

NASA CONTRACTOR REPORT

NASA CR-1493



NASA CR-1493

0060694



TECH LIBRARY KAFB, NM

LOAN COPY: RETURN TO
AFWL (WL0L)
KIRTLAND AFB, N MEX

STUDY PROGRAM FOR LIFT FAN NOISE REDUCTION AND SUPPRESSION

by M. J. Benzakein and L. J. Volk

Prepared by

GENERAL ELECTRIC COMPANY

Cincinnati, Ohio

for Ames Research Center



STUDY PROGRAM FOR LIFT FAN NOISE REDUCTION AND SUPPRESSION

By M. J. Benzakein and L. J. Volk

Distribution of this report is provided in the interest of information exchange. Responsibility for the contents resides in the author or organization that prepared it.

Prepared under Contract No. NAS 2-4763 by
GENERAL ELECTRIC COMPANY
Cincinnati, Ohio

for Ames Research Center

NATIONAL AERONAUTICS AND SPACE ADMINISTRATION

SUMMARY

This report describes a nine-month program to evaluate noise reduction methods in terms of their effects on lift fan design. Two lift fans designed under Contracts NAS2-3077 and AF33657-67-C-0812 were used as design points. These fans were analytically modified to study acoustic reduction by trade-offs in fan pressure ratio, tip speed, rotor-stator spacing, number of blades and vanes and the use of various types of acoustic materials.

The quiet OGV fan is summarized in Table IX. The fan is shown in Figure 74. The basepoint LF475 OGV fan has a 500 feet sideline noise of 119 PNdB. The quiet version of this fan has a 500 feet sideline noise of only 99 PNdB, a reduction of 20 PNdB. The fan lift is unchanged. The fan diameter is increased by 1 inch, the fan weight is increased by 17%, and the fan thickness is increased by 3 inches.

The selected quiet IGV fan design is summarized in Table X. The fan is shown in Figure 75. The LF387 basepoint IGV fan has a 500 feet sideline noise of 131 PNdB. The quiet version of the fan has a 500 feet sideline of 106 PNdB, a reduction of 25 PNdB. The fan lift and size are unchanged. The fan weight is increased by 6% and the fan thickness is increased by 4 inches. This fan could have been made more quiet by increasing the number of blades, leaning the stators, and using an H-type rear frame, but the penalties in weight and size would have been as large as with the OGV fan.



CONTENTS

SUMMARY iii

LIST OF ILLUSTRATIONS vi

LIST OF TABLES ix

INTRODUCTION 1

LIST OF SYMBOLS 3

BASEPOINT LIFT FANS 7

 Fan Descriptions 7

 Noise Predictions 7

NOISE PARAMETRIC DATA 16

 Range of Studies 16

 Noise Parametric Data for OGV Fans 16

 Noise Parametric Data for IGV Fans 27

TRADE-OFF STUDIES 35

 Performance & Installation Parametric Data for OGV Fans 35

 Performance & Installation Parametric Data for IGV Fans 50

SELECTION OF QUIET LIFT FAN DESIGNS 61

 Selected OGV Fan Design 61

 Selected IGV Fan Design 65

CONCLUSIONS 68

APPENDICES 69

 A. Theoretical Prediction of Aerodynamically Generated Noise in Fans and Compressors 69

 B. Aero-Acoustic Data Used to Calculate the Fan Parametric Noise Curves. 93

REFERENCES 109

<u>Figure</u>	<u>Page</u>
25	Power Levels at the Fundamental of Blade Passing Frequency Versus Fan Tip Diameter, for IGV Fans 29
26	Perceived Noise Levels Versus Tip Diameter, for IGV Fans 29
27	Power Levels at the Fundamental of Blade Passing Frequency Versus Tip Speed at Constant Thrust, for IGV Fans 31
28	Perceived Noise Levels Versus Tip Speed at Constant Thrust, for IGV Fans 31
29	Power Levels at the Fundamental of Blade Passing Frequency Versus Number of Blades, for IGV Fans 32
30	Perceived Noise Levels Versus Number of Blades, for IGV Fans . . . 32
31	Power Levels at the Fundamental of Blade Passing Frequency Versus Number of Vanes, for IGV Fans 33
32	Perceived Noise Levels Versus Number of Vanes, for IGV Fans 33
33	Power Levels at the Fundamental of Blade Passing Frequency Versus Blade Row Spacing, for IGV Fans 34
34	Perceived Noise Levels Versus Blade Row Spacing, for IGV Fans . . . 34
35	Radius Ratio Versus Tip Speed and Pressure Ratio, for OGV Lift Fans. 36
36	Lift Versus Tip Speed and Pressure Ratio, for OGV Fans 36
37	Fan Tip Diameter Versus Tip Speed and Pressure Ratio, for OGV Fans. 37
38	Area Versus Tip Speed and Pressure Ratio, for OGV Fans 37
39	Weight Versus Tip Speed and Pressure Ratio, for OGV Fans 38
40	Rotor Weight Versus Tip Speed, for OGV Fans 38
41	Effect of Tip Speed on Weight, for OGV Fans 40
42	Lift/Area Ratio Versus Tip Speed and Pressure Ratio, for OGV Fans . 40
43	Lift/Weight Ratio Versus Tip Speed and Pressure Ratio, for OGV Fans 41
44	Effect of Input Power on Fan Diameter and Lift, for OGV Fans . . . 41
45	Effect of Diameter on Lift/Weight and Lift/Area Ratios, for OGV Fans 42
46	Inlet Mach Number Limits for OGV Lift Fans 42
47	Effects of Fan Inlet Mach Number on Fan Lift, Weight and Area . . . 44
48	Number of Blades Versus Fan Tip Diameter and Tip Speed 44
49	Rotor Weight Versus Number of Blades 46
50	Fan Weight Versus Number of Blades, for OGV Fans 47
51	Stator Vane Row With Part-Span Vanes in the Outer Annulus 47



<u>Figure</u>		<u>Page</u>
52	Fan Weight Versus Number of Tip Vanes for OGV Fans	48
53	Stator Vane Row With Stub Vanes at the Tip	48
54	Stator Vane Row With Lean	49
55	Fan Weight Versus Number of Tip Vanes With Lean, for OGV Fans . .	49
56	Conventional Front Frame with Cross Struts	51
57	Front Frame with Lean	51
58	Fan Thickness Ratio Versus Number of Fan Blades and Rotor-Stator Spacing, for OGV Fans	52
59	Weight Increase for Rotor-Stator Spacing, For OGV Fans	52
60	Fan Radius Ratio Versus Fan Tip Speed, for IGV Fans	53
61	Lift Versus Tip Speed and Pressure Ratio, for IGV Fans	53
62	Fan Tip Diameter Versus Tip Speed and Pressure Ratio, for IGV Fans	54
63	Area Versus Fan Tip Speed and Pressure Ratio, for IGV Fans	54
64	Weight Versus Tip Speed and Pressure Ratio, for IGV Fans	55
65	Lift/Area Ratio Versus Tip Speed and Pressure Ratio, for IGV Fans	55
66	Lift/Weight Ratio Versus Tip Speed and Pressure Ratio, for IGV Fans	57
67	Effect on Input Power on Fan Diameter and Lift, for IGV Fans . . .	57
68	Effect of Fan Diameter on Lift/Weight and Lift/Area Ratios, for IGV Fans	58
69	Inlet Mach Number Limits for IGV Lift Fans	58
70	Effects of Fan Inlet Mach Number on Fan Lift, Weight and Area, for IGV Fans	59
71	Fan Weight Versus Number of Blades, for IGV Fans	59
72	Fan Weight Versus Number of Vanes, for IGV Fans	60
73	Weight Increase for Rotor-Stator Spacing, for IGV Fans	60
74	Quiet OGV Lift Fan	64
75	Quiet IGV Lift Fan	67

TABLES

<u>Table</u>		<u>Page</u>
I	LF475 OGV Lift Fan Description	8
II	LF387 IGV Lift Fan Description	8
III	LF475 OGV Fan Aero-Acoustic Data	10
IV	LF387 Fan Aero-Acoustic Data	10
V	Range of Studies	13
VI	Acoustic Run Log for OGV Fans	17
VII	Acoustic Run Log for IGV Fans	17
VIII	Vane/Blade Ratios of Other Fan Designs	46
IX	OGV Quiet Fan Summary	64
X	IGV Quiet Fan Summary	67

INTRODUCTION

The feasibility of commercial lift fan V/STOL transport aircraft for intercity short-haul transportation has been extensively investigated by the aeronautical community. However, the commercial success of these aircraft depends on community acceptance. To gain this acceptance, fan noise will have to be reduced without major compromises in performance, weight or volume.

To achieve this goal, an investigation of lift fan noise generation, as well as a study of methods for noise reduction of reasonably thin lift fans were undertaken.

The basic differences between this study and other studies of turbofan engines is that the lift fan is a single-stage machine with a tip turbine rather than a central, concentric turbine. Furthermore, the rotational axis of the fan is vertical rather than horizontal, thus the noise problem is confined to the 180° arc comprising the lift fan exhaust. A further difference is, since volume is of primary importance, little space is available for acoustic material treatment of exhausts or inlets.

This study has integrated existing noise reduction technology and lift fan design technologies by predicting basic fan noise levels and defining the trade-offs in fan weight, performance and installation dimensions for various methods of fan noise reduction.

NOMENCLATURE

Symbol

A_{nm}	Fourier-Bessel coefficient
a_n	Coefficients of the radial unsteady circulation distribution
B	Number of rotor blades
b	Axial distance between the centers of adjacent blade rows
b'	Axial distance between adjacent blade rows
C_d	Drag coefficient
C_r	Rotor blade chord
C_s	Stator vane chord
c	Speed of sound, or airfoil semi-chord
D	Number of rotating line vorticies
DFT	Fan tip diameter
D_r	Rotor diffusion factor
D_s	Stator diffusion factor
d	Blade-to-blade tangential spacing
f(r)	Radial distribution of unsteady tangential velocity
FPR	Fan pressure ratio
G_m	See Equation (A2) or (A10), Appendix A
H_m	See Equation (A11) or (A15), Appendix A
IGV	Inlet guide vanes
I_j	See Equation (A46), Appendix A
$J (m^{(j)}_r)$	See Equation (A7), Appendix A
J_n, Y_n	First and second kind Bessel functions of order n
K_n	Modified Bessel function of the second kind of order n

k	Integer index
M	Mach number
M_{nm}^*	Mode cut-off tip Mach number
m	Integer index
n	Integer index, or spinning mode number
\hat{n}	Integer index
\bar{n}	Integer indicator of the harmonic of blade passing frequency
OGV	Outlet guide vanes
P	Pressure
PWL	Sound power level referenced to 10^{-13} watts
$R_n(\lambda_{nm} r)$	Bessel cylinder function
R_o	Duct outside radius
r, θ , z	Polar coordinates
S	Rotor-stator axial spacing, expressed as a multiple of the true tip chord of the upstream blade row
S (m ω)	See Equation (A8), Appendix A
t	time
U	Rotor linear wheel speed
UFT	Rotor linear wheel tip speed
V	Air velocity, or stator vane number
V/B	Vane to blade ratio
v^r	Upwash (or downwash) velocity on the rotor
W	Sound power
w	Axial velocity
x'	See Equation (A3), Appendix A
x	Distance measured along the blade chord

z_r	See Equation (A12), Appendix A
α	Air flow angle
α_1	Rotor inlet absolute air angle
α_2	Rotor exit absolute air angle
β_1	Rotor inlet relative air angle
β_2	Rotor exit relative air angle
Γ_o	Steady blade circulation
Γ	Unsteady blade circulation
γ	See Equation (A20)
∇	$\frac{\partial}{\partial r} + \frac{1}{r} \frac{\partial}{\partial \theta} + \frac{\partial}{\partial z}$
δ	Impulse Function
ζ	See Equation (A21), Appendix A
η_{nm}	See Equation (A42), Appendix A
λ	See Equation (A14), Appendix A
λ_{nm}	Eigenvalue
μ	Radius ratio
ν	Circular frequency = $\frac{2 \pi U}{d}$
ρ	Density
σ	Blade Row Solidity
ϕ	Velocity potential
ω	Reduced frequency = $\frac{\nu c}{V}$

Subscripts

n	Spinning mode number
m	Radial mode number
r	Rotor
s	Stator
z	Axial direction
θ	Tangential direction
1	Rotor inlet
2	Rotor discharge

BASEPOINT LIFT FANS

Lift Fan Descriptions

Two existing lift fan designs, a rotor-OGV fan and an IGV-rotor fan, were selected as basepoints for the studies. The OGV fan, designated LF475, is a 75 inch diameter tip turbine lift fan. Preliminary design of this fan was done under contract AF33657-67-C-0812. The power source is an advanced gas generator of the GE1 family. Certain design and performance features of the LF475 are classified Confidential and are not included in this report. A drawing of the fan is shown in Figure 1. Table I summarizes the design features. The LF475 rear frame combines the OGV's and the load-carrying struts. There is no front frame. The fan inlet is integral with the double walled tip turbine scroll.

The IGV fan, designated LF387, is an 86.5 inch diameter tip turbine lift fan. Conceptual design for this fan was done under contract NAS2-3077 and is described in Reference 1. The power source is an assumed advanced gas generator representing the technology of the 1967-1970 period. A drawing of the fan is shown in Figure 2. Table II summarizes the design features. The LF387 has a front frame incorporating the IGV's as load-carrying struts. There is no rear frame.

The two basepoint fans were designed for wing installation and are in the 25,000 to 30,000 pound thrust bracket. Design technology advancements in blade fabrication and structural design concepts were incorporated.

Noise Predictions

Fan on the Ground. - Noise was predicted for the two basepoint fans when near the ground. Broad band noise was predicted using a technique similar to that of Smith & House (Reference 2). The prediction of the maximum 500 foot sideline PNdB was based on the pure tone calculation described in Appendix A. The calculation procedure is outlined below:

1. The pure tone power levels are calculated from basic aerodynamic and geometric parameters which define the fan.
2. The sound directivity is calculated and the sound is obtained along a 250 foot arc.
3. The angle of maximum sound on a 500 foot sideline is determined and the sound is calculated at that position taking into account directivity, air attenuation, and ground reflection.

The aero-acoustic data for the LF475 are given in Table III. The predicted pure tone sound directivity is shown in Figure 3. The maximum

Table I. LF475 OGV Lift Fan Description

Fan Tip Diameter, inches	75.0
Turbine Tip Diameter, inches	82.2
Fan Pressure Ratio	1.39
Fan Radius Ratio	0.45
Fan Bypass Ratio	8.1
Fan Tip Speed, ft/sec	1114
RPM	3440
Fan Inlet Axial Mach No	0.58

	Fan Rotor Blades			Fan OGV's		
	Hub	Pitch	Tip	Hub	Pitch	Tip
Diameter, inches	33.8	54.4	75	36.4	53.4	70.4
Chord, inches	3.9	4.3	4.7	5.26	5.26	5.26
Solidity	2.35	1.66	1.34	1.65	1.13	.864
Orientation Angle, deg	7.1	34.1	50.3	14.9	11.9	9.0
Camber, degrees	46.1	24.2	23.7	37.7	43.7	33.4
Number		66			36	
Length, inches		20.6			17.0	
Aspect Ratio		4.8			3.2	

Table II. LF387 IGV Lift Fan Description

Fan Tip Diameter, inches	86.5
Turbine Tip Diameter, inches	93.2
Fan Pressure Ratio	1.26
Fan Radius Ratio	0.45
Fan Bypass Ratio	11.1
Fan Tip Speed, ft/sec	1000
RPM	2650
Fan Inlet Axial Mach No	0.51

	Fan Rotor Blades			Fan IGV's		
	Hub	Pitch	Tip	Hub	Pitch	Tip
Diameter, inches	39.9	63.2	86.5	30.6	60.0	89.4
Chord, inches	6.0	6.0	6.0	7.5	7.5	7.5
Solidity	1.92	1.21	0.89	2.18	1.11	0.75
Orientation Angle, deg	41	49	61	22	18	28
Camber, degrees	22	12	23	41	40	67
Number		40			28	
Length, inches		23.3			29.4	
Aspect Ratio		3.9			3.9	

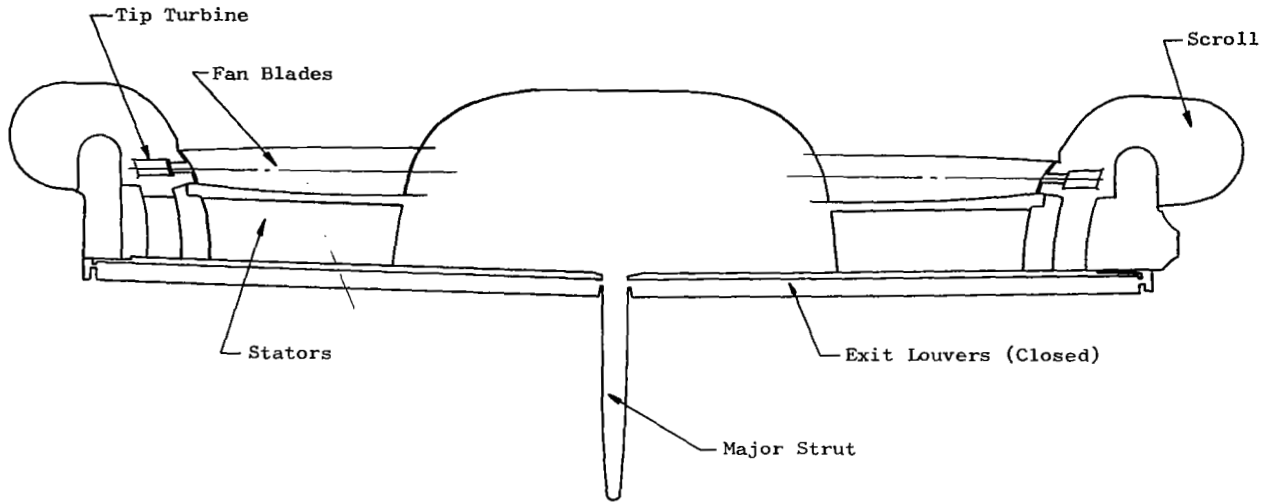


Figure 1. LF475 Basepoint OGV Lift Fan

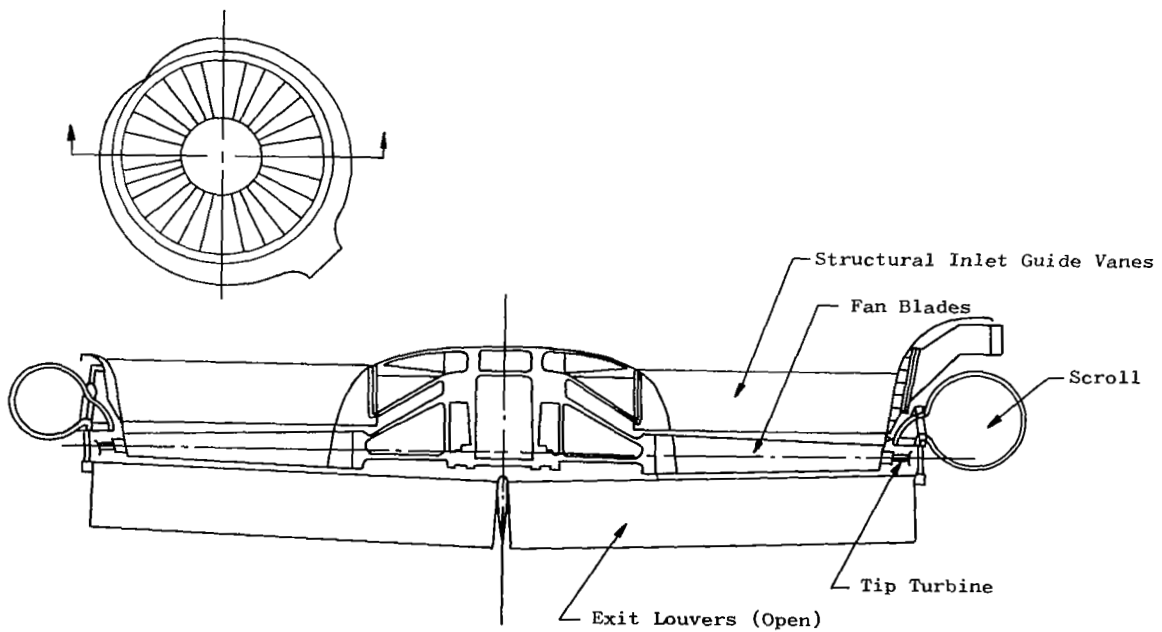


Figure 2. LF387 Basepoint IGV Lift Fan

Table IV LF387 IGV Fan Aero-Acoustic Data			
Pressure Ratio	1.26		
Radius Ratio	0.45		
Fan Tip Speed, fps	1000		
Fan Tip Diameter, inches	86.5		
Number of Rotor Blades	40		
Number of Stator Vanes	28		
Vane/Blade Ratio	0.70		
Rotor-Stator Tip Spacing, in vane chords	0.20		
	HUB	PITCH	TIP
Rotor Inlet Radius, inches	19.46	31.36	43.25
Rotor Inlet Absolute Air Angle, α_1 , deg	-46.4	-27.2	-25.0
Rotor Inlet Relative Air Angle, β_1 , deg	61.5	59.3	65.6
Rotor Exit Absolute Air Angle, α_2 , deg	0	0	0
Rotor Exit Relative Air Angle, β_2 , deg	46.9	54.3	59.3
Rotor Inlet Speed, U_1 , fps	450	781	1000
Rotor Exit Speed, U_2 , fps	499	769	964
Rotor Blade Chord, C_r , inches	5.87	5.95	6.04
Stator Vane Chord, C_s , inches	7.5	7.5	7.5
Rotor Solidity, σ_r	1.92	1.21	0.89
Stator Solidity, σ_s	2.18	1.11	0.75
Rotor Diffusion Factor, D_r	0.451	0.336	0.313
Stator Diffusion Factor, D_s	-0.738	-0.364	-0.334
Stator Drag Coefficient, C_{ds}	0.0504	0.0666	0.0939
Rotor-Stator Spacing, inches	0.75	1.10	1.50

Table III LF475 OGV Fan Aero-Acoustic Data			
Pressure Ratio	1.39		
Radius Ratio	0.45		
Fan Tip Speed, fps	1114		
Fan Tip Diameter, inches	75.0		
Number of Rotor Blades	66		
Number of Stator Vanes	36		
Vane/Blade Ratio	0.55		
Rotor-Stator Tip Spacing, in blade chords	0.23		
	HUB	PITCH	TIP
Rotor Inlet Radius, inches	16.88	27.2	37.5
Rotor Inlet Absolute Air Angle, α_1 , deg	0	0	0
Rotor Inlet Relative Air Angle, β_1 , deg	38.3	51.72	60.8
Rotor Exit Absolute Air Angle, α_2 , deg	39.05	34.80	31.75
Rotor Exit Relative Air Angle, β_2 , deg	0	26.63	39.67
Rotor Inlet Speed, U_1 , fps	501	808	1114
Rotor Exit Speed, U_2 , fps	535	796	1057
Rotor Blade Chord, C_r , inches	3.77	4.28	4.78
Stator Vane Chord, C_s , inches	5.30	5.30	5.30
Rotor Solidity, σ_r	2.35	1.65	1.34
Stator Solidity, σ_s	1.67	1.14	0.864
Rotor Diffusion Factor, D_r	0.322	0.399	0.390
Stator Diffusion Factor, D_s	0.243	0.380	0.505
Rotor Drag Coefficient, C_{dr}	0.315	0.0528	0.0615
Rotor-Stator Spacing, inches	0.90	1.00	1.10

Fundamental Tone SPL,
de re 0.0002 Microbar

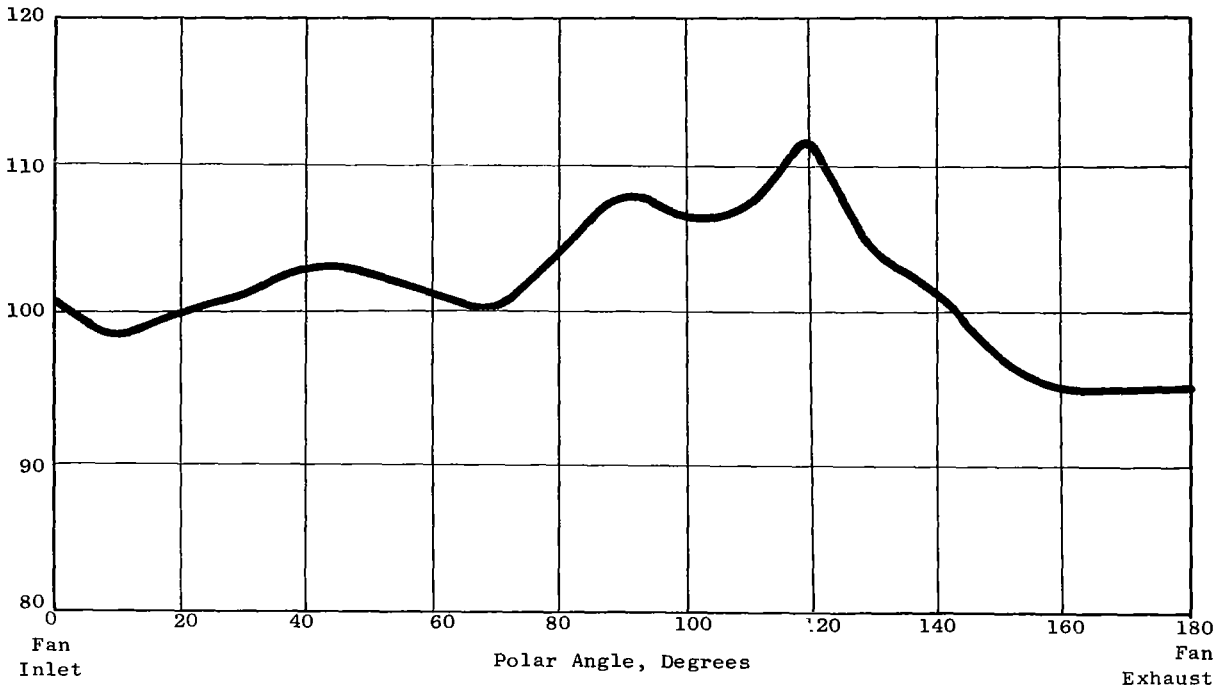


Figure 3. Predicted Fundamental Sound Pressure Levels of the LF475 at 100% Speed, 250 Ft. Arc

Fundamental Tone SPL
dB re 0.0002 Microbar

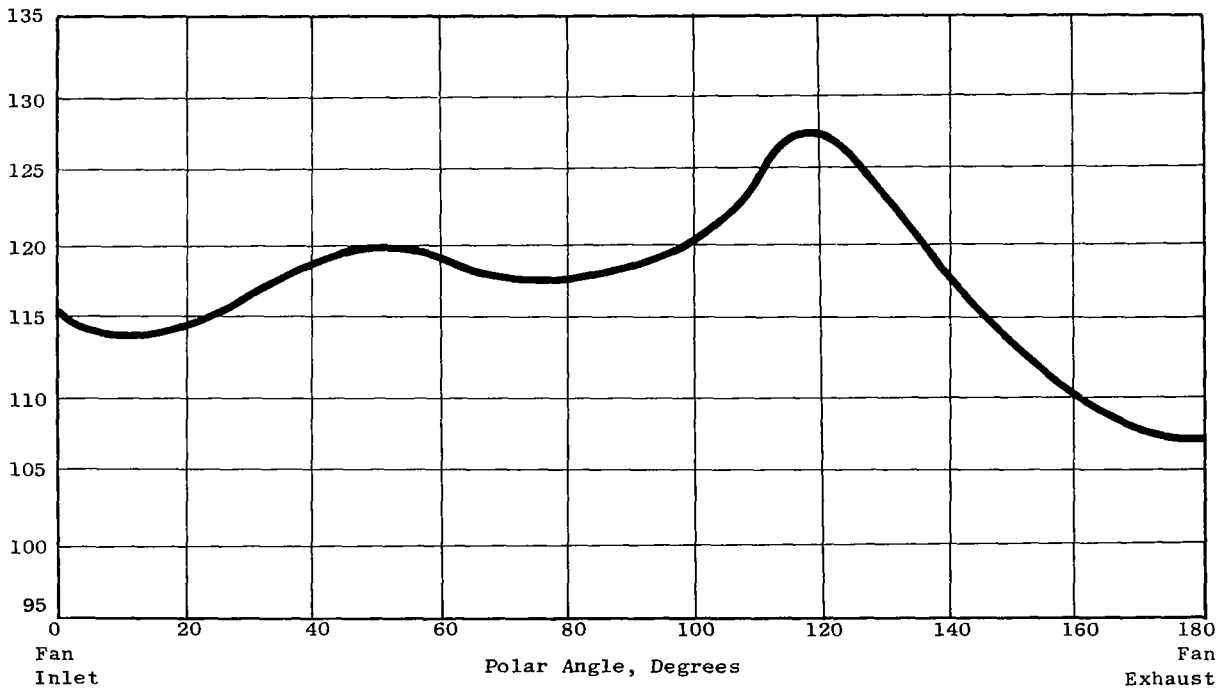


Figure 4. Predicted Fundamental Sound Pressure Levels of the LF387 at 100% Speed, 250 Ft. Arc

500 feet sideline noise was calculated to be 119 PNdB. It can be seen that the point of maximum noise is 60 degrees from straight down. The point of maximum PNdB will therefore not necessarily be below the aircraft but will depend on the height of the aircraft above the ground.

The aero-acoustic data for the LF387 is given in Table IV. The predicted pure tone sound directivity is shown in Figure 4. The maximum 500 feet sideline noise was found to be 131 PNdB.

It is seen that the LF387 is louder than the LF475. This is primarily due to the much stronger potential interaction and unfavorable wake geometry of the IGV stage. (See Figure 5. For a given axial spacing, the IGV wakes travel a much shorter distance before interacting with the rotor than do the rotor wakes to interact with the OGV's in the OGV fans. This causes the stronger wake interaction.)

Fan Noise During Landing and Take-Off. - The effective perceived noise levels (EPNdB) were calculated for one LF475 fan, and noise contours were obtained for take-off and landing cases. The lift fan was assumed to be mounted in the wing of an aircraft that would operate through the take-off and landing profiles shown on Figure 6. The computation procedure of EPNdB's used in the study conforms to the Federal Aviation Agency's revised draft circular, "Aircraft Noise Analysis and Measurement" dated May 22, 1968. It consists of a series of computer programs:

1. The first program corrects the sound pressure data for the line of sight distance from the source to the receiver.
2. The second program calculates the tone correction for the noise spectrum as perceived by the receiver.
3. The third program adds the duration correction.
4. The fourth program performs the EPNdB calculation.

The static ground source data were the predicted sound pressure levels reported in Figure 3. For both the take-off and landing cases, a number of ground level receiver positions were established. At each receiver position the SPL values for each spectrum angle were calculated for a standard (59°F and 70% relative humidity) day by accounting for humidity corrections, ground attenuation corrections and square law divergence. Using these estimated SPL values, the EPNdB values were calculated. From these EPNdB calculations the maximum EPNdB value at each ground microphone position was chosen. Given these maximum values representative of the aircraft passing overhead, the contour plots were prepared for the ground level noise. The results are shown for the take-off and landing cases in Figures 7 and 8.

It is obvious that lift fans are noisy and that quieting will be required. Straight-up climbs to high altitude to minimize noise are possible but will be costly in airplane range or in direct operating costs. Lift fan noise can, however, be reduced by quieting at the source through design changes and by judicious use of acoustic treatment.

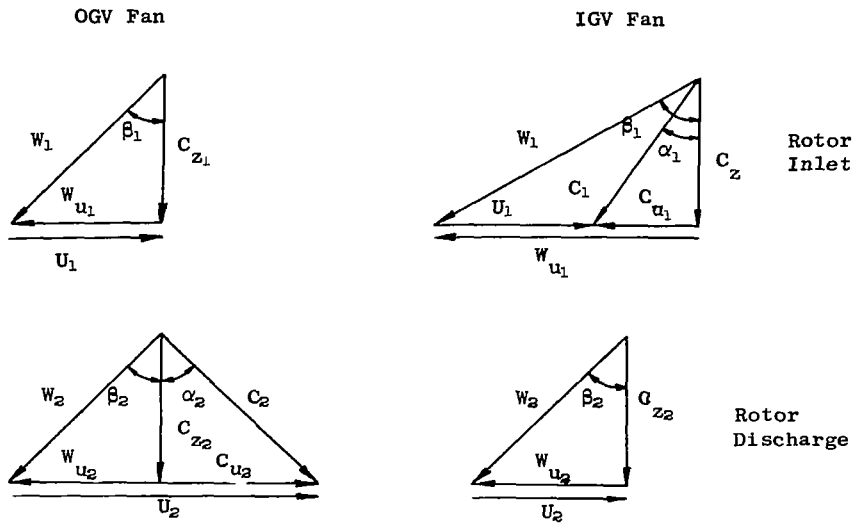


Figure 5. Fan Flow Vector Diagrams for OGV and IGV Fans

TABLE V Range of Studies		
Range of Studies for OGV ¹ Fans	LF475	Study Range
Fan Tip Diameter, inches	75	36-100
Fan Stage Pressure Ratio	1.39	1.2-1.4
Fan Tip Speed, fps	1114	800-1200
Fan Rotor Inlet Axial Mach Number	0.58	0.50-0.60
Fan Rotor Blade Number	66	30-80
Fan Stator Vane Number	36	30-200
Fan Stator Vane Lean Angle, deg	0	0-30
Rotor-Stator Tip Axial Separation, Expressed in fan rotor blade tip chords	0.23	0.10-2.0
Range of Studies for IGV Fans	LF387	Study Range
Fan Tip Diameter, inches	86.5	36-100
Fan Stage Pressure Ratio	1.26	1.15-1.30
Fan Tip Wheel Speed, fps	1000	800-1100
Fan Rotor Inlet Axial Mach Number	0.51	0.30-0.55
Fan Rotor Blade Number	40	30-80
Fan Stator Vane Number	28	28-100
Rotor-Stator Tip Separation, expressed in fan IGV tip chords	0.15	0.10-2.0

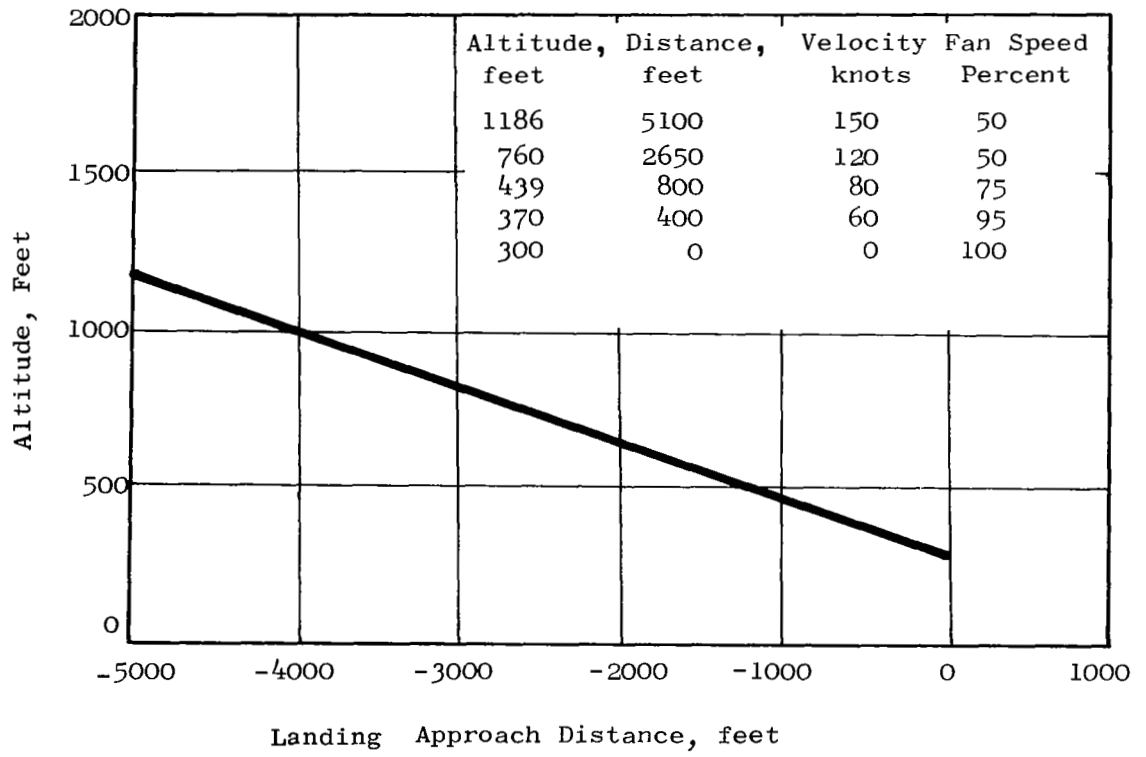
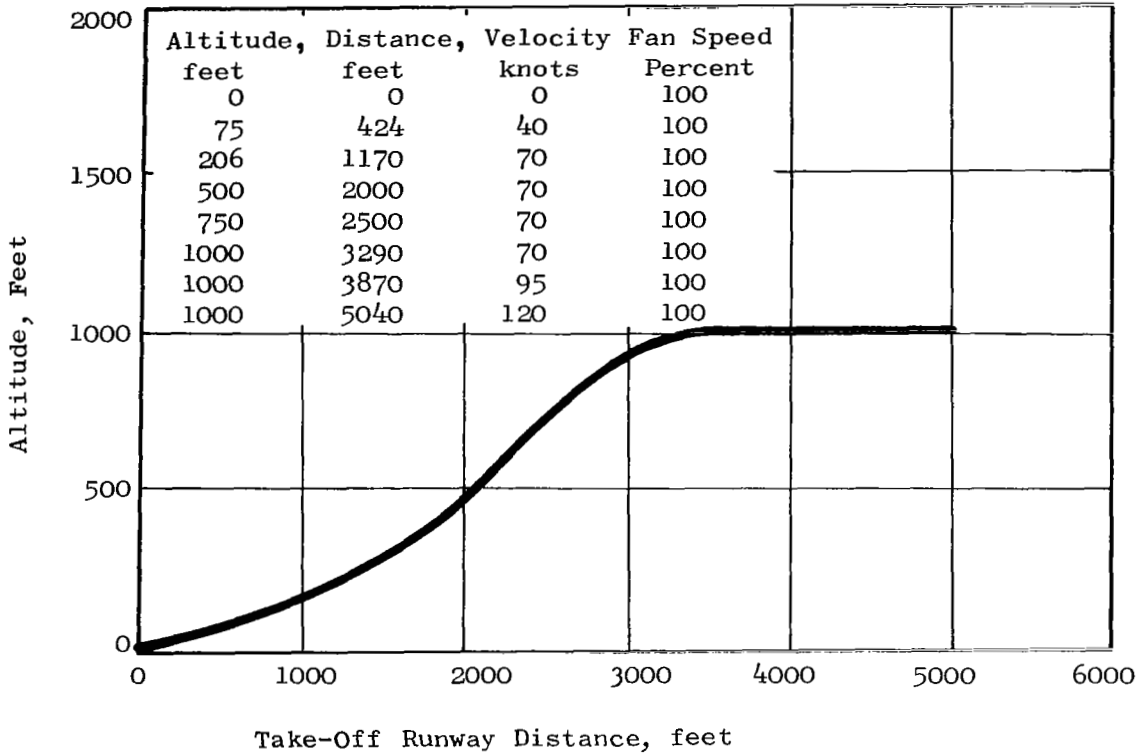


Figure 6. Take-Off & Landing Paths Definitions

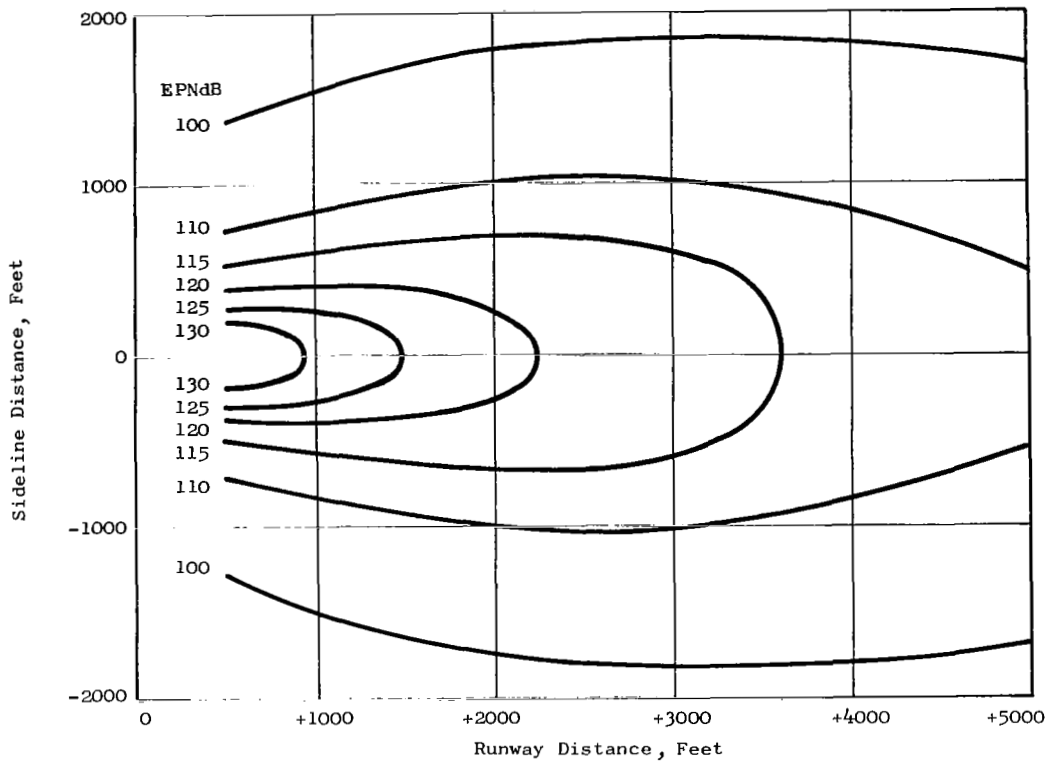


Figure 7. Takeoff Noise Contours for the LF475

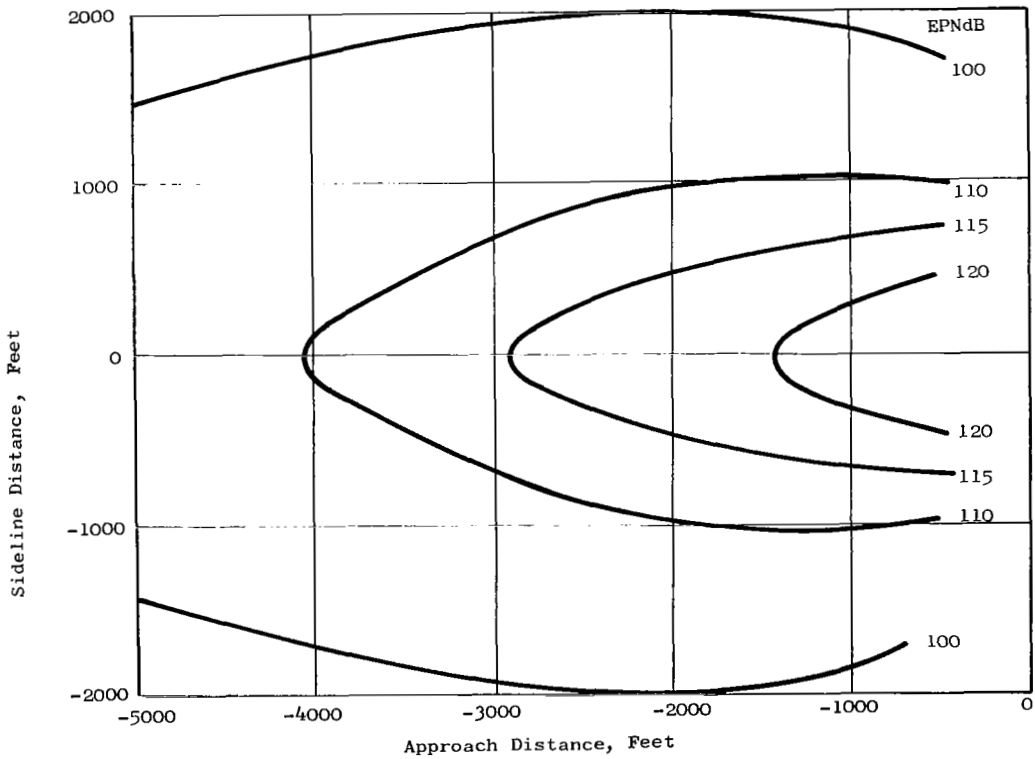


Figure 8. Landing Noise Contours for the LF475

NOISE PARAMETRIC DATA

Range of Studies

Table V defines the selected range of studies for the OGV and IGV fans. Fan sizes from 36 inches to 100 inches, fan pressure ratios between 1.15 and 1.4, and fan tip speeds from 800 to 1200 fps will include most lift fan applications. These studies were made to determine the functional relationships between the fan pure tone noise generation (blade passing frequency tones of the fundamental and higher harmonics) and the fan aerodynamic and geometric parameters of pressure ratio, wheel speed, size, number of blades, vane/blade ratio, and spacing. These studies were based on the theoretical analyses described in Appendix A, which has been taken from Reference 3. These analyses agree well with experimental results, as shown in Figures A7 to A11 of Appendix A.

Noise Parametric Data for OGV Fans

Numerical values of each fan parameter were selected while holding all other parameters constant. A matrix of points was formed to cover the range of studies. The noise level of each of the resulting fan configurations was calculated and curves of the relative noise levels were then constructed.

A matrix of 16 points was chosen for the OGV fans. This matrix is shown in Table VI. The basepoint LF475 OGV fan appears in each of the six groupings. The detailed aero-acoustic data for each of these configurations are given in Tables B1 - B16 in Appendix B. The fan flow vector diagrams for OGV & IGV fans are given in Figure 5.

Fan Pressure Ratio. - The effect of pressure ratio on pure tone power levels is shown in Figure 9. An increase in pressure ratio without a change in wheel speed requires the blade row to do more turning of the flow. This in turn increases the blade loading. The velocity ratio and the air angle contained in the expression for the coefficient of unsteady upwash increase. (See equation (A2) in Appendix A.) These cause the increase in the pure tone power levels. It can be seen from Figure 9 that a decrease in fan pressure ratio from 1.39 to 1.20 reduces the pure tone levels by about 8 dB for a constant-size fan, and about 4 dB for a constant-thrust fan. Pressure ratio is therefore an important parameter than cannot be neglected. The use of correlation formulas that do not include this effect may therefore give misleading results.

Figure 10 shows the effect of including broad band noise in addition to the pure tone. It can be seen that the PNdB trend with pressure ratio is the same as for the pure tone.

Table VI. Acoustic Run Log for the OGV Fans

RUN	FPR	UFT	DFT	B	V/B	S
1	1.2	1114	75	66	.55	.23
2	1.3	↓	↓	↓	↓	↓
3	1.39	↓	↓	↓	↓	↓
4	1.39	800	75	66	.55	.23
5	↓	1000	↓	↓	↓	↓
3	↓	1114	↓	↓	↓	↓
6	↓	1200	↓	↓	↓	↓
7	1.39	1114	36	66	.55	.23
8	↓	↓	50	↓	↓	↓
3	↓	↓	75	↓	↓	↓
9	↓	↓	100	↓	↓	↓
10	1.39	1114	75	20	.55	.23
3	↓	↓	↓	66	↓	↓
11	↓	↓	↓	80	↓	↓
3	1.39	1114	75	66	.55	.23
12	↓	↓	↓	↓	1.5	↓
13	↓	↓	↓	↓	2.1	↓
14	1.39	1114	75	66	.55	.10
3	↓	↓	↓	↓	↓	.23
15	↓	↓	↓	↓	↓	1.0
16	↓	↓	↓	↓	↓	2.0

Table VII. Acoustic Run Log for IGV Fans

RUN	FPR	UFT	DFT	B	V/B	S
1	1.15	1000	86.5	40	.70	.15
2	1.26	↓	↓	↓	↓	↓
3	1.30	↓	↓	↓	↓	↓
4	1.26	800	86.5	40	.70	.15
2	↓	1000	↓	↓	↓	↓
5	↓	1100	↓	↓	↓	↓
6	1.26	1000	36	40	.70	.15
7	↓	↓	50	↓	↓	↓
2	↓	↓	86.5	↓	↓	↓
8	↓	↓	100	↓	↓	↓
9	1.26	1000	86.5	20	.70	.15
2	↓	↓	↓	40	↓	↓
10	↓	↓	↓	80	↓	↓
2	1.26	1000	86.5	40	.70	.15
11	↓	↓	↓	↓	1.5	↓
12	↓	↓	↓	↓	2.1	↓
2	1.26	1000	86.5	40	.70	.15
13	↓	↓	↓	↓	↓	1.0
14	↓	↓	↓	↓	↓	1.5
15	↓	↓	↓	↓	↓	2.1

Fan Tip Speed. - The effect of fan tip speed on pure tone levels is shown in Figure 11. It can be seen that the pure tone levels at a constant pressure ratio are lower for a high speed, low loading coefficient machine. This can be explained by considering the fact that for a constant pressure ratio the designs with high tip speed will have a lower velocity ratio and rotor turning angle, which will be translated into lower pure tones. The concept that noise increases with speed can be quite misleading. It is true that the pure tone levels go up as the speed is increased on a particular vehicle, but so do the rotor loading and stage pressure ratio. It is not the speed, but the higher work the stage is doing which is generating higher pure tone levels. It can be seen from Figure 11 that for a particular design pressure ratio, a higher speed can be a favorable noise feature.

When the broadband noise is added to the pure tone and the PNdB calculated, one can see a different trend (see Figure 12). The fan white noise component increases with speed and results in the PNdB rating increasing with speed. The curve of PNdB versus tip speed is, however, very flat. When the design speed is increased from 800 to 1200 ft/sec the noise rises only by about 1.5 PNdB. The results indicate that the design speed does not have a major effect on the PNdB rating of this basepoint OGV fan.

Fan Diameter. - The effect of size on pure tone noise is shown in Figure 13. The PNdB levels are shown in Figure 14. If the LF475 fan diameter is reduced by a factor of 2, this will result in a 4 to 1 decrease of fan air flow and thrust. The pure tone power levels will consistently decrease by 6 dB. The noise rating of four new 37.5" fans will, however, be quieter than the LF475 (see Figure 14). This is due to the fact that if the tip speed and the number of blades are kept constant, a smaller fan will have a higher rpm and, consequently, a higher blade passing frequency. (The fan fundamental blade passing frequency is the product of blade number and rpm: $f = B \times \text{RPM}/60$, Hertz.)

Figure 15, from Reference 4, shows the relationship between sound pressure level, frequency, and the annoyance rating called NOY's. Figure 16 shows the NOY values versus frequency for a constant 100 dB SPL, obtained by crossplotting the data of Figure 15. The LF475 frequency is 3740 Hertz. Now, it is seen that as the size of the fan is reduced, with blade number and tip speed held constant, the fan will move toward the right, away from the peak of the NOY curve of Figure 16, thus lowering the annoyance (NOY) rating of the fan. Figure 14 points out that it will be advantageous, from the noise viewpoint, to select two 53" fans or even four 37.5" fans to replace one 75" fan.

Number of Blades. - The number of rotor blades is an important parameter in noise generation and can be modified within certain mechanical and aerodynamic bounds to suit the acoustic designer. In the present study the pressure ratio, tip speed, blade row spacing and the vane/blade ratio were constant and the numbers of blades were varied from 20 to 80. It can be seen on Figure 17 that a large blade number design reduces the pure tone levels

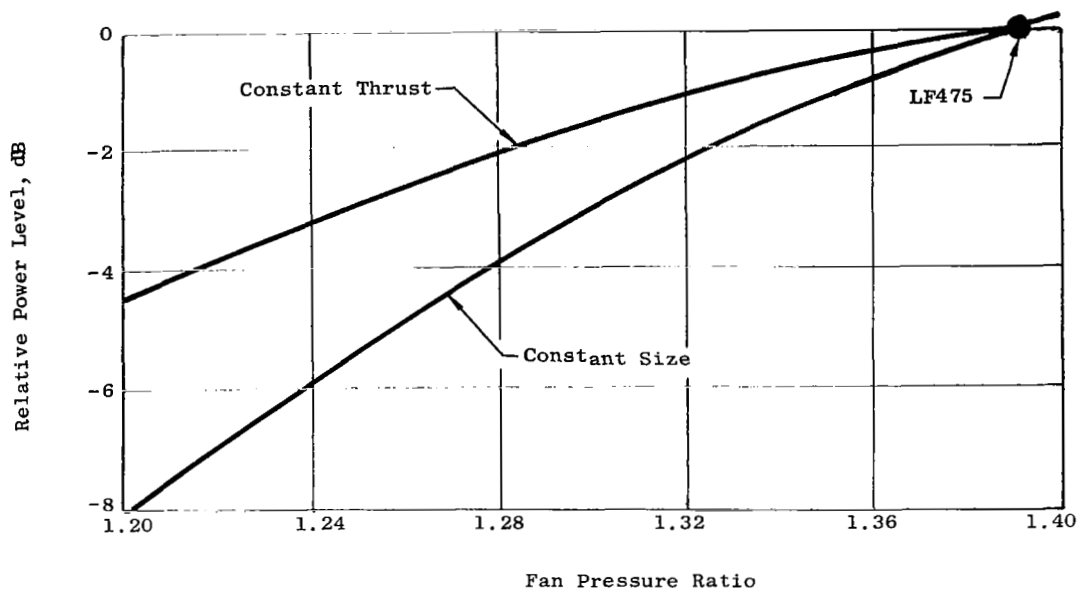


Figure 9. Power Levels at the Fundamental of Blade Passing Frequency vs. Pressure Ratio, for OGV Fans

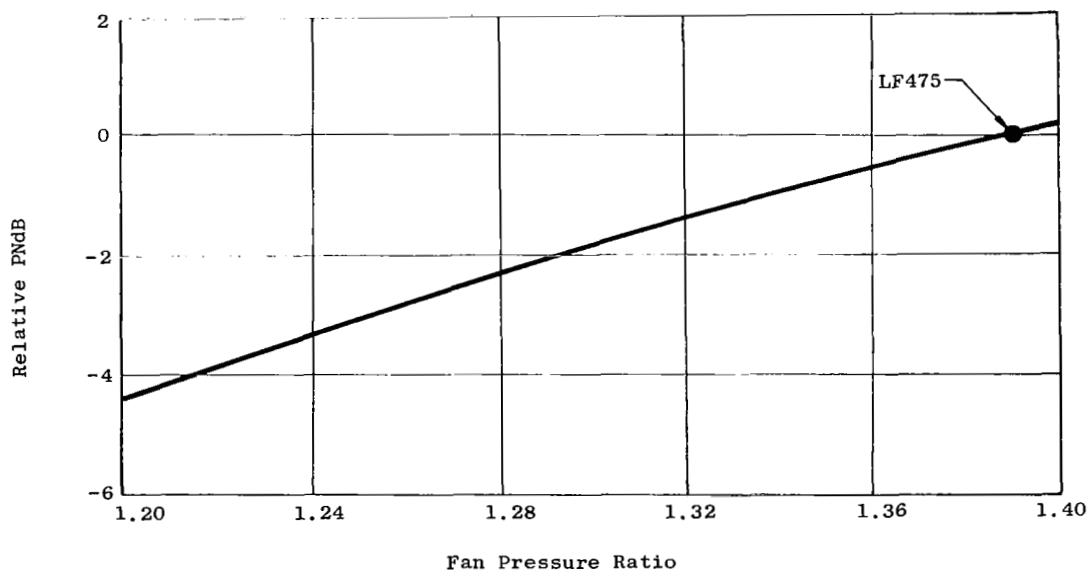


Figure 10. Perceived Noise Levels vs. Pressure Ratio at Constant Tip Speed and Constant Size, for OGV Fans

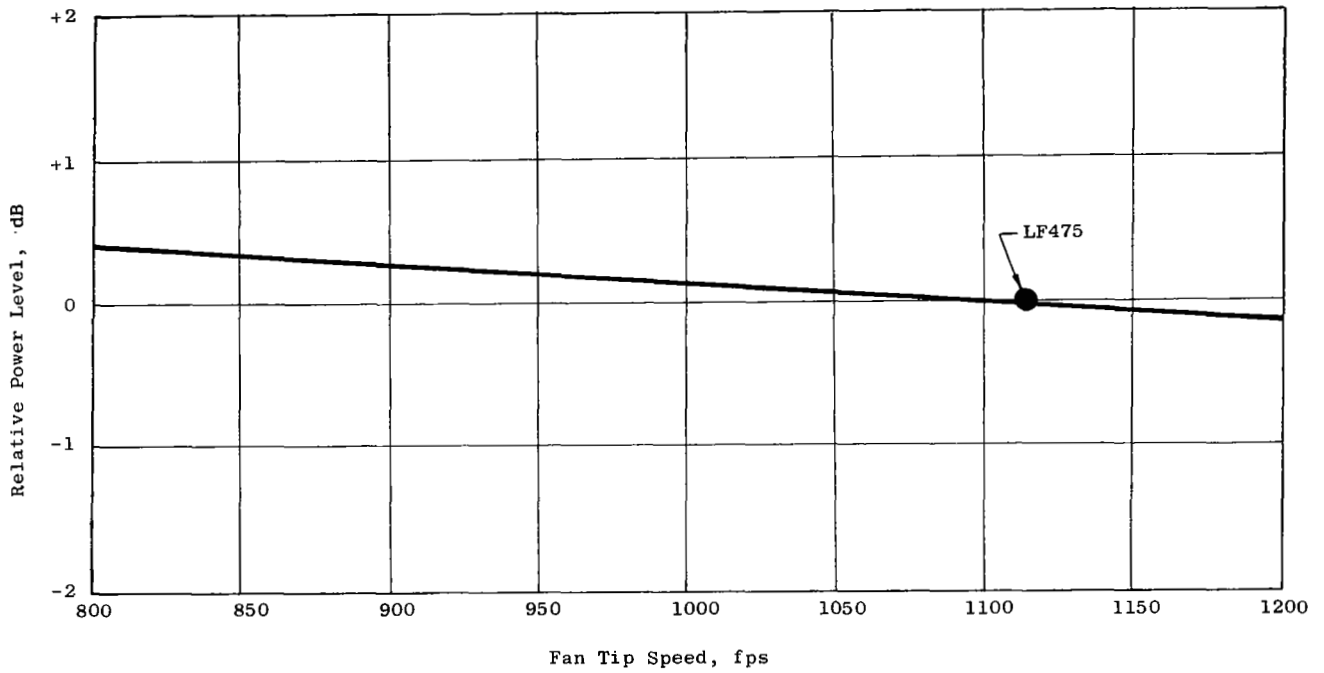


Figure 11. Power Levels at the Fundamental of Blade Passing Frequency vs. Tip Speed at Constant Thrust, for OGV Fans

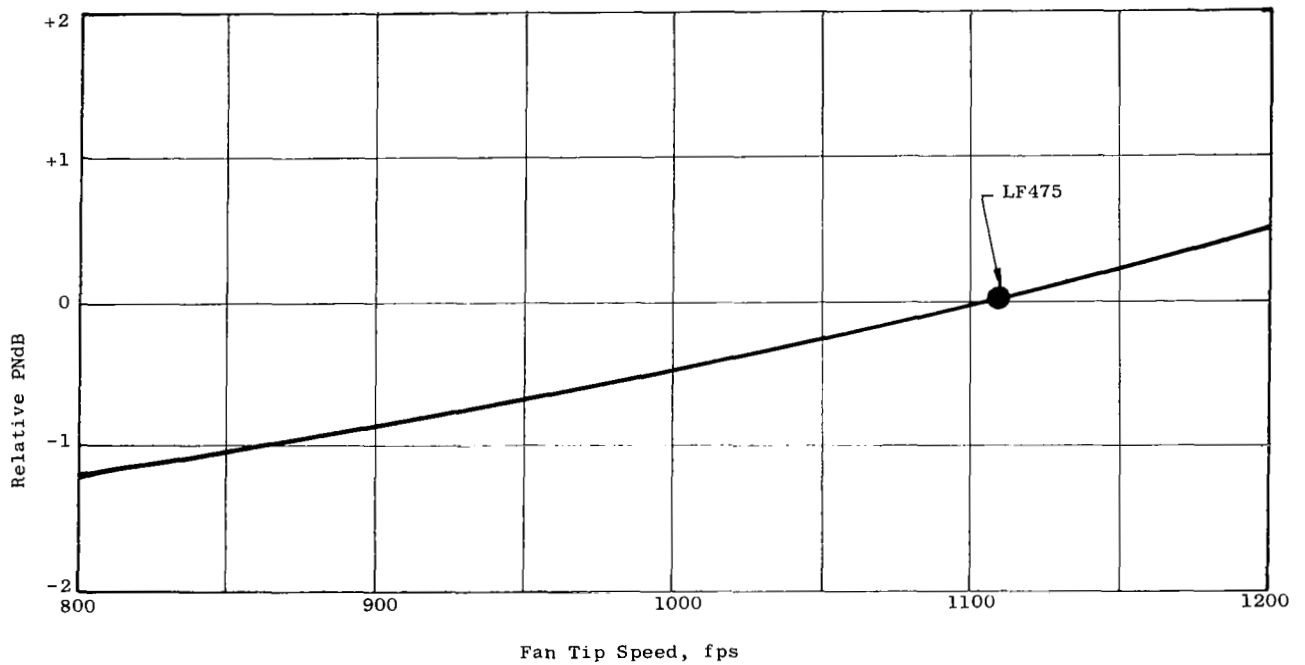


Figure 12. Perceived Noise Levels vs. Tip Speed at Constant Thrust, for OGV Fans

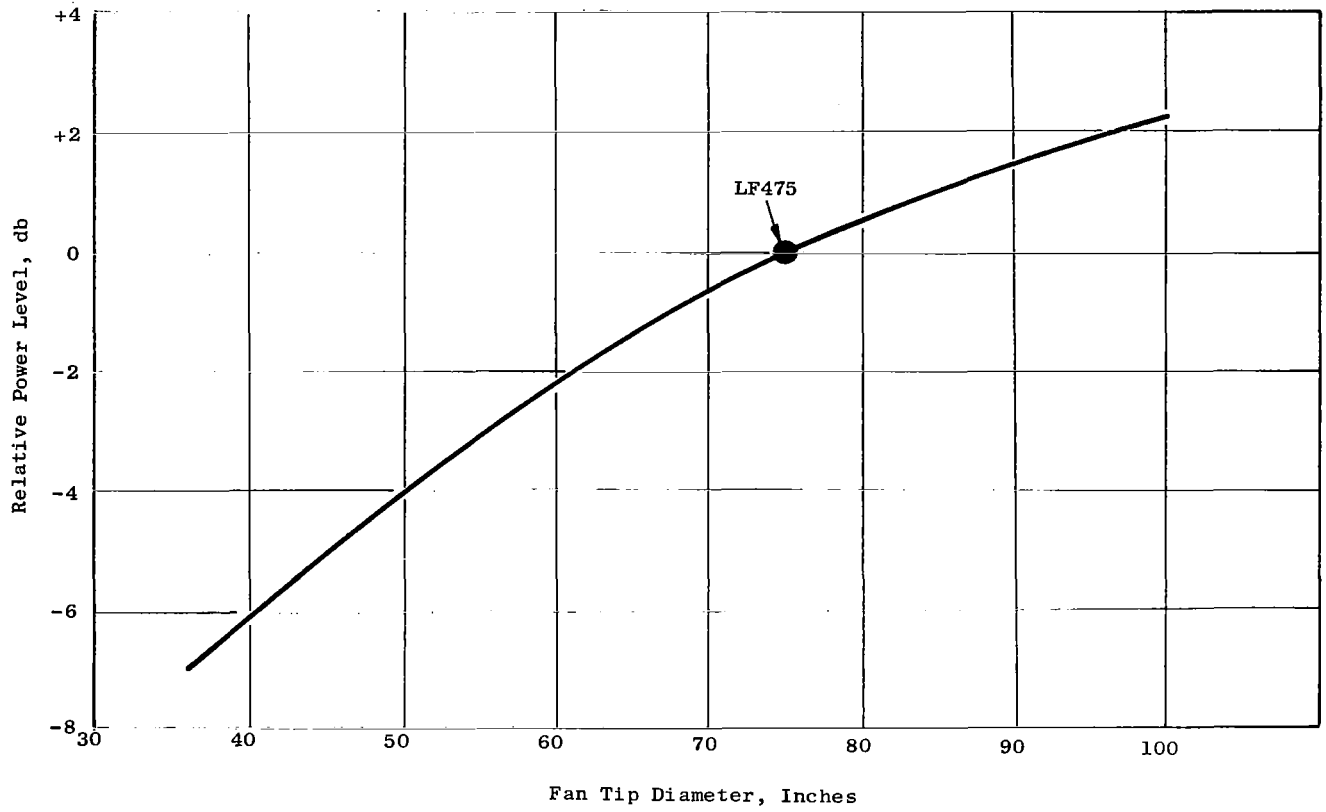


Figure 13. Power Levels at the Fundamental of Blade Passing Frequency vs. Tip Diameter, for OGV Fans

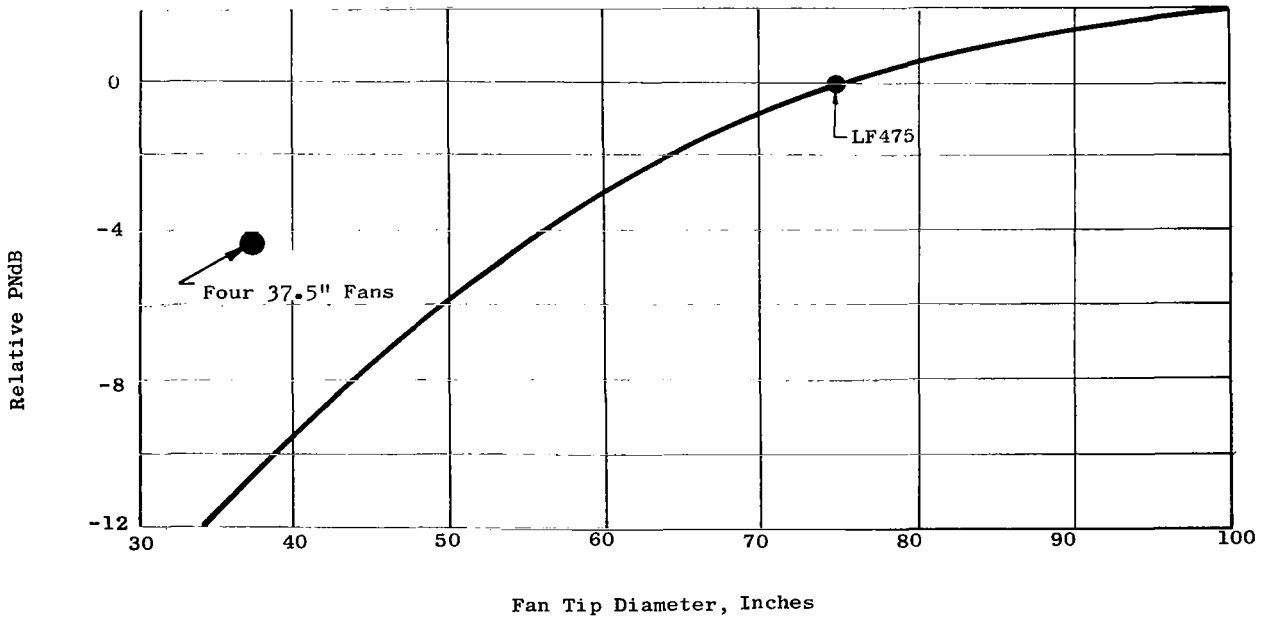


Figure 14. Perceived Noise Levels vs. Fan Tip Diameter, for OGV Fans

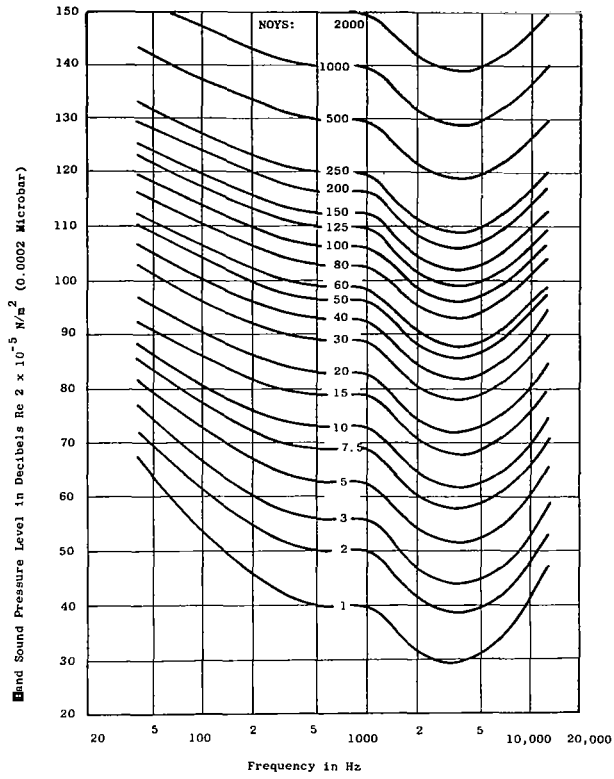


Figure 15 Noys As Function Of Sound Pressure Level

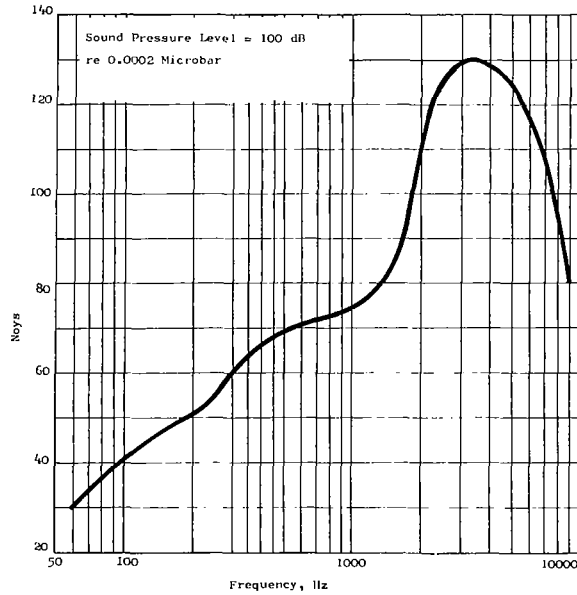


Figure 16. Noise Annoyance Frequency Dependency

appreciably. A similar trend can be observed on the PNdB curve of Figure 18. After having passed a peak at about 48 blades (due to the "NOY" rating curve peak versus frequency) the PNdB decreases appreciably as the number of blades is increased.

Vane/Blade Ratio. - The analysis of the sound generated by the wake interaction indicates the vane/blade ratio is an important parameter. Figure 19 shows that an appreciable reduction in pure tone levels can be obtained by increasing the number of vanes to twice the number of blades. Figure 20 shows the corresponding reduction in PNdB's.

Rotor-Stator Spacing. - It is well known that increasing the spacing between blade rows will decrease the interaction noise. Several experimental investigations (for example, References 5, 6 & 7) have been made to determine quantitatively the reduction in pure tone levels that can be obtained by going to one or two chord spacings. Some of the results have been summarized by Lowson in Reference 5. An examination of Figure 3 of Reference 5 shows, however, how inconsistent those results are. Some researchers show 2 dB reduction per doubling the axial separation, while others prescribe 4 or even 6 dB. This inconsistency is no surprise if one considers the fact that several other parameters besides axial spacing are involved in the interaction process. Geometric quantities like solidity of the upstream blade row, the outlet angle, as well as aerodynamic quantities such as the drag coefficient, are of major importance in the wake interaction decay. These parameters vary from one configuration to another and ignoring them is bound to lead the designer to erroneous conclusions. Figure 21 shows the results for spacings of from .1 to 2 rotor chords. It can be seen that an appreciable reduction in pure tones can be obtained by going to large spacings. Figure 22 shows the corresponding reduction in PNdB's.

Vane Lean. - A leaned vane is a non-radial vane. The lean angle is the angle, at the fan annulus hub, between a radial and a non-radial vane. It has been reported in the literature (for example, References 8 & 9), that non-radial vanes can reduce noise by radially phasing the wake interaction between the rotating & stationary blade rows. Le S Filleul (Reference 9) obtained a large noise reduction (about 1 dB for each 8 degrees of lean) in a controlled experiment. Reference 10 showed, however, that there was no noise reduction due to lean in a high speed fan. The effectiveness of this noise reduction feature needs further experimental investigation.

For very close spacing between the rotor & stator, the direction of vane lean is immaterial. But there is some phasing of the wakes due to spacing. The difference between the fan velocity triangles (see Figure 5 and Tables III and IV) at the hub & tip cause the rotor wakes to become increasingly non-radial as the spacing between the rotor & stator is increased. This phasing is in the direction of fan rotation. Therefore, when spacing is used, the lean angle of the vanes should also be in the direction of rotation so as to further increase the wake phase angles. Otherwise, vane lean could offset some of the advantage gained by spacing.

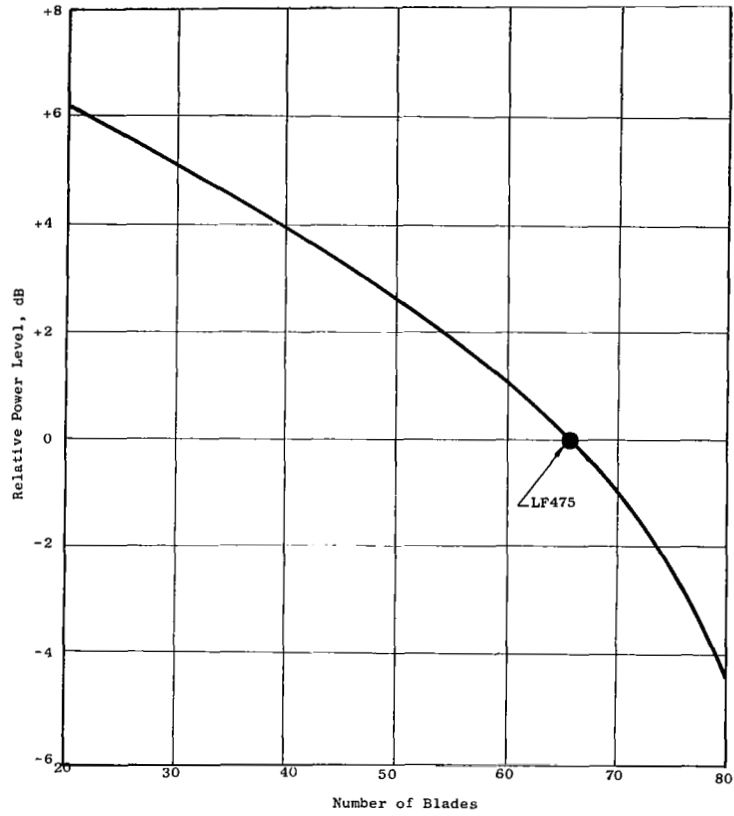


Figure 17 Power Levels at the Fundamental of Blade Passing Frequency Vs. Number of Blades, for OGV Fans

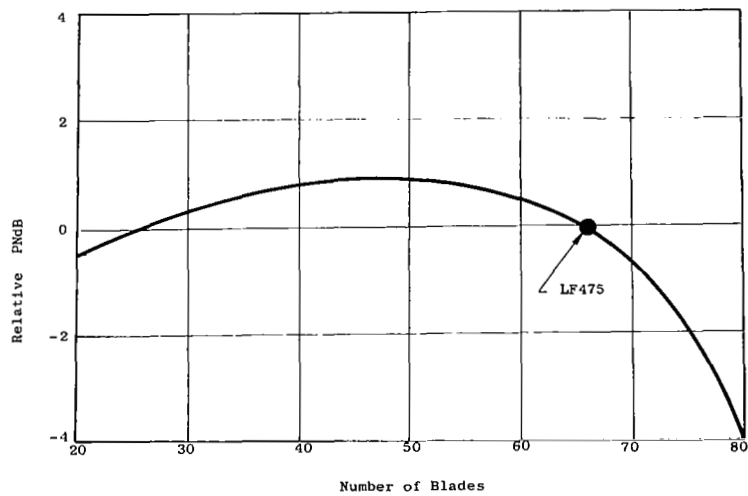


Figure 18 Perceived Noise Levels Versus Number of Blades, for OGV Fans

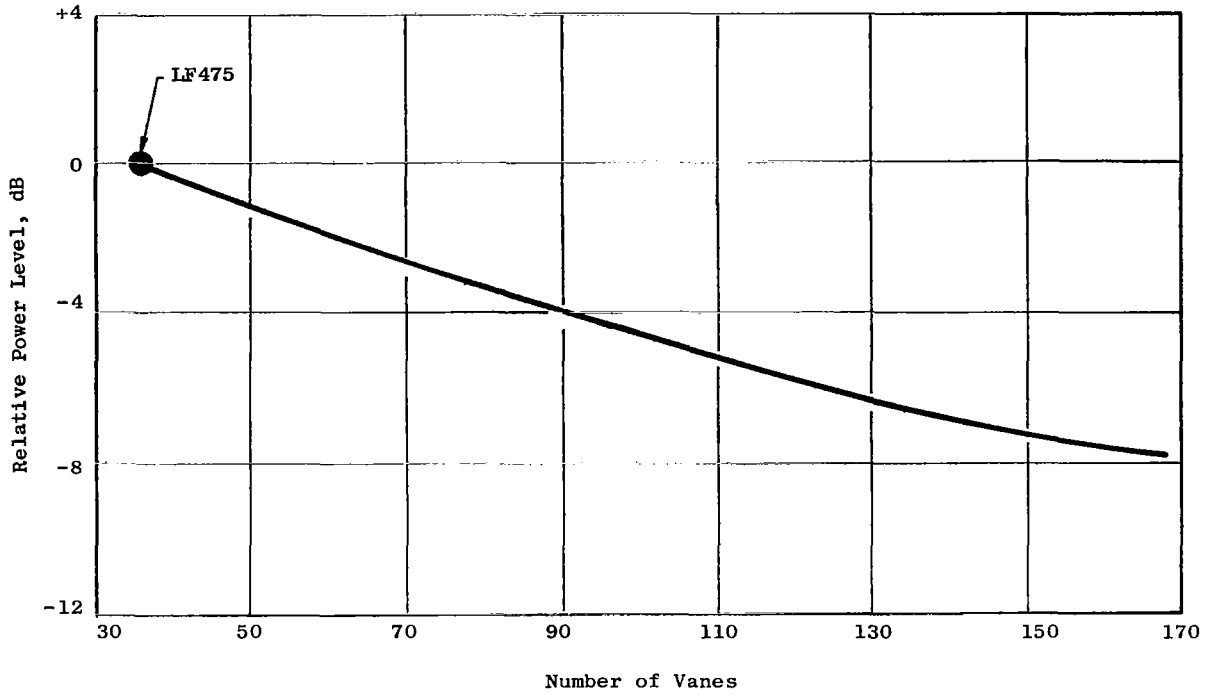


Figure 19. Power Levels at the Fundamental of Blade Passing Frequency vs. Number of Vanes, for OGV Fans

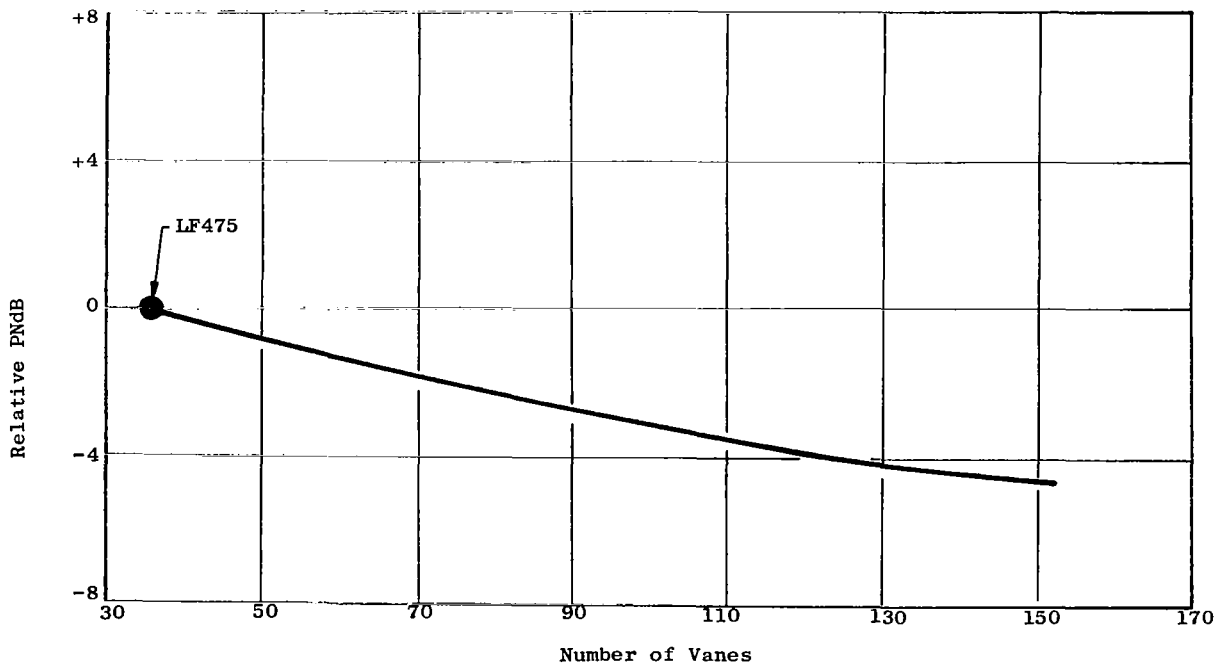


Figure 20. Perceived Noise Levels vs. Number of Vanes for OGV Fans

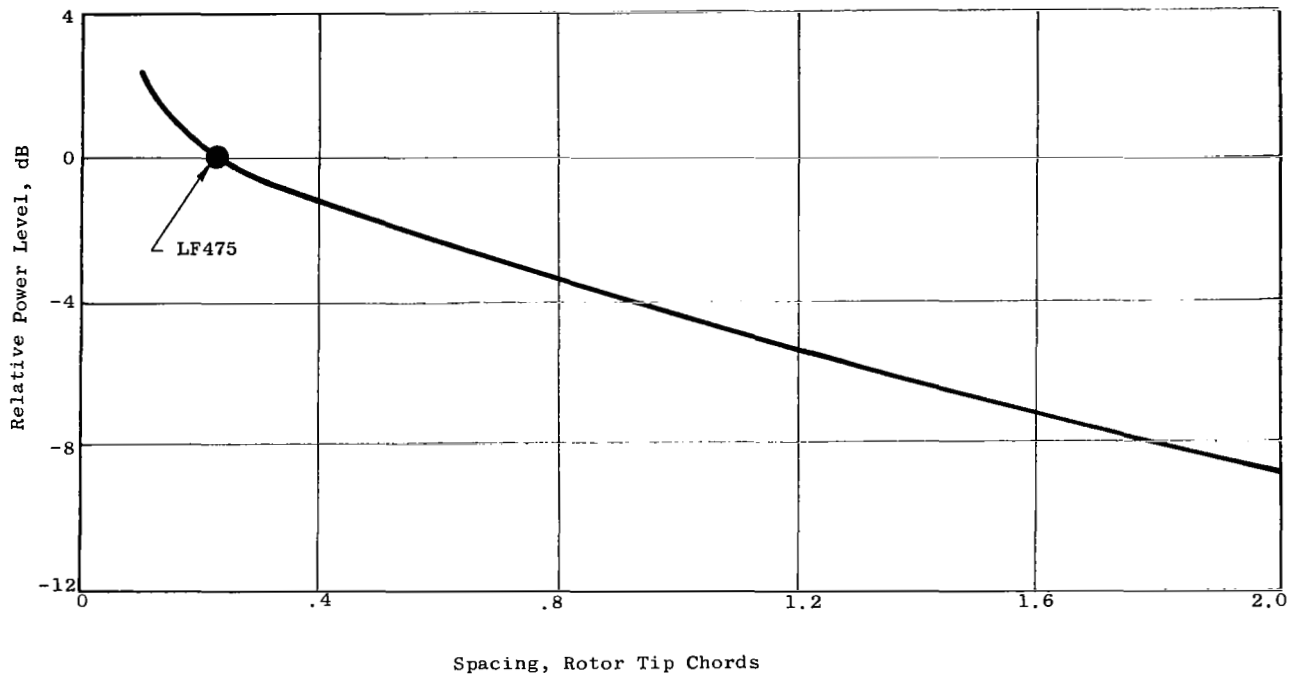


Figure 21. Power Levels at the Fundamental of Blade Passing Frequency vs. Blade Row Spacing, for OGV Fans

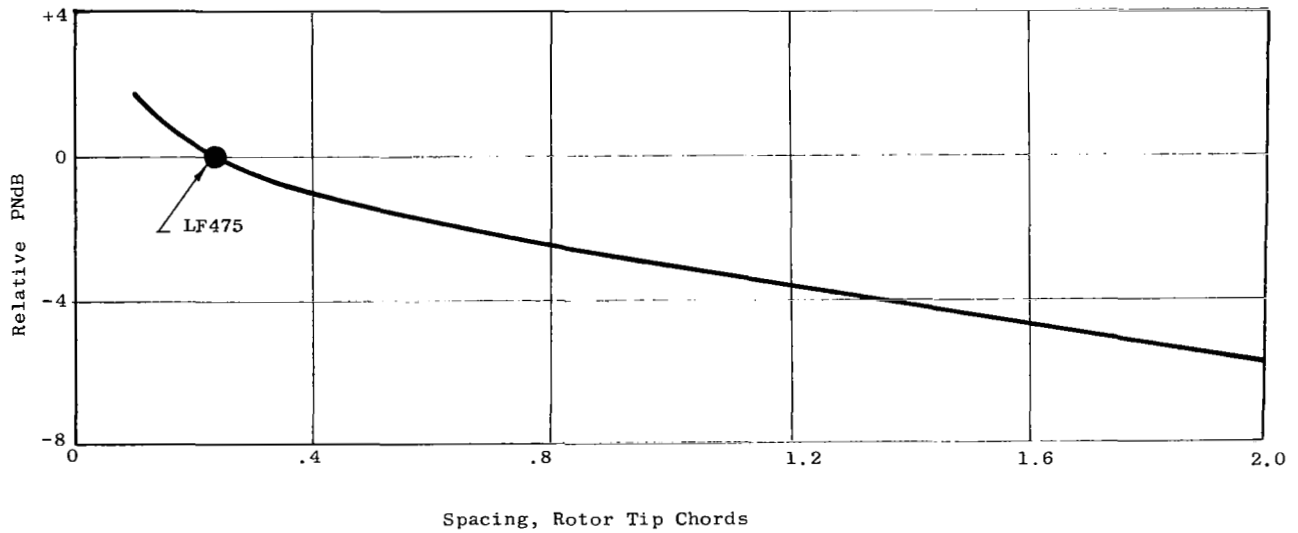


Figure 22. Perceived Noise Levels vs. Blade Row Spacing, for OGV Fans

Acoustic Material. - It is desirable to design acoustic material such that the peak absorption occurs at or near the fundamental of the blade passing frequency. The basic design variable which determines the peak absorption frequency is the material thickness. The required thickness decreases with increasing frequency.

Fiber or foam acoustic materials absorb moisture, have environmental temperature limitations, and have a short service life. The acoustic material selected for lift fan applications is a honeycomb resonator panel formed by a properly-sized honeycomb core sandwiched between inner & outer skins. The honeycomb core geometry and the outer skin thickness & porosity (ratio of hole area to total surface area) are functions of the desired absorption frequency.

For high vane/blade ratios, the fan acoustic energy tends to concentrate in radial modes, with high pressure peaks in the outer annulus. Acoustic treatment of the fan tip walls therefore offers potential for noise reduction. Acoustic treatment of the fan hub wall could also be helpful, but is expected to be less effective than the tip wall treatment. The addition of an acoustic splitter in the fan annulus also offers high potential for noise reduction. This splitter would consist of a circular ring concentrically mounted in the stator row, and acoustically treated on one or both sides. With increased rotor-stator spacing, the treated passage lengths would be sufficient to obtain significant noise reduction. Reference 11 summarizes some recent research on acoustic materials.

Noise Parametric Data For IGV Fans

Similar studies were done for the IGV fans. A matrix of 15 points, shown in Table VII, was used. The basepoint LF387 IGV fan appears in each of the six groupings. The detailed aero-acoustic data for these configurations are given in Tables B17 - B31 in Appendix B.

Fan Pressure Ratio. - The effect of pressure ratio on pure tone levels is given in Figure 23. It is seen that for constant thrust, a change in pressure ratio to 1.15 will decrease the pure tone about 1.5 dB. Figure 24 shows the effect on PNdB. A decrease of 3 PNdB is possible by changing to 1.15 pressure ratio.

Fan Diameter. - The effect of size on the pure tone noise is shown in Figure 25. The effect of size on the PNdB level is shown in Figure 26. Unlike the OGV fans, a decrease in the fan size of the basepoint IGV fan will increase the noise. Figure 26 shows that four 43.25 inch IGV fans at the same pressure ratio and tip speed (same lift) will have a noise increase. This is explained by the NOY curve of Figure 16. The basepoint IGV fan is on the left of the NOY peak which occurs at about 3100 Hertz. The basepoint fan has a fundamental frequency of 1770 Hertz. The smaller fans increase the blade passing frequency and thereby raise the NOY rating.

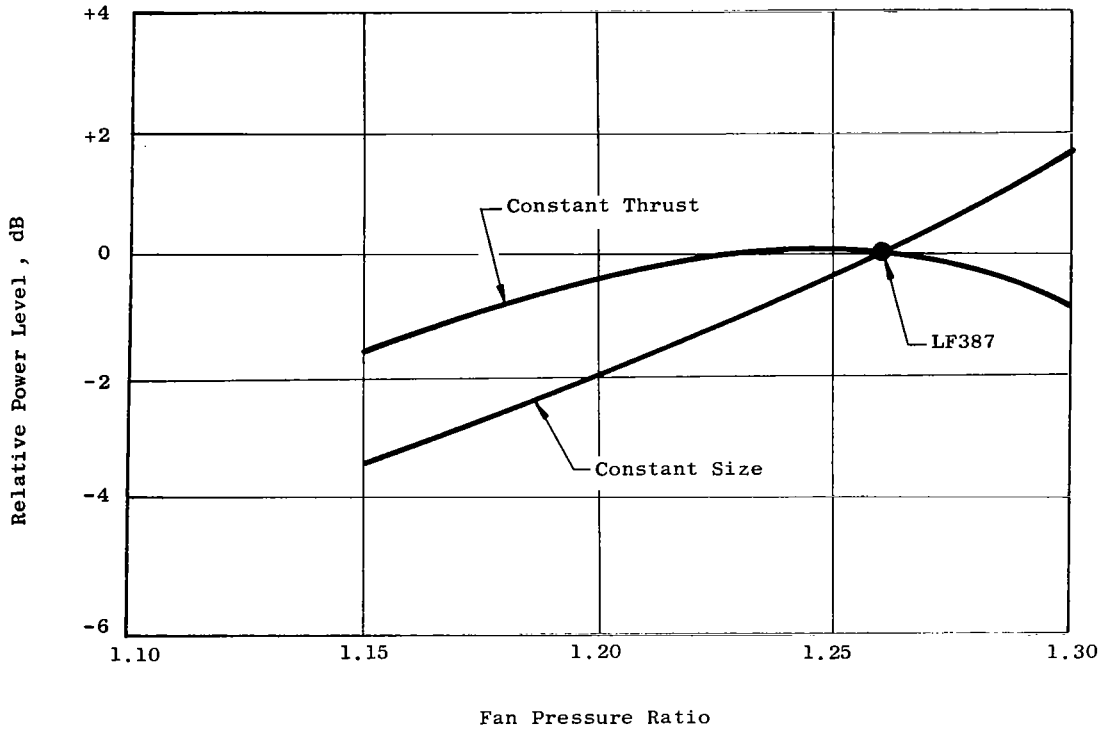


Figure 23. Power Levels at the Fundamental of Blade Passing Frequency vs. Pressure Ratio, for IGV Fans

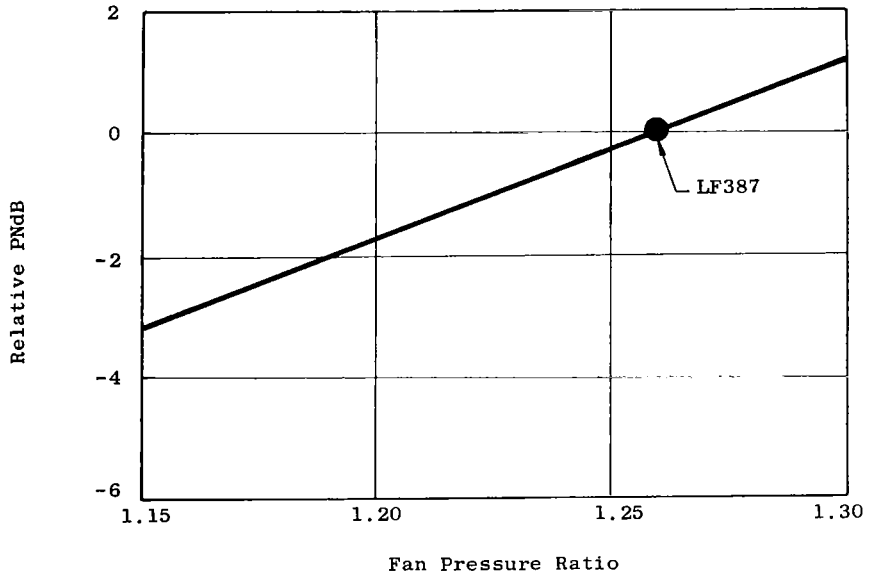


Figure 24. Perceived Noise Levels vs. Fan Pressure Ratio at Constant Speed and Constant Size, for IGV Fans

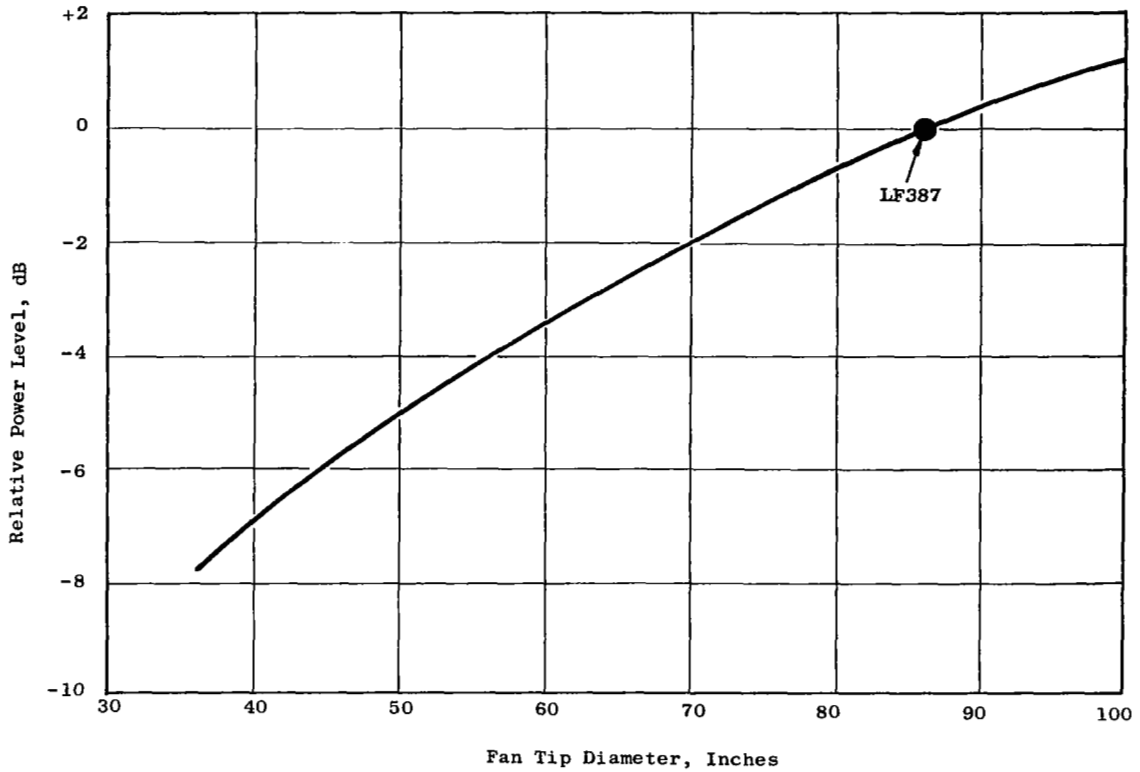


Figure 25. Power Levels at the Fundamental of Blade Passing Frequency vs. Fan Tip Diameter, for IGV Fans

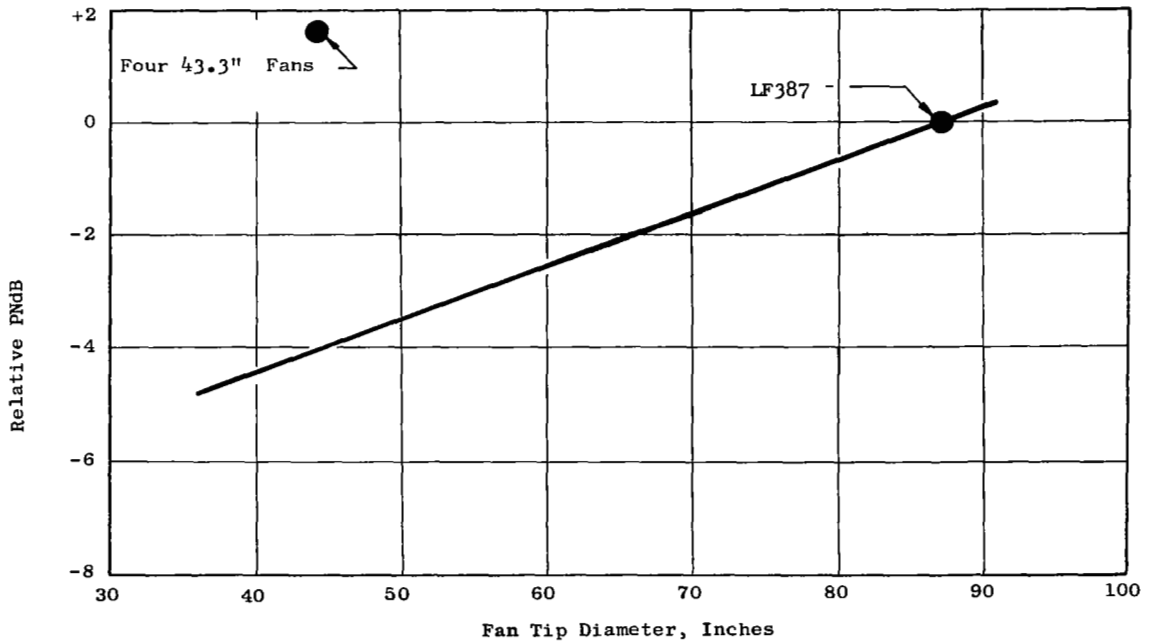


Figure 26. Perceived Noise Levels vs Tip Diameter, for IGV Fans

Fan Tip Speed. - The effect of fan tip speed on pure tone levels is shown in Figure 27. Figure 28 shows the effect on the perceived noise levels. For constant thrust, the tip speed has only a slight effect on fan noise.

Number of Blades. - Figure 29 shows the effect of blade number on the pure tone levels. Figure 30 shows the effect on the PNdB. The noise decrease with increase in blade number for the IGV fan is not as large as was obtained for the OGV fan. Again, the effect of blade passing frequency on the NOY rating is the cause. The increase in blade number lowered the absolute sound power level of the fan, but the increase in the NOY rating partly offset this noise reduction.

Vane/Blade Ratio. - Figure 31 shows the effect of vane/blade ratio on the pure tone levels. Figure 32 shows the effect on the perceived noise levels. The basepoint fan has a vane/blade ratio of 0.70. Figure 32 shows a reduction of over 10 PNdB for a vane/blade ratio of 2.1 (84 vanes).

Rotor-Stator Spacing. - Figure 33 shows the effect of tip spacing on the pure tone levels. Figure 34 shows the effect on the PNdB levels. The tip spacing for the IGV fans is expressed in multiples of the true tip chord of the inlet guide vanes. The decrease in noise levels with increased spacing for the IGV fans is greater than for the OGV fans. The IGV's apply counter-swirl to the flow, which causes a severe interaction between the vane and rotor of the IGV fan. Increased spacing decreases this interaction and therefore lowers the noise more than does an equal spacing on the OGV fan.

Vane Lean. - The effect of phasing the wakes between the IGV & rotor is expected to be similar to that described for the OGV fans.

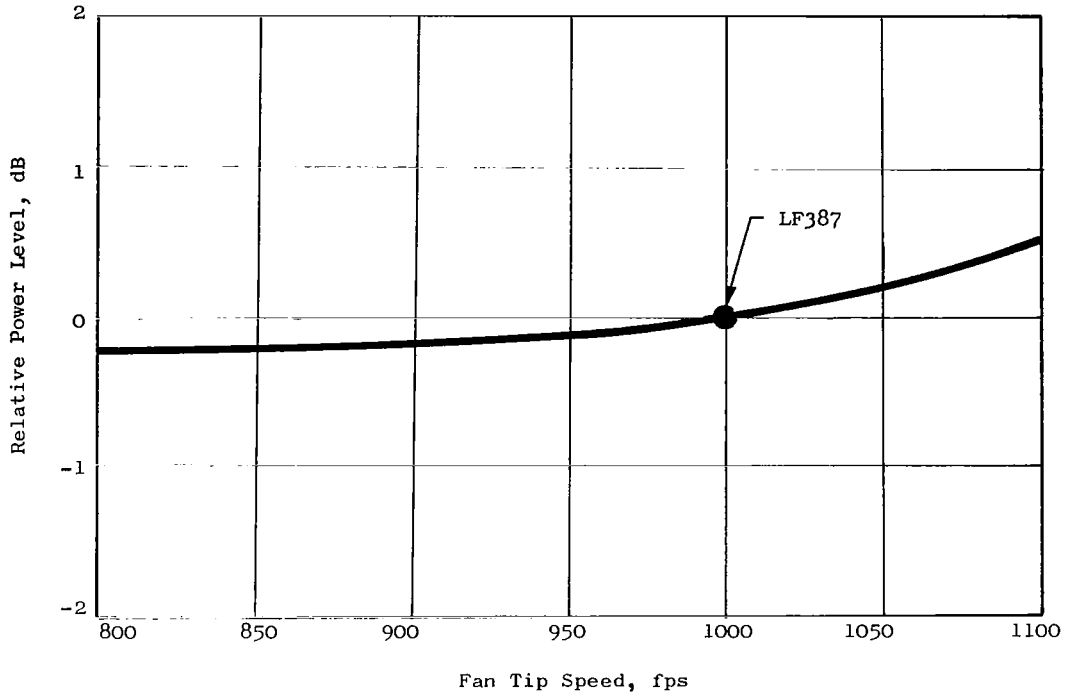


Figure 27. Power Levels at the Fundamental of Blade Passing Frequency vs. Tip Speed at Constant Thrust, for IGV Fans

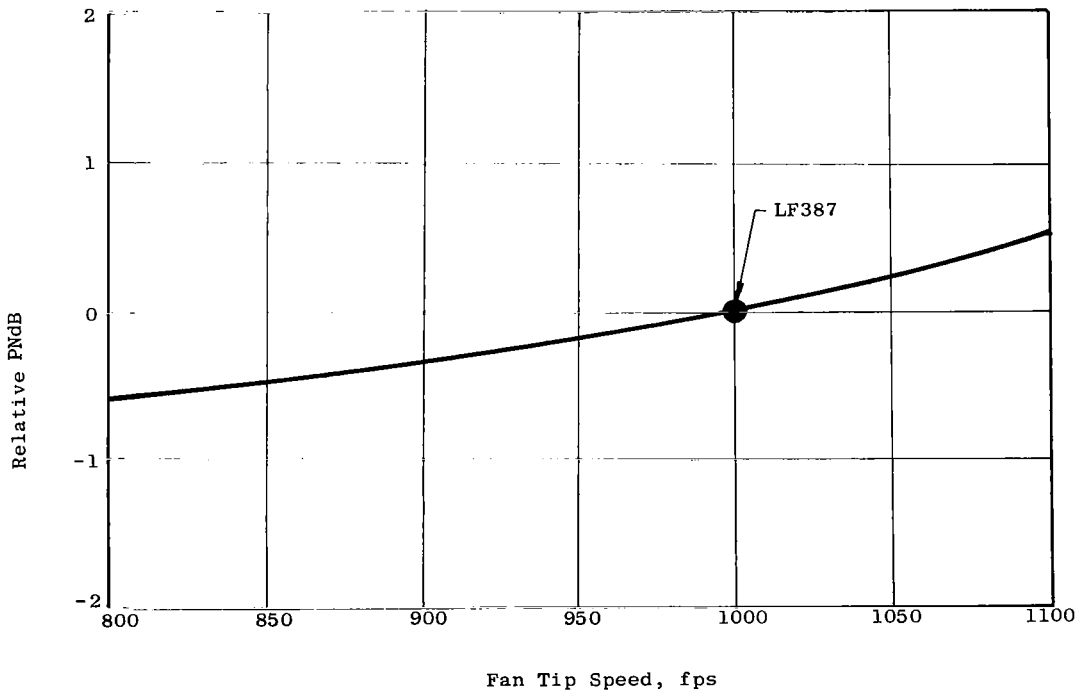


Figure 28. Perceived Noise Levels vs. Tip Speed at Constant Thrust, for IGV Fans

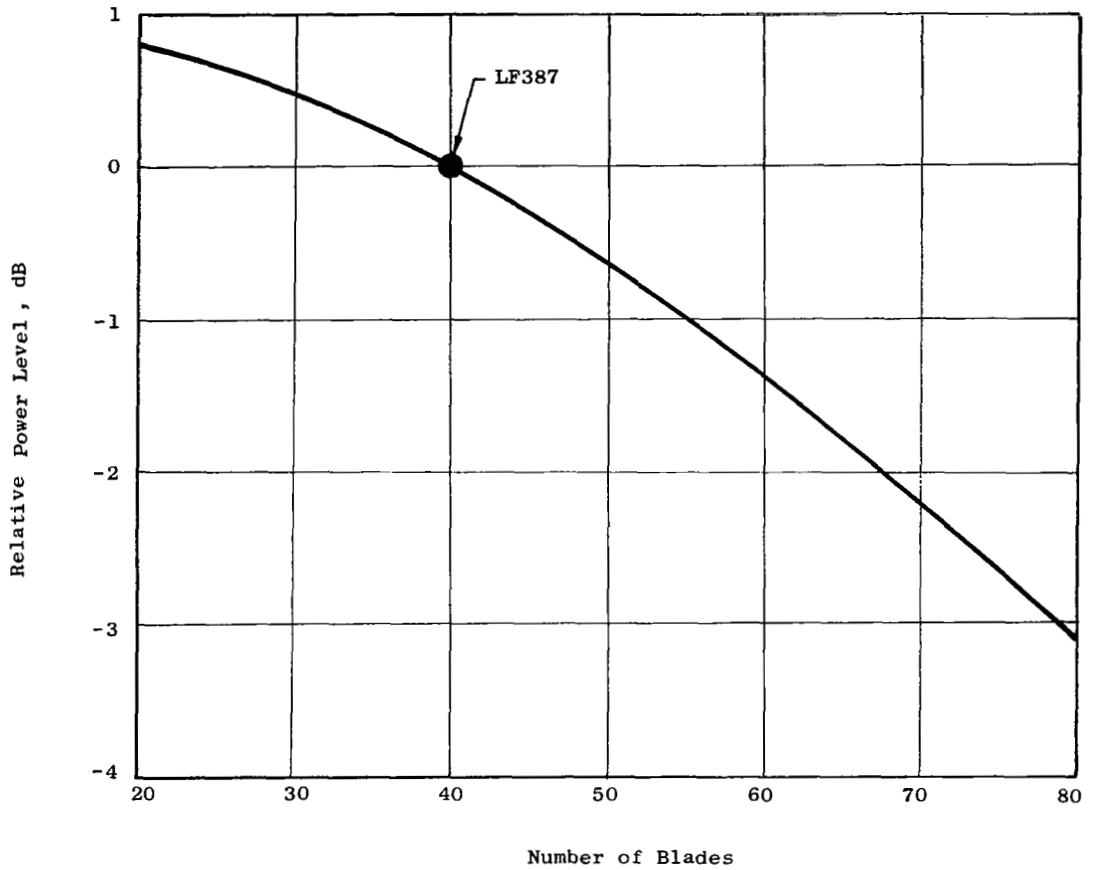


Figure 29. Power Levels at the Fundamental of Blade Passing Frequency vs. Number of Blades, for IGV Fans

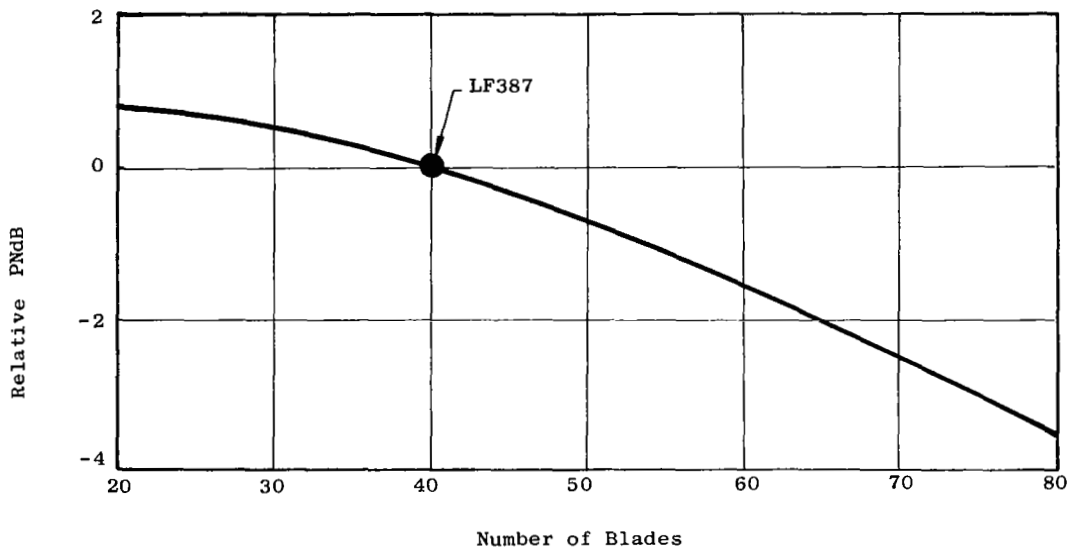


Figure 30. Perceived Noise Levels vs. Number of Blades, for IGV Fans

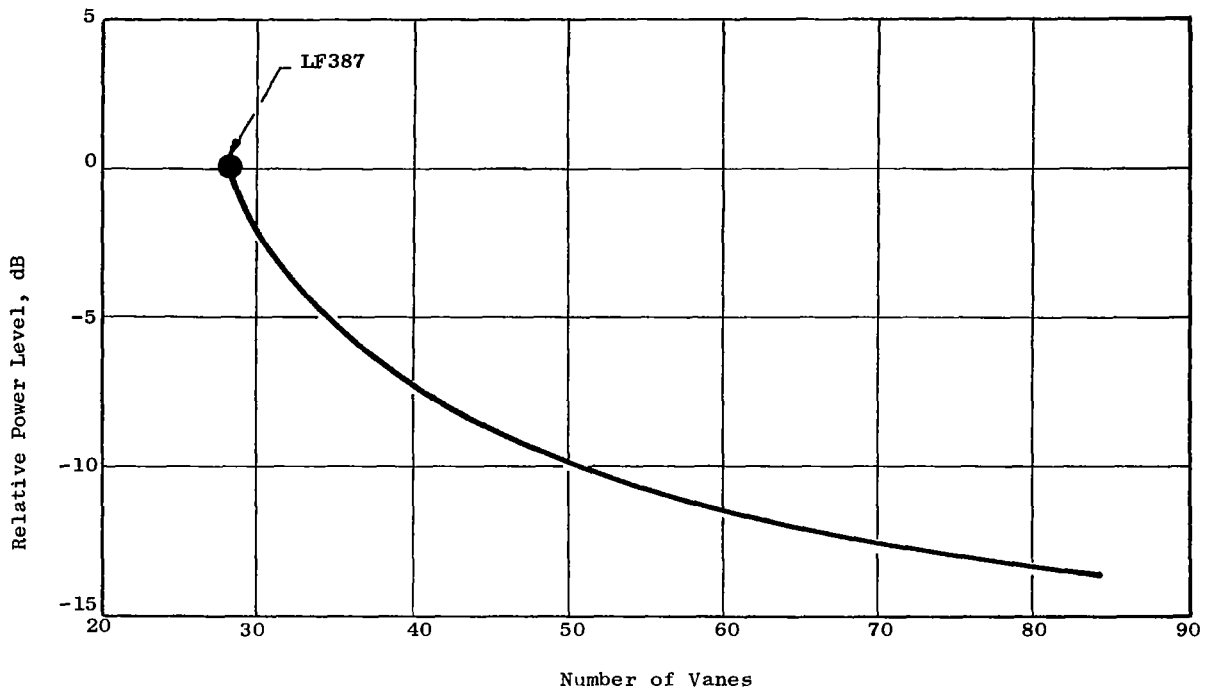


Figure 31. Power Levels at the Fundamental of Blade Passing Frequency vs. Number of Vanes, for IGV Fans

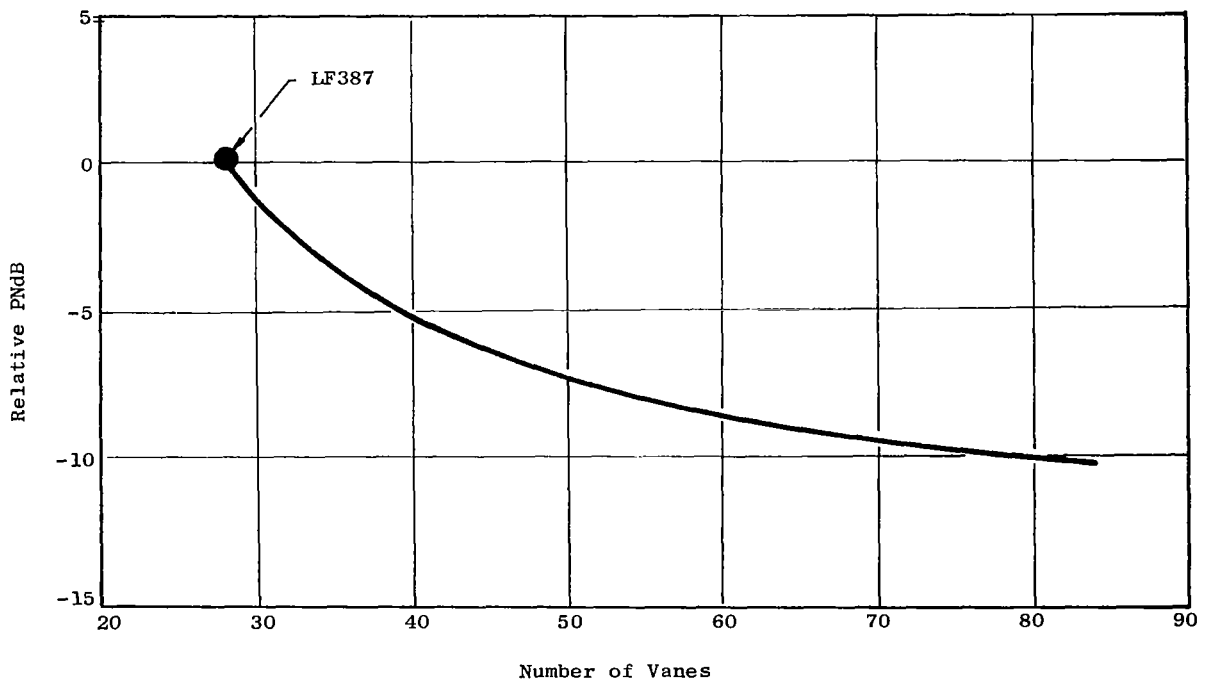


Figure 32. Perceived Noise Levels vs. Number of Vanes, for IGV Fans

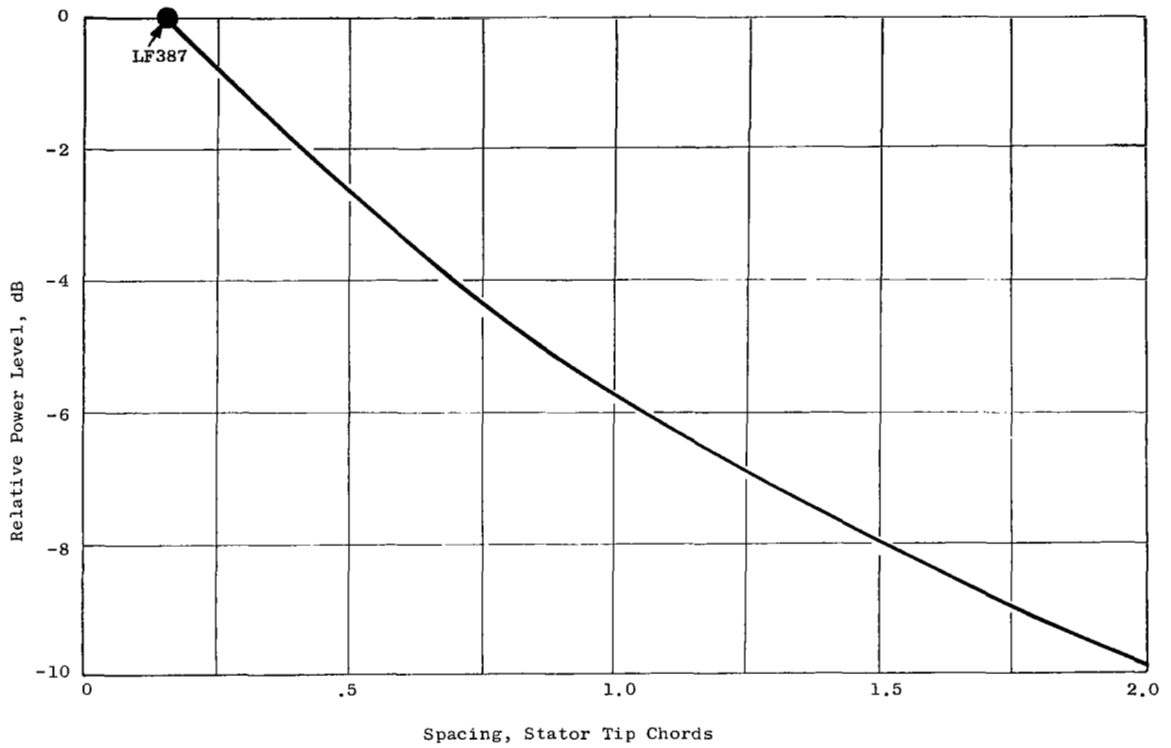


Figure 33 Power Levels at the Fundamental of Blade Passing Frequency vs Blade Row Spacing, for IGV Fans

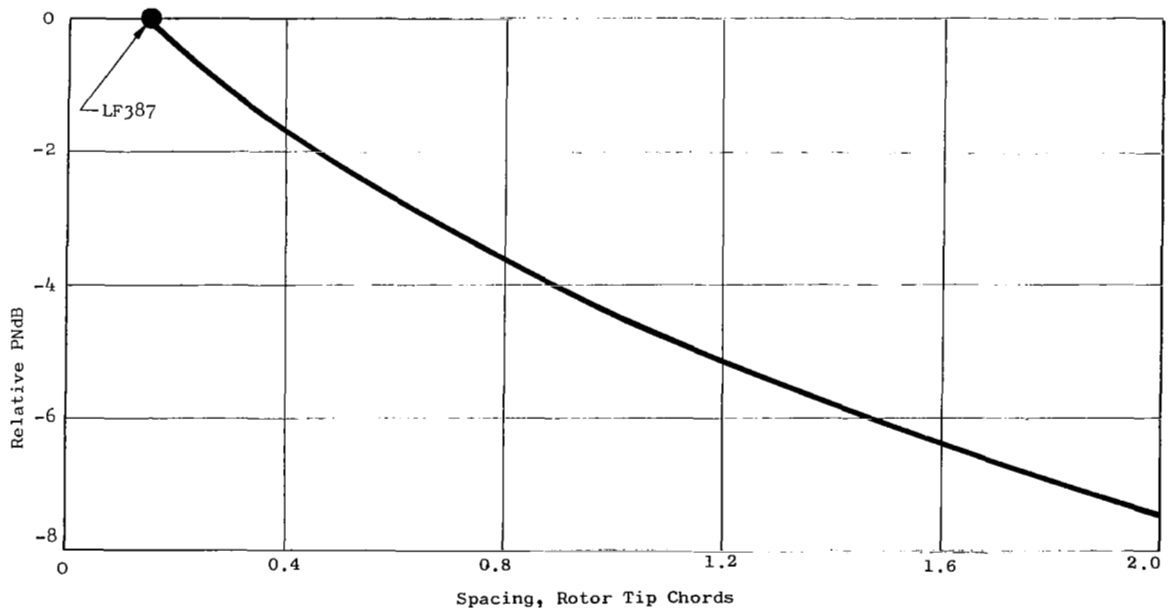


Figure 34. Perceived Noise Levels Vs. Blade Row Spacing For IGV Fans

TRADE-OFF STUDIES

Parametric performance & installation data were determined for the range of studies previously discussed (Table V). Computer programs were used to calculate fan parametric data for lift, size & weight for this range of studies.

Performance & Installation Parametric Data for OGV Fans

Fan Pressure Ratio & Tip Speed. - Figure 35 shows the fan radius ratio relationship to tip speed and pressure ratio. This curve is based on a minimum practical value of wheel speed at the hub for any given pressure ratio. This minimum hub speed is independent of radius ratio and is that wheel speed which produces the required pressure ratio when the relative air flow angle at the rotor exit is axial at the hub. The assumption that the rotor hub turning angle be limited to turning to axial is considered good compressor design practice by most designers, and is based on the fact that the stage characteristic becomes flat at this point. Thus, at the hub, no change in total pressure ratio would be expected with small changes in exit static pressure. It has been assumed that the hub pressure ratio is less than the average pressure ratio. A radial variation of local pressure ratio has been used.

Figures 36, 37 and 38 show lift, diameter and planform area as functions of fan tip speed and pressure ratio, for the OGV lift fans. All data are normalized to the design point values of the LF475 basepoint fan. For these data, scroll inlet horsepower was held constant, while fan efficiency and fan pressure ratio were varied. The fan lift is shown in Figure 36 and is the total fan lift, including the tip turbine residual thrust, and including corrections for inlet and exit losses. The maximum lift is obtained with a tip speed between 1050 and 1150 fps, and at low pressure ratios (high bypass ratios). The fan tip diameter is shown in Figure 37. The fan area is shown in Figure 38, and is defined as the total planform area including the area occupied by the tip turbine scroll bubble. The trends of area and diameter are similar.

The fan weight is shown in Figure 39 and represents the total uninstalled fan weight, including the fan exit louvers and fan inlet, but excluding any mount attachments and inlet closure doors since these items are functions of a particular installation. For constant input horsepower, the low pressure ratio fans are larger and heavier. Figure 40 shows the effect of tip speed on rotor weight. Figure 41 shows the weight of the rotating and static components of the fan, relative to total fan weight, verses tip speed at the design pressure ratio of the LF475. The total fan weight line of Figure 41 corresponds to the dashed line of Figure 39.

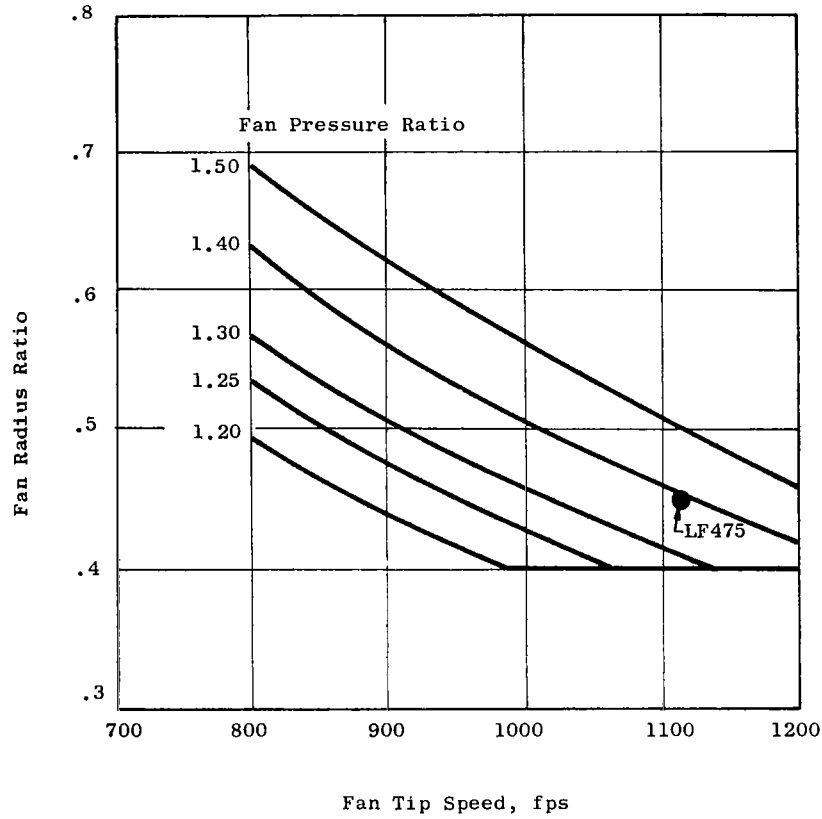


Figure 35. Radius Ratio Versus Tip Speed and Pressure Ratio for OGV Lift Fans

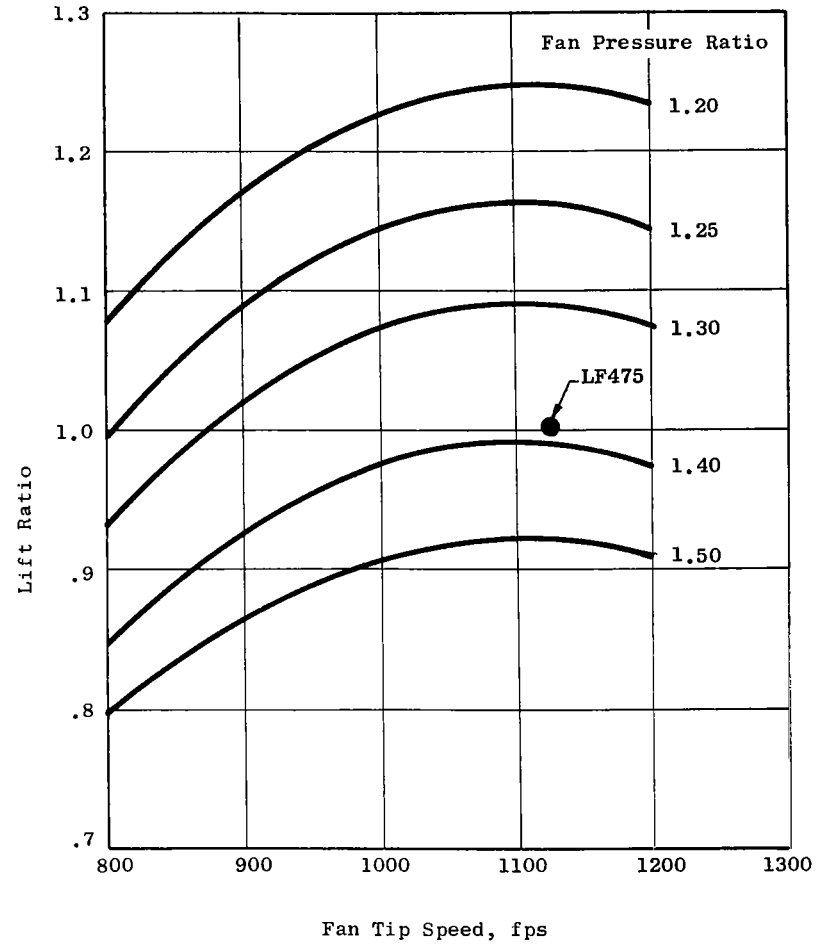


Figure 36. Lift vs. Tip Speed and Pressure Ratio, for OGV Fans

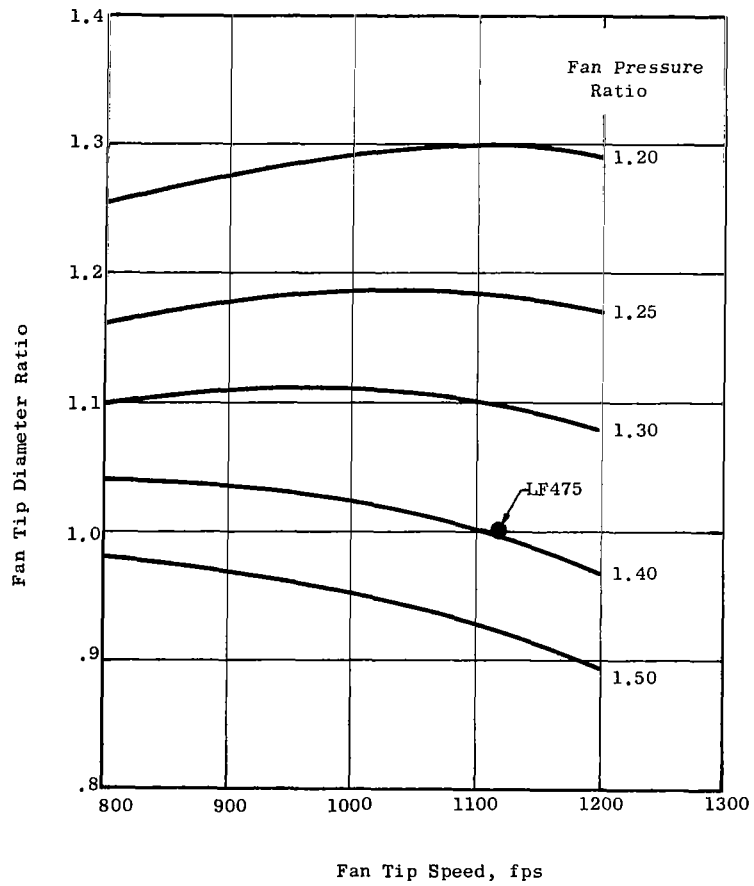


Figure 37. Fan Tip Diameter vs Tip Speed and Pressure Ratio, for OGV Fans

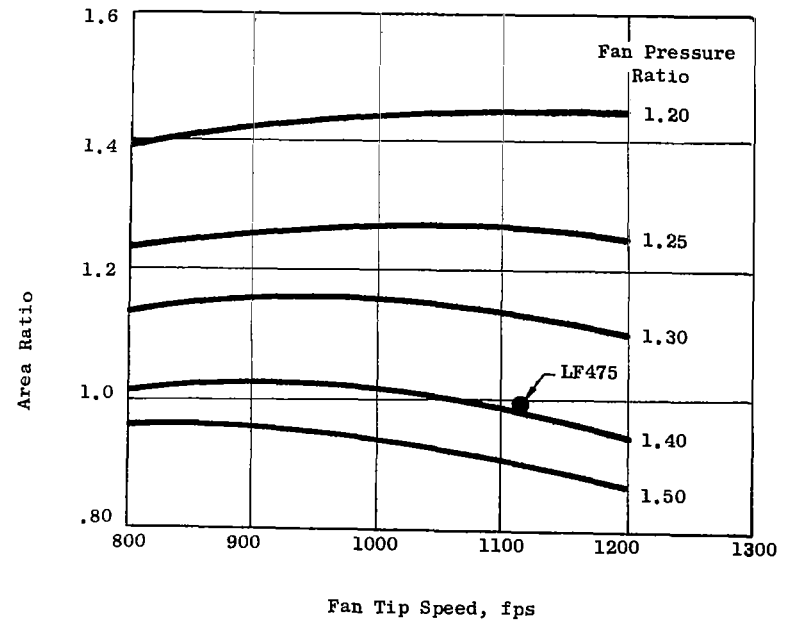


Figure 38. Area vs. Tip Speed and Pressure Ratio, for OGV Fans

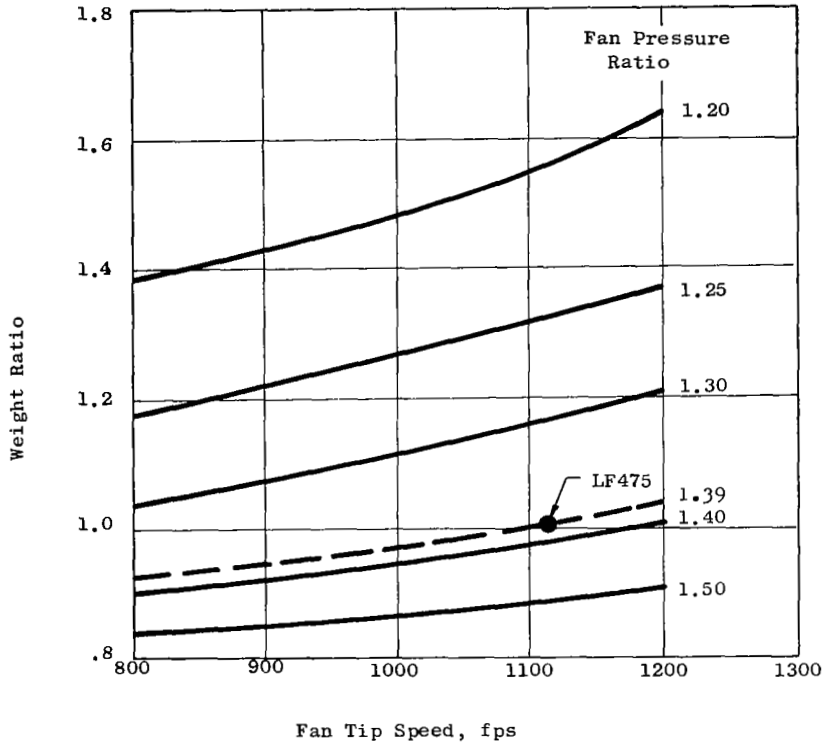


Figure 39. Weight vs. Tip Speed and Pressure Ratio, for OGV Fans

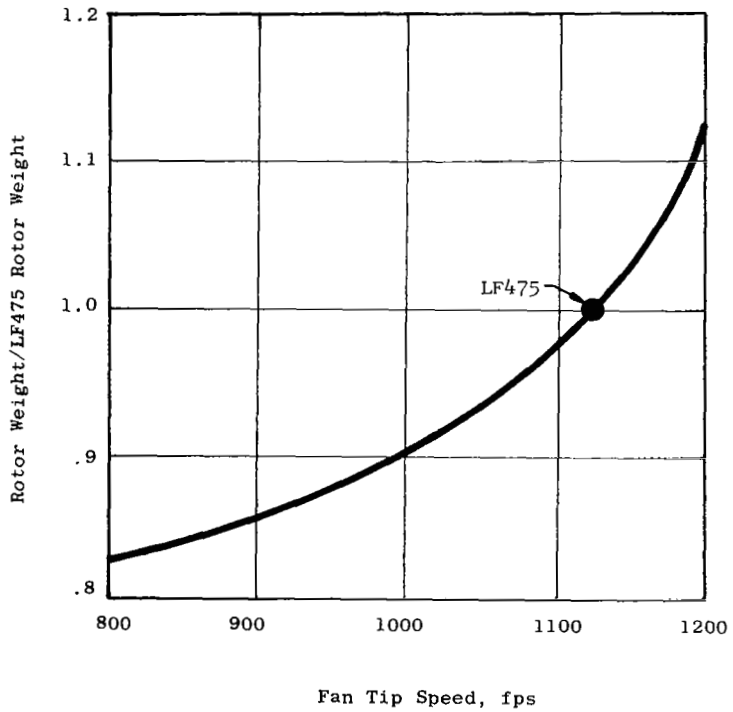


Figure 40. Rotor Weight vs Tip Speed, for OGV Fans

Figures 42 and 43 illustrate the trends of lift/weight ratio and lift/planform area ratio as functions of fan tip speed and pressure ratio at constant input horsepower. The highest values of lift/weight are obtained with tip speeds between 1000 fps at 1.2 pressure ratio, and 1050 fps at 1.5 pressure ratio. The highest values of lift/area are obtained with tip speeds of 1100 fps at 1.2 pressure ratio and above 1200 fps at 1.5 pressure ratio.

Fan Diameter. - These previous data were for constant input power. The fan diameter & lift may be changed by varying the input power, as shown in Figure 44. Figure 44 illustrates the effect of changes in input power on fan lift and size when tip speed and pressure ratio are fixed at the LF475 values. Figure 45 shows the resulting lift/weight and lift/area ratios as functions of size. Size has a strong effect on lift/weight ratio. To illustrate, two 53" fans would provide the same total lift as one LF475 at the same tip speed and pressure ratio, but at an uninstalled lift/weight ratio about 18% higher.

Fan Inlet Axial Mach Number. - Figure 46 shows the envelope of the average fan inlet axial Mach number for OGV fans. The envelope is bounded by three limit lines labeled axial diffusion limit, tip slope limit, and choke limit. The axial diffusion limit defines the limiting amount of reduction in the average axial velocity across the fan from inlet to exit. Since the average exit velocity is closely fixed by the fan pressure ratio, the diffusion limit puts an upper limit on the inlet Mach number as a function of fan pressure ratio. In a similar way a lower limit may be established by placing a limit on the velocity increase through the fan. Reasons for placing limits on the axial velocity increase or decrease through the fan are as follows:

1. Too large a decrease in axial velocity results in high static pressure rises through the fan blading and requires increases in blade solidities and chords.
2. Too large an increase in axial velocity results in highly converging flow paths with steep slopes and high curvatures at the exit if the flow is to exit axially.

A third limit may also be placed on the inlet axial Mach number by choke considerations at the throat of the upstream blade row. The flow area is reduced by turning in the blade passage. The choke limit shown in Figure 46 is not the Mach number at which flow actually becomes sonic at the blade throat, but is instead, a practical upper limit.

Figure 47 illustrates the effect of changes in fan inlet axial Mach number on lift, weight and area for OGV fans. It is clear that for considerations of high lift/weight and lift/area ratios, the fan inlet Mach number should be chosen as high as the limits of Figure 47 allow.

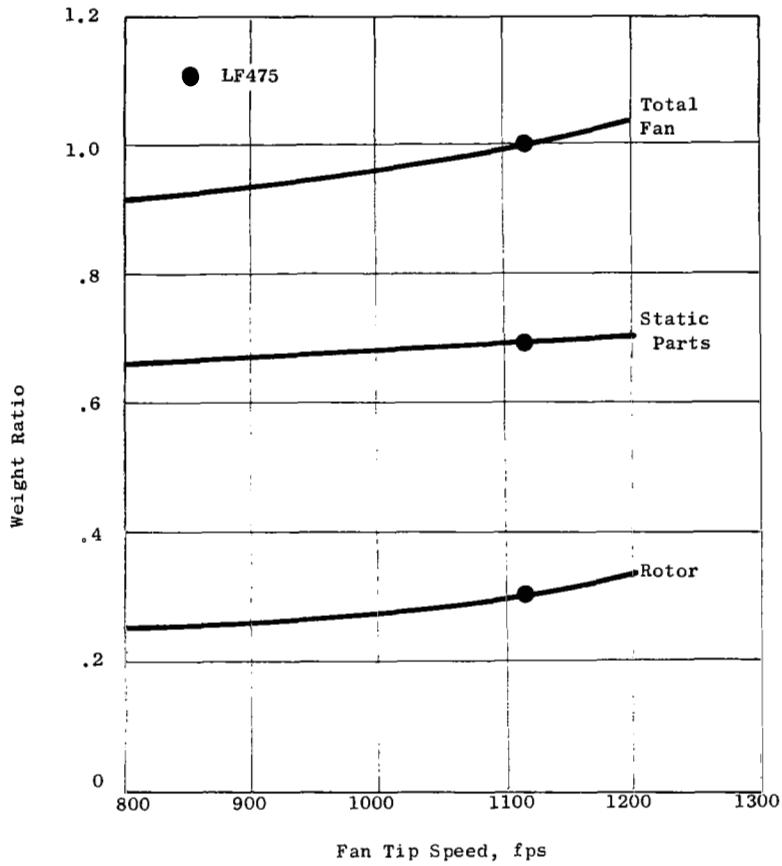


Figure 41. Effect of Tip Speed on Weight, for OGV Fans

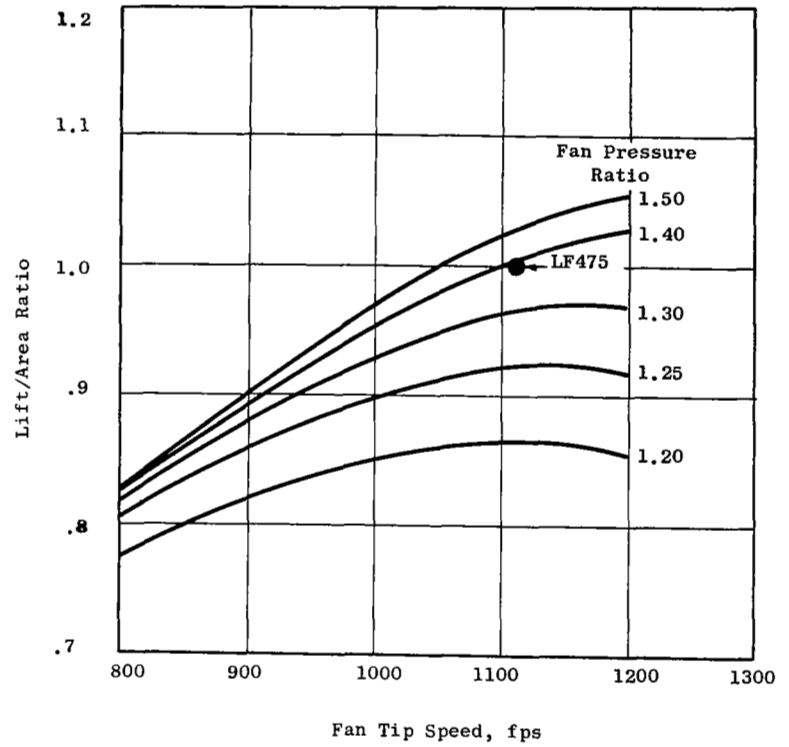


Figure 42. Lift/Area Ratio vs Tip Speed and Pressure Ratio, for OGV Fans

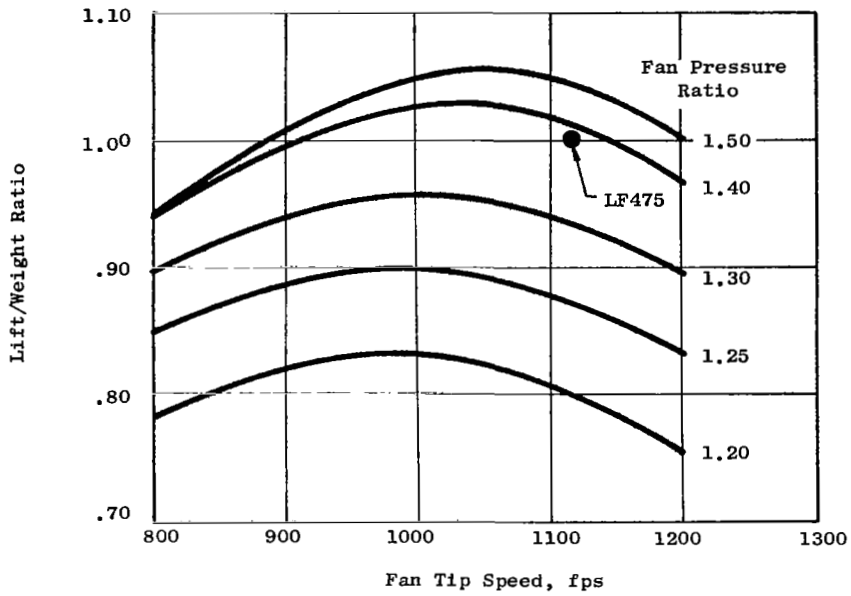


Figure 43. Lift/Weight Ratio vs. Tip Speed and Pressure Ratio, for OGV Fans

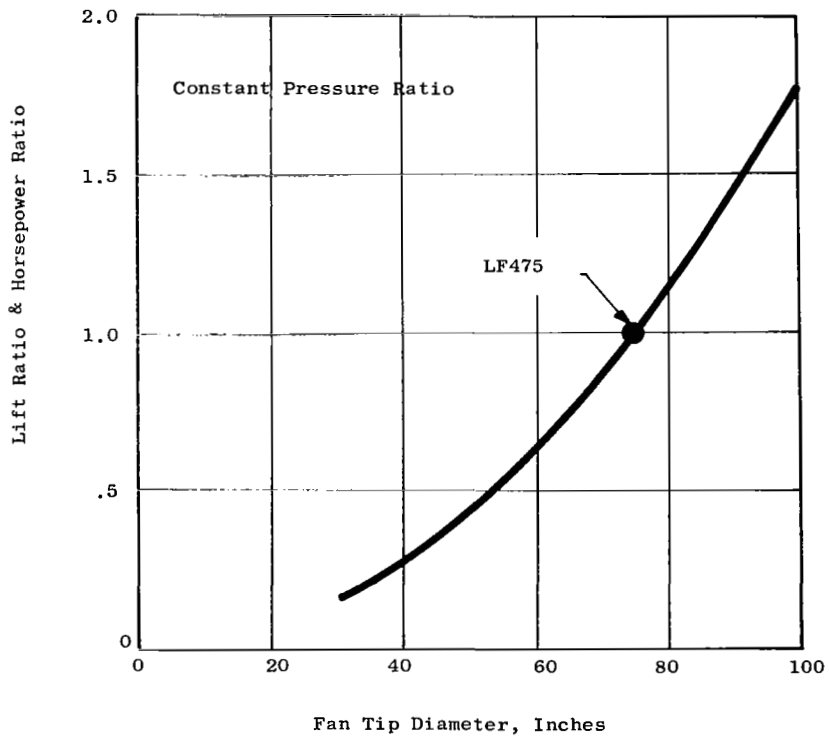


Figure 44. Effect of Input Horsepower on Fan Diameter and Lift for OGV Fans

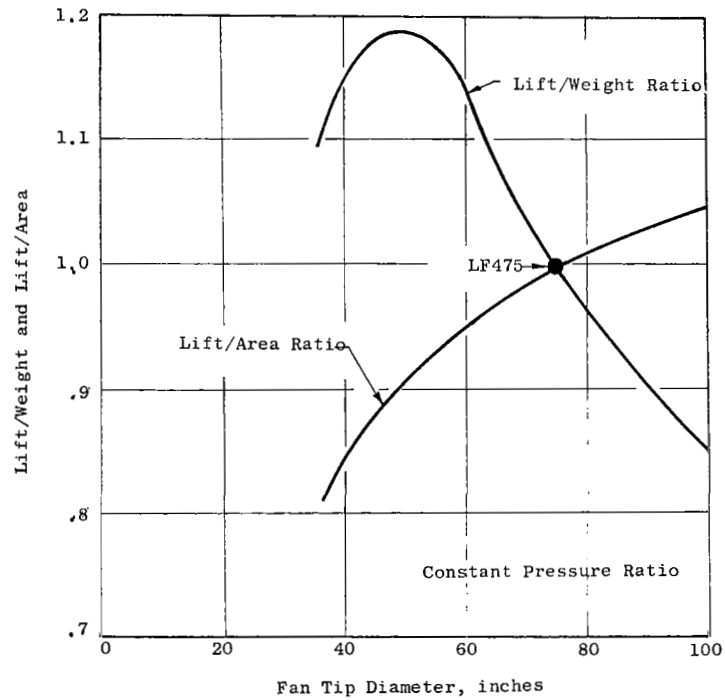


Figure 45 Effect of Diameter on Lift/Weight & Lift/Area Ratios, for OGV Fans

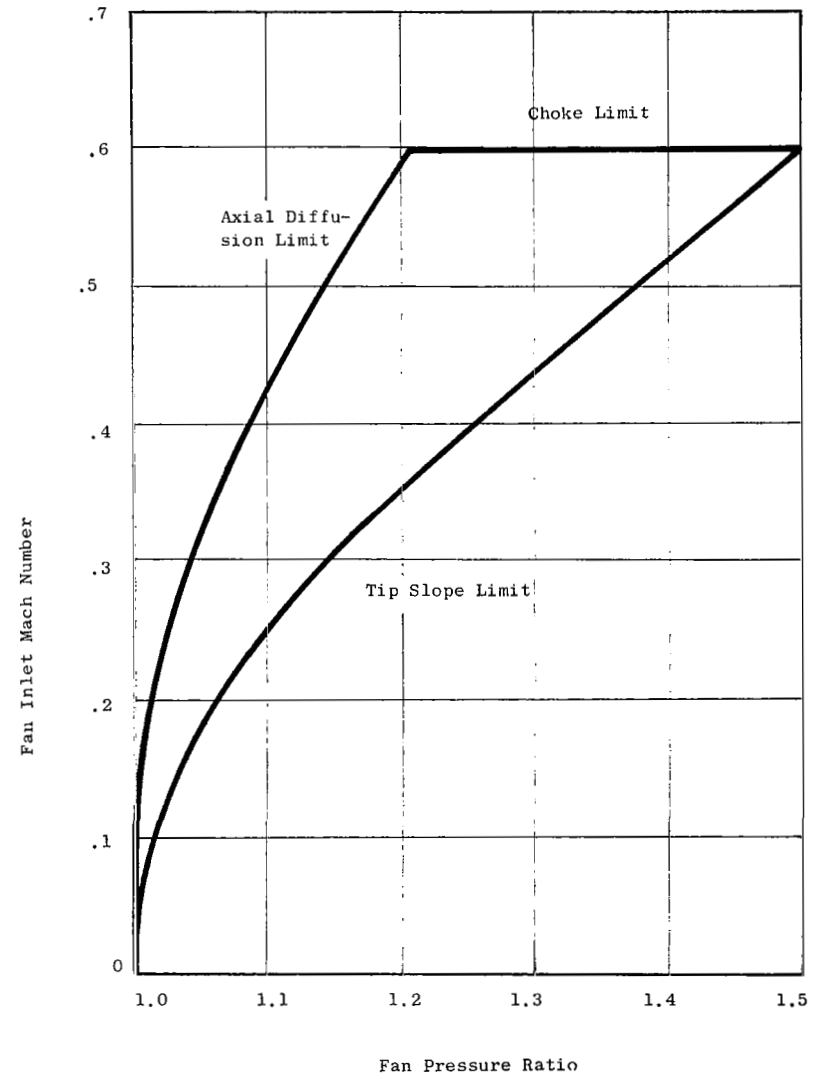


Figure 46 Inlet Mach Number Limits For OGV Lift Fans

Blade Number Increases, At Constant Blade Chord. - When chord is kept constant the solidity will be directly proportional to blade number. The diffusion losses are reduced by increased blade number & solidity, but friction or compressibility losses are increased. The usual outcome is a less efficient rotor. Increased solidity at constant chord reduces fan annulus area thus reducing flow capacity unless blading leading edge angles are reduced (opened) so that throat area is maintained. Manufacturing and structural limitations on edge radius and maximum airfoil thickness do not usually permit throat area increases by thinning the blade sections. Further, excessively opened blades have increased loss and poor stall margin. Solidity can therefore only be increased within narrow limits. Blade number increases accompanied by chord decreases are therefore more desirable.

Blade Number Increases With Chord Reduction. - Chord reduction can affect the fan flowpath, fan aerodynamic parameters, and the fan mechanical design. Hub wheel speed, wall curvatures, and aspect ratio are among the affected parameters. With chord reduction it is desirable to maintain the stall capability of the stage. For a fixed blade height, this means that the product of chord and solidity must remain constant, so that the number of blades increases as the square of the ratio of old to new chord. Reduced chord, higher aspect ratio blade and vane rows may require part-span shrouds, which have efficiency penalties.

Higher solidity in a higher blade number design may require some reduction in inlet average axial Mach number. The LF475 rotor inlet annulus was sized for an average axial Mach number of approximately 0.58. Streamline slope and inlet blockage made the average meridional Mach number even higher. Incidences in the LF745 design were largely set by choke margin rather than by low speed minimum loss criteria because of Mach number levels.

A flowpath with reduced fan inlet Mach number should also have somewhat reduced stator inlet Mach numbers also. A slight increase in fan inlet radius ratio may also be required with an increased blade number design to keep up hub wheel speed, avoid high stator hub inlet Mach numbers, and to maintain LF475 and LF387 loading levels.

Another major factor that would have to be considered in a many-bladed design is the effect of the high stress levels on fan life. At high stress levels the low cycle fatigue effects of start-stop cycles can consume fatigue life as rapidly as ordinary vibration considerations.

The net cross-sectional area of the blades and the blade centrifugal stress are functions of the number of blades. As the number of blades is increased, an upper limit is reached. This limit in blade number can be exceeded by use of newer and stronger materials or by new technologies for the turbine-fan attachment. Fan size also affects this blade number limit because the net blade cross-section decreases faster with size than does the tip load. Figure 48 shows the maximum number of fan blades as a function of fan size and tip speed, for 6-6-2 Titanium alloy. This curve is valid for both OGV and IGV fans.

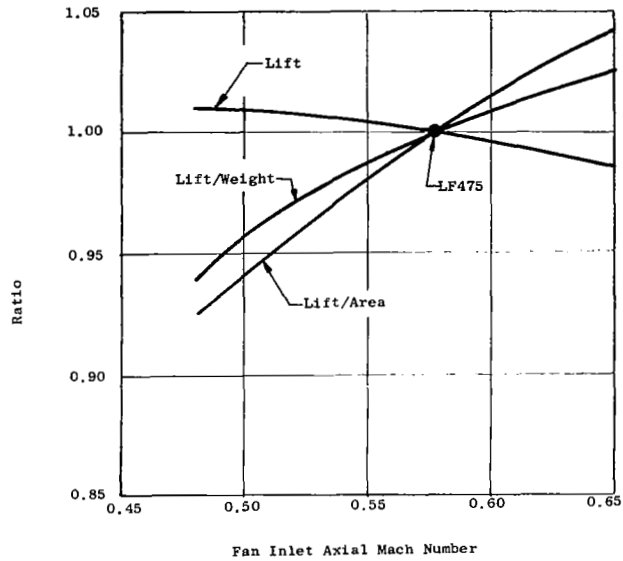


Figure 47 Effects of Fan Inlet Mach Number on Fan Lift, Weight & Area, for OGV Fans

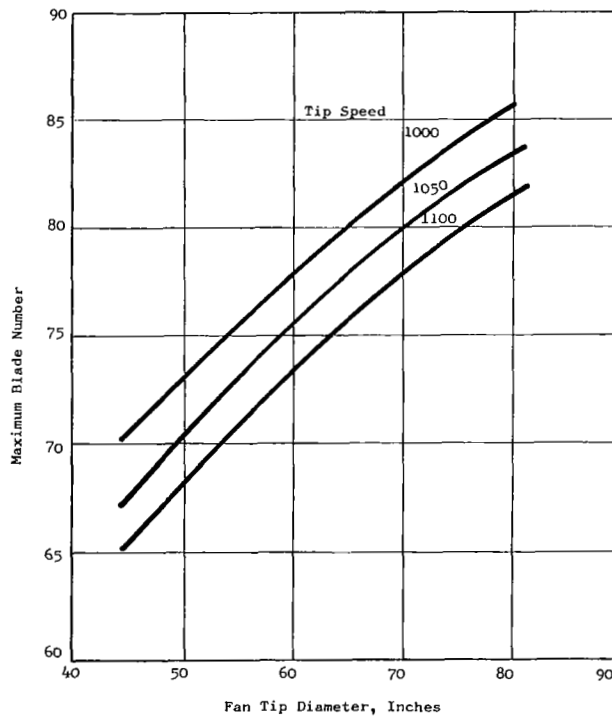


Figure 48. Number of Blades Versus Fan Tip Diameter & Fan Tip Speed

Figure 49 shows the effect of changes in blade number on rotor weight alone, & Figure 50 shows the effect of blade number on the total fan weight, for the LF475 basepoint fan. Increases in blade number reduce fan weight because of the reduction in net blade cross-sectional area (and volume) just discussed.

Vane/Blade Ratio. - Table VIII compares the vane/blade ratios of several lift fan designs. The LF475 basepoint fan has 36 vanes and a vane/blade ratio of 0.55. The LF1 (XV-5B wing fan) has 90 vanes and a vane/blade ratio of 2.5. One stiffening ring was used in the LF1 stator. But the LF475 stator has about four times the load of the LF1 because of the higher lift & fan pressure ratio of the LF475. Therefore, any increase in LF475 vane number is correspondingly more difficult.

The LF475 vane number can be increased to 72 by using solid vanes and by adding two stiffening rings to support vane bending loads. Further increases in vane number will require additional stiffening rings. Each of these rings will have a performance loss equivalent to about 1.5% of fan efficiency.

There is a radial variation of fan acoustic energy, with the majority of fan noise being generated in the outer region of the fan annulus. It would therefore seem logical to reduce vane weight and performance penalties by having a vane/blade ratio of two only in the fan outer annulus. Figure 51 illustrates such an arrangement. The short vanes extend only over the outer one third of the fan annulus, thus reducing the weight penalty and performance losses. Figure 52 shows the change in fan weight versus vane number for this configuration.

To proceed yet one step further, Figure 53 illustrates a minimum-penalty vane number increase. Shown is a conventional vane row having only stub vanes placed at the tip, to increase the vane/blade ratio in this region only.

The benefit of these concepts can only be estimated. There are no test data as yet available to support the assumption of noise reduction due to high vane/blade ratios only in the outer fan annulus.

Vane Lean. - It is not possible to incorporate lean into the LF475 stators because the load-carrying struts and the aerodynamic vanes are combined into an integral structure. To incorporate lean, it is necessary to change to a fan assembly having a structural front frame, a rotor and an OGV row, such as the LF1 used in the XV-5B aircraft. Figure 54 shows the vane row of Figure 51 which was previously discussed, with lean added. Figure 55 defines the weight increase as a function of the lean angle, for the basepoint fan with this vane row. The discontinuity in the curves occurs at the transition from hollow to solid vanes, required for mechanical considerations.

Table VIII Vane/Blade Ratios of Existing Fan Designs			
Fan Design	Fan Rotor Blades	Fan Stator Vanes	Vane/Blade Ratio
PF1	36	52	1.44
LF1	36	90	2.50
LF2	36	90	2.50
LFX	50	40	0.80
LF336	42	45	1.07
LCF380	40	18	0.45
LF387	40	28	0.70
LF475	66	36	0.55

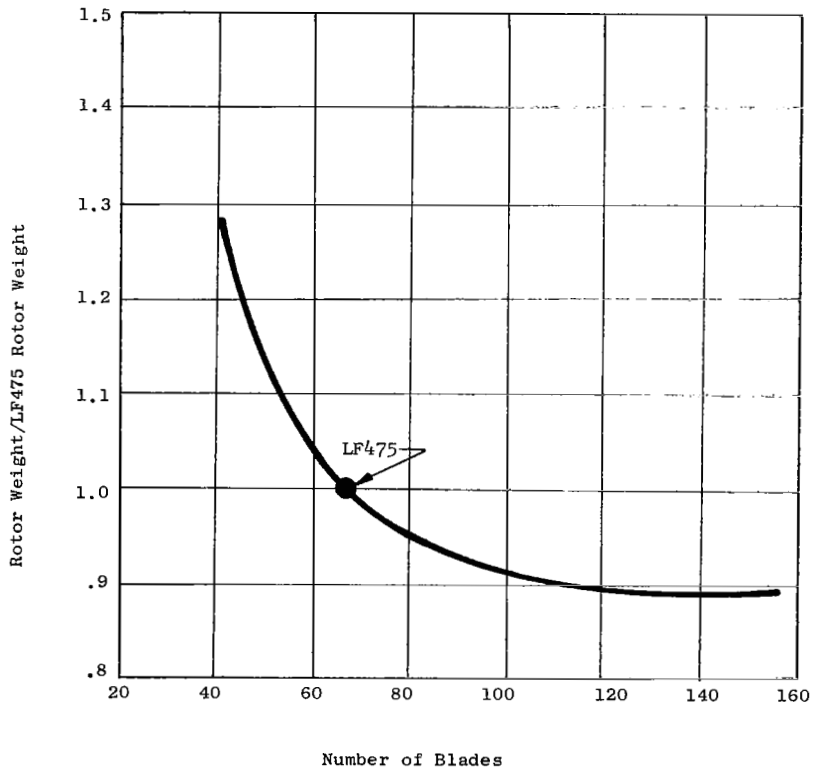


Figure 49 Rotor Weight vs No. Of Blades

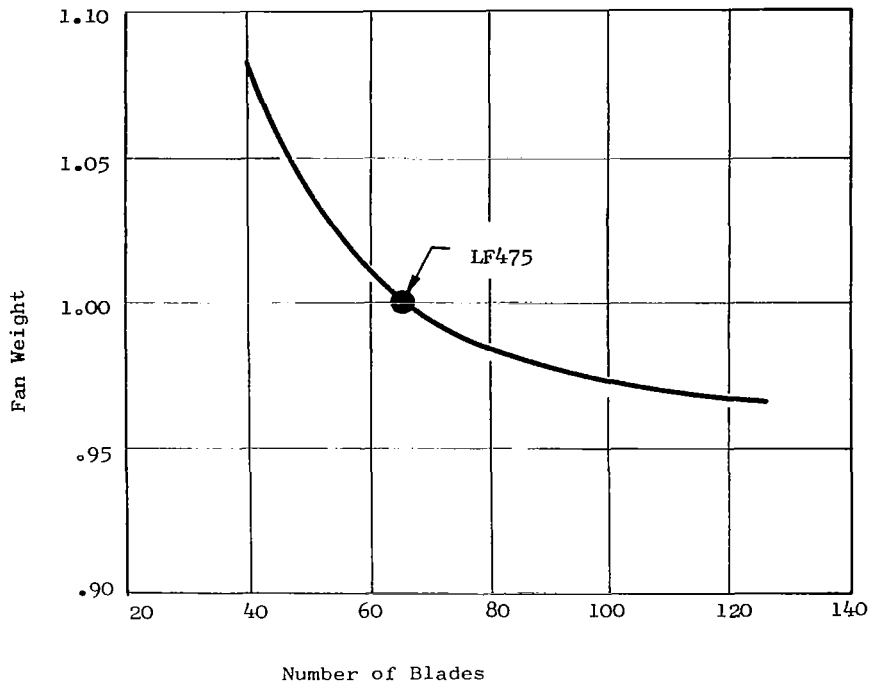


Figure 50. Fan Weight Vs. Number of Blades, for OGV Fans

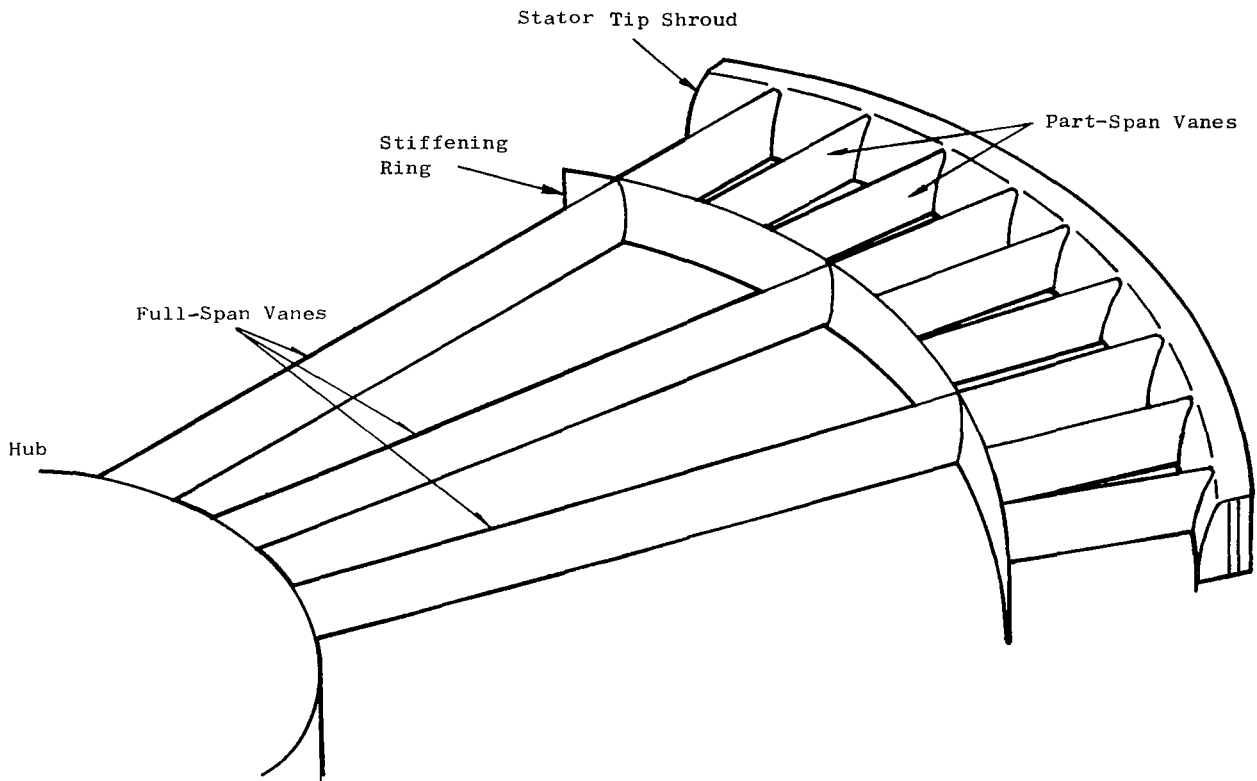


Figure 51. Stator Vane Row with Part-Span Vanes in the Outer Annulus

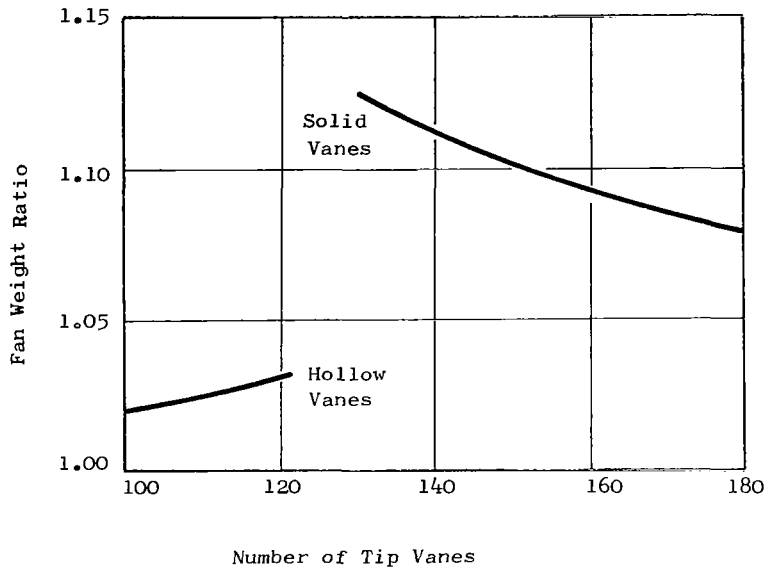


Figure 52. Fan Weight Vs. Number of Tip Vanes for OGV Fans

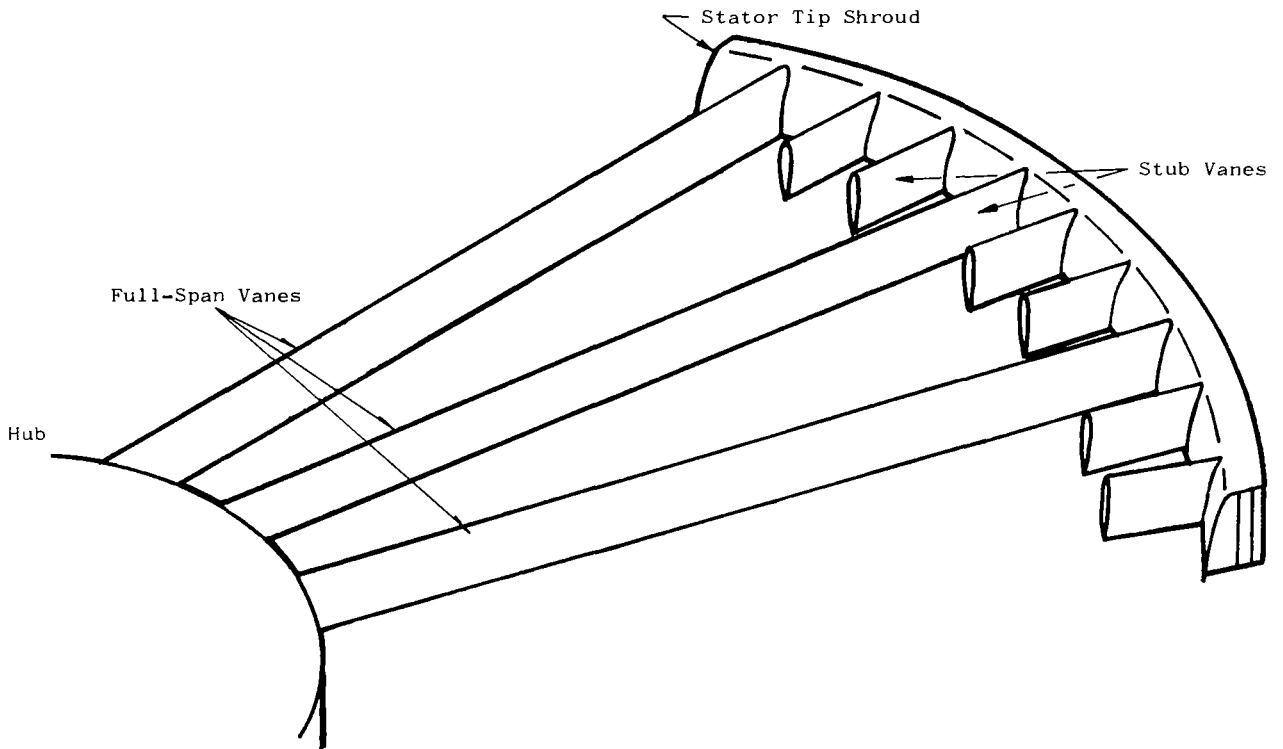


Figure 53. Stator Vane Row with Stub Vanes at the Tip

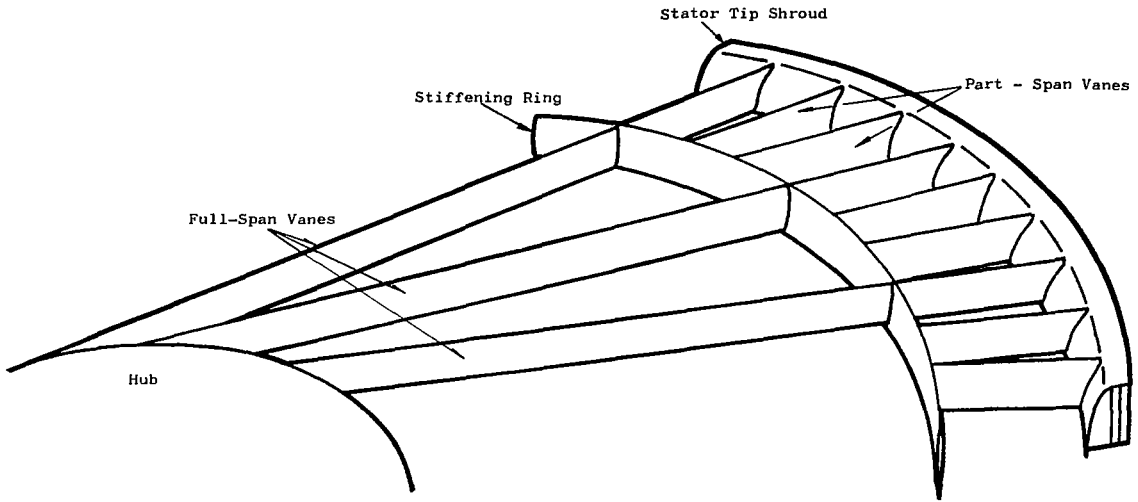


Figure 54 Stator Vane Row With Lean

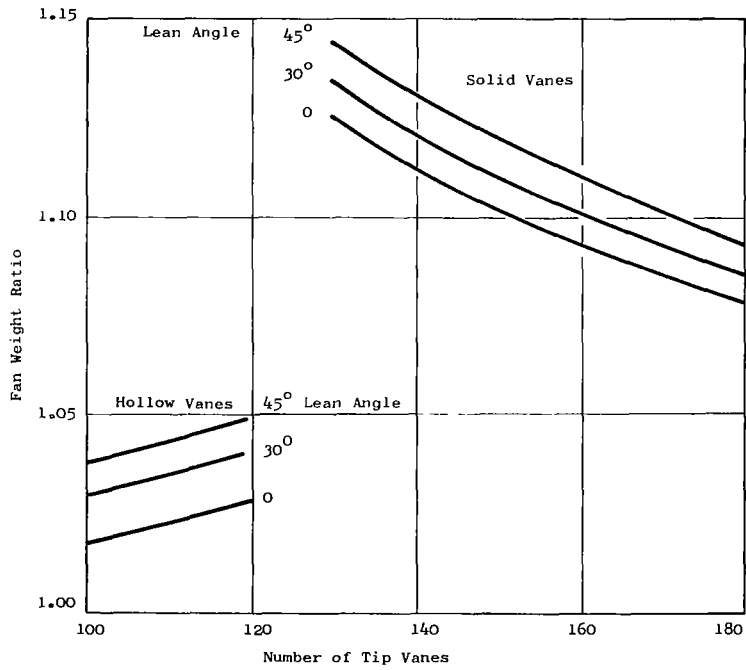


Figure 55 Fan Weight Versus Number of Vanes With Lean, for OGV Fans

Strut Lean. - It is also possible to incorporate lean into the structural front frame. Figure 56 illustrates the conventional structural front frame with the major and minor struts forming a cross. These struts can be made non-radial by employing the so-called H-frame concept illustrated in Figure 57. This H-frame consists of two parallel struts aligned with the airflow, and eliminates the need for the minor struts of the cross frame of Figure 56. The rotor lift loads and gyro moments must be transferred through the hub to the struts. The gyro moment loads the hub in torsion, with high shear loads generated in the hub-strut attachment area. Hub stiffness is therefore critical to keep the rotor tip deflection within design limits. The H-frame front frame is estimated to increase the LF475 fan weight by about 2%. The performance penalty due to the non-radial frame is estimated to be small.

Spacing. - The rotor-stator spacing is the axial spacing between the vane and blade rows at the fan tip. Spacing is expressed in multiples of the true tip chord of the upstream blade row.

One obvious effect of increased spacing is increased fan thickness. Figure 58 shows fan thickness ratio (fan thickness/fan tip diameter) as a function of spacing and blade number, for OGV fans. There is little or no performance loss for increased spacing. This has been substantiated in numerous references, for example, References 6 & 7. The weight penalty for increased spacing is shown in Figure 59.

Performance & Installation Parametric Data for IGV Fans

Fan Pressure Ratio & Tip Speed. - Figure 60 shows the fan radius ratio relationship to pressure ratio and tip speed for IGV fans. This is similar to Figure 35 for the OGV fans, but is based on the LF387 aerodynamic design.

Figures 61 through 64 show lift, diameter, planform area and weight as functions of fan tip speed and pressure ratio. All data are normalized to the design point values of the LF387 basepoint IGV fan. For these data, scroll inlet horsepower was held constant while fan efficiency and fan radius ratio were variables. The fan lift is shown in Figure 61. Maximum lift is obtained with tip speeds of 1000 fps at a 1.15 pressure ratio and at 1050 fps at a 1.3 pressure ratio. Fan tip diameter, fan area and fan weight are shown on Figures 62, 63 and 64. For constant input horsepower, the lower pressure ratio fans are larger, have higher thrust augmentation ratios and higher bypass ratios. Figures 65 and 66 show the lift/weight and lift/area trends with tip speed and pressure ratio at constant input horsepower. The highest values of lift/area are obtained with tip speeds between 950 fps at 1.20 pressure ratio and about 1000 fps at 1.30 pressure ratio.

Fan Diameter. - These previous data were for constant input power. The fan diameter and lift may be changed by varying the input power.

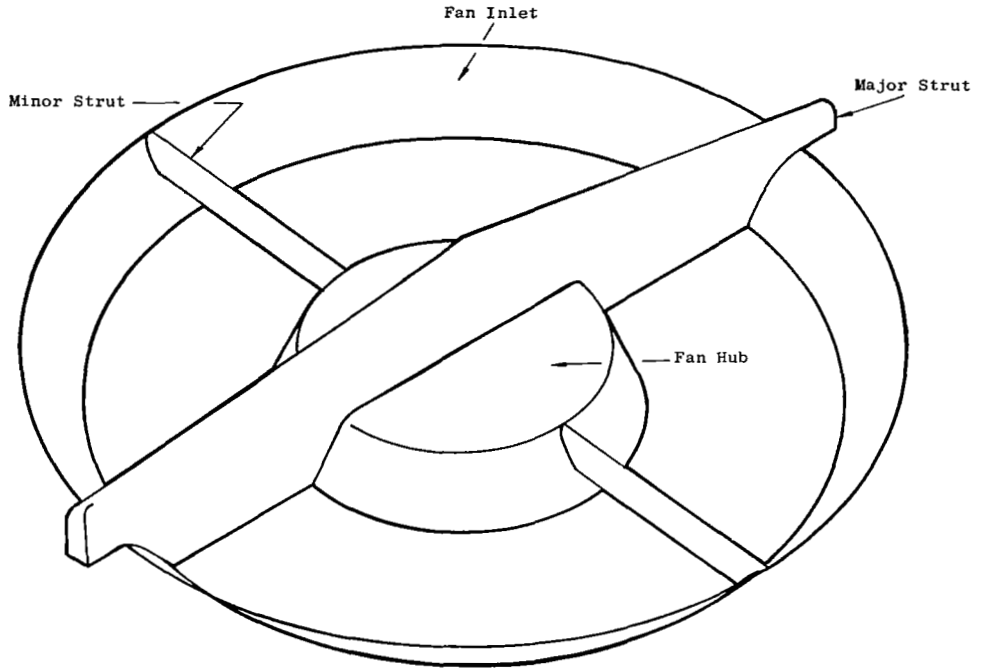


Figure 56 Conventional Front Frame with Crossed Struts

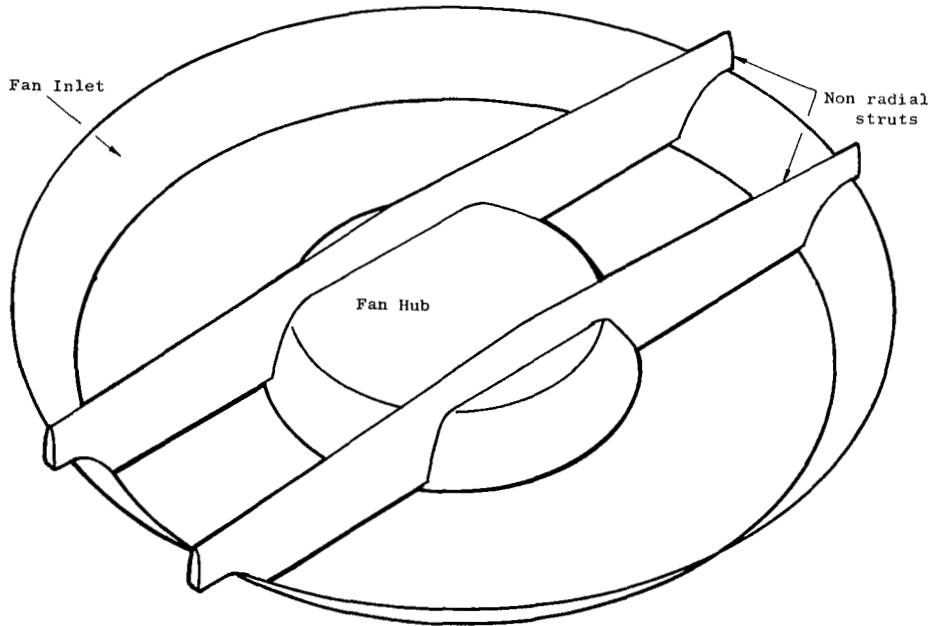


Figure 57 Front Frame with Lean

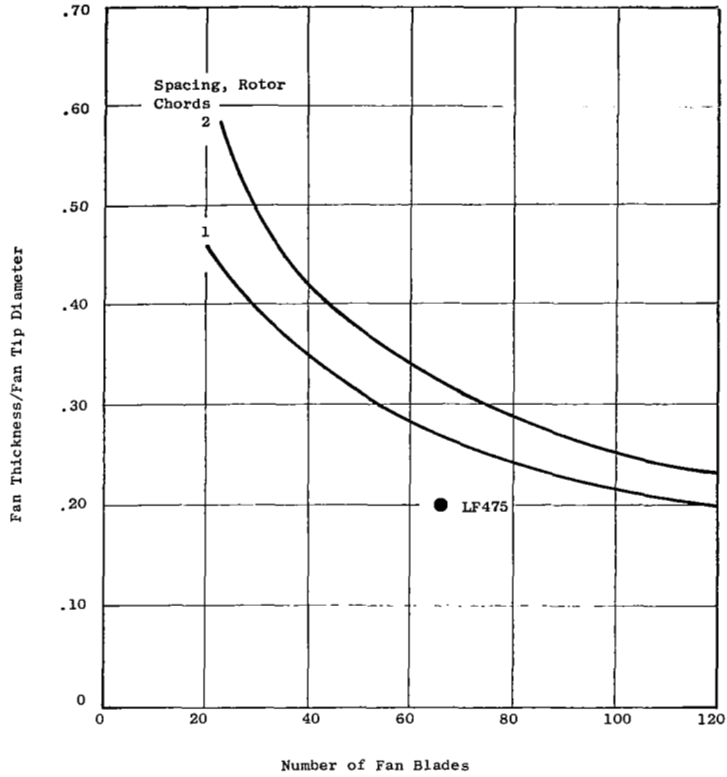


Figure 58 Fan Thickness Ratio Vs. Number of Fan Blades & Rotor - Stator Spacing, for OGV Fans

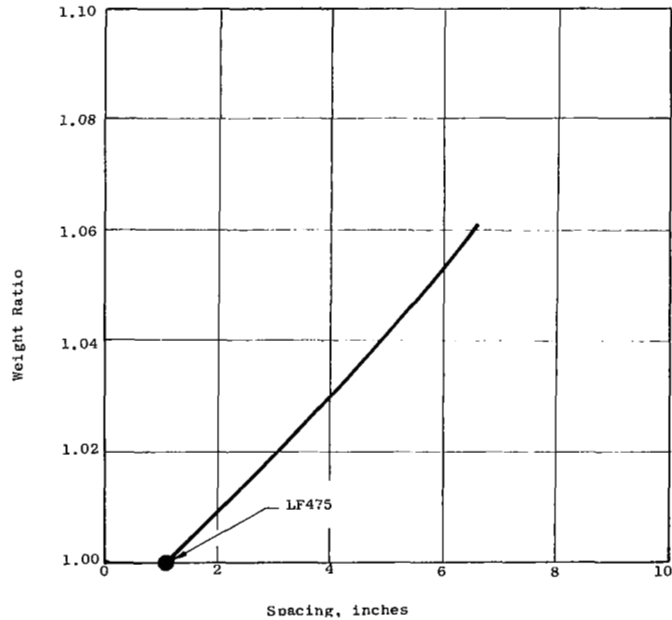


Figure 59 Weight Increase for Rotor-Stator Spacing, for OGV Fans

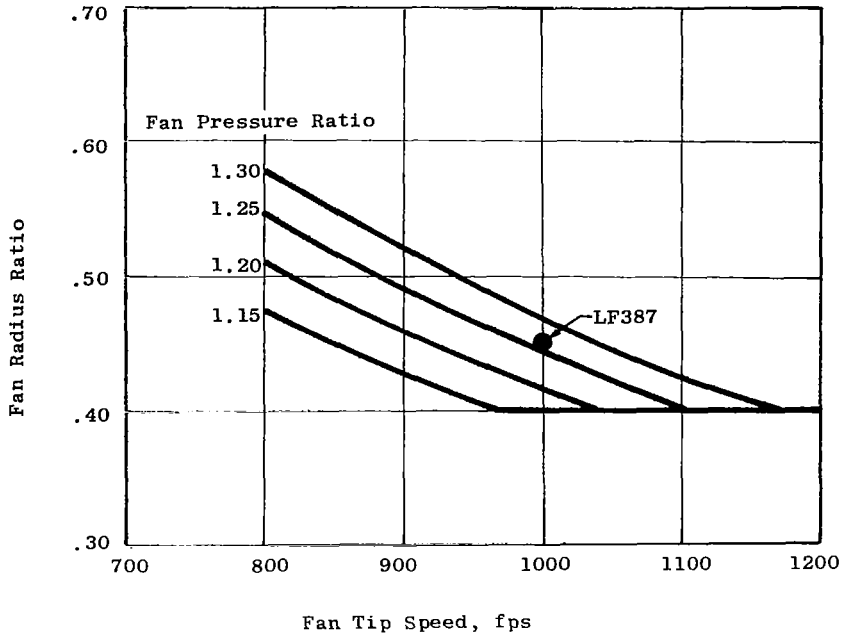


Figure 60. Fan Radius Ratio vs. Fan Tip Speed, for IGV Fans

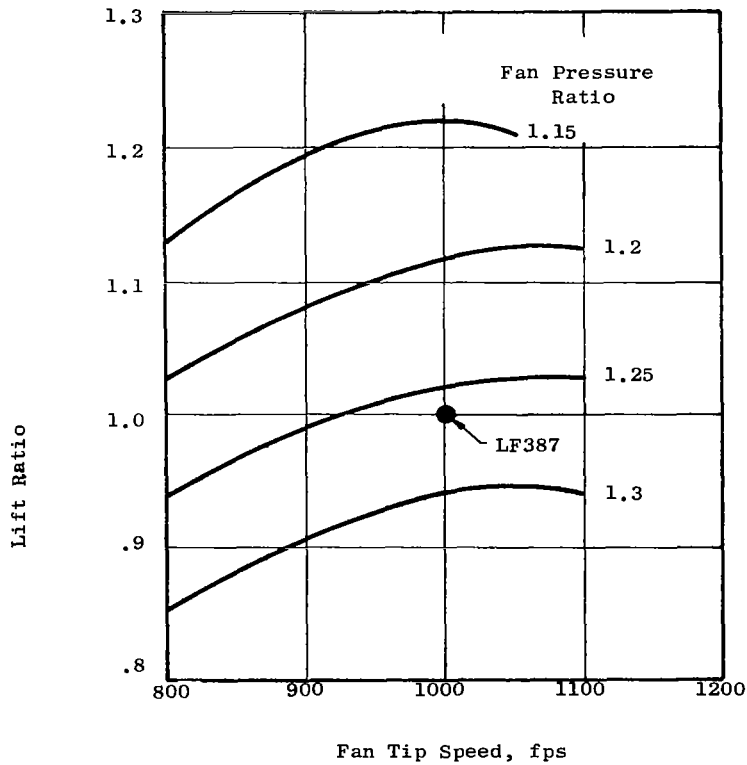


Figure 61. Lift vs. Tip Speed and Pressure Ratio, for IGV Fans

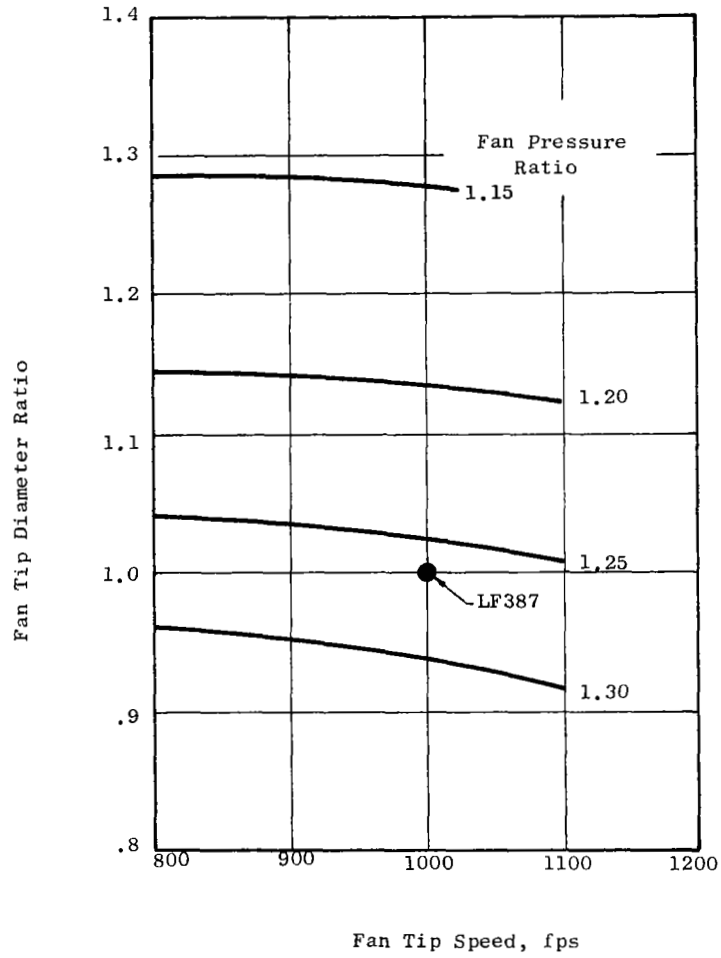


Figure 62. Fan Tip Diameter vs. Tip Speed and Pressure Ratio, for IGV Fans

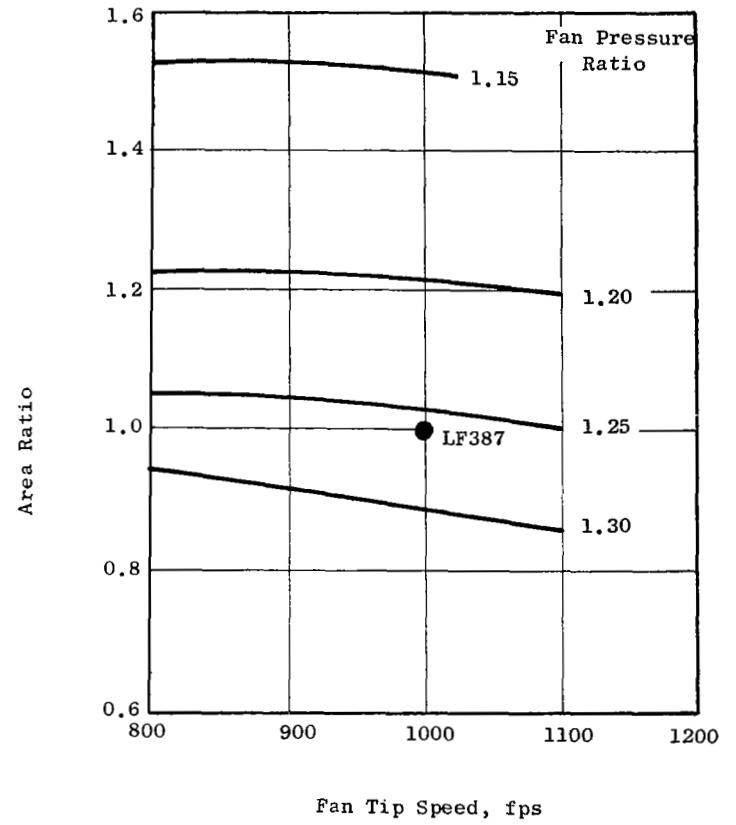


Figure 63. Area vs. Fan Tip Speed and Pressure Ratio, for IGV Fans

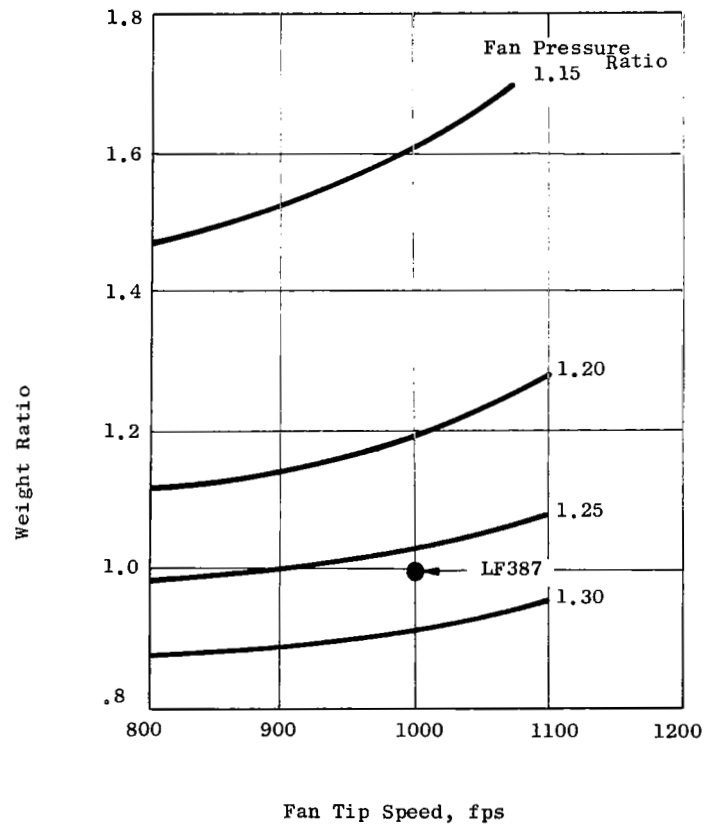


Figure 64. Weight vs. Tip Speed and Pressure Ratio, for IGV Fans

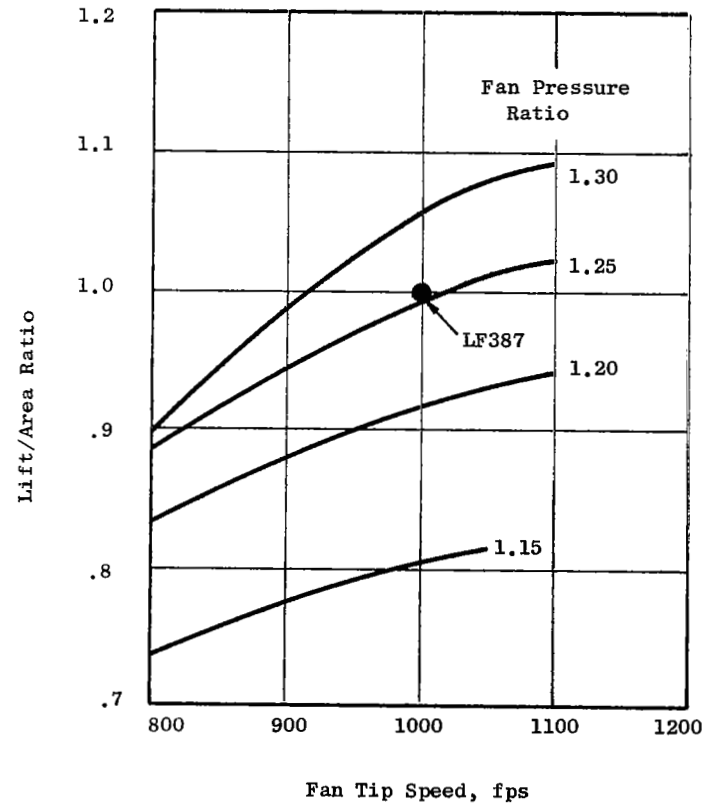


Figure 65. Lift/Area Ratio Vs. Tip Speed and Pressure Ratio, for IGV Fans

Figure 67 shows the effect of input horsepower on lift & fan tip diameter. Figure 68 shows the effect of varying input power on fan lift/weight and lift/area ratios for the LF387 design values of pressure ratio & tip speed. The same trends are evident for both OGV and IGV fans, i.e., the lift/weight ratio of the fan is strongly affected by fan size.

Fan Inlet Axial Mach Number. - Figure 69 shows the envelope within which the fan inlet average axial Mach number should be for IGV fans. The same axial diffusion limit and tip slope limit that were given in Figure 46 for OGV fans apply also to IGV fans. The choke limit for IGV fans is determined by choke considerations at the throat of the upstream IGV row, since the flow area is reduced by turning through the IGV's. These choke limits represent a practical maximum for IGV fans. Figure 70 shows lift, lift/weight, and lift/area versus the fan inlet axial Mach number for IGV fans. For maximum lift/weight and lift/area, the fan inlet axial Mach number should be chosen as high as the limits of Figure 70 allow.

Blade Number Increases. - For both IGV and OGV fans, the same considerations for increases in blade number apply. Figure 48 shows the maximum number of fan blades as a function of fan size and tip speed, for 6-6-2 Titanium alloy. Further increases in blade number require new tip turbine attachment methods or new and stronger materials. Figure 71 shows the effect of blade number on fan weight for the LF387 basepoint IGV fan.

Vane/Blade Ratio. - The basepoint fan has 28 vanes and a vane/blade ratio of 0.70. The basepoint fan has 40 blades, so that a vane/blade ratio of 2.1 can be obtained with only 84 vanes. But the LF387 has no separate load-carrying frame, the 28 IGV's are themselves the load-carrying members. Increases in vane number therefore require that structural frames such as shown in Figure 56 be incorporated into the design. Figure 72 shows the change in the basepoint fan weight as vane number is increased. The weight increase to obtain the 2.1 vane/blade ratio is about 2%.

Vane Lean. - Vane lean cannot be incorporated into an integral front frame - IGV row because of the struts. It is necessary to change to an IGV-rotor - rear frame assembly if vane lean is required.

Spacing. - The tip axial spacing for IGV fans is expressed in multiples of the true tip chord of the inlet guide vanes. The fan inlet and the fan rotor define the fan thickness for IGV fans. Some increase in spacing is therefore possible with no increase in fan thickness. A spacing of 0.6 IGV chords can be obtained on the basepoint fan with no increase in fan thickness. As the vanes are raised in the inlet to increase spacing, their length increases. This, plus the necessary stiffening of the hub and shaft assembly, represent the weight change due to increased spacing, up to .6 IGV chords. Further increases in spacing increase fan thickness & fan weight in the same way as for the OGV fans. Figure 73 shows the fan weight increase for increased spacing for IGV fans.

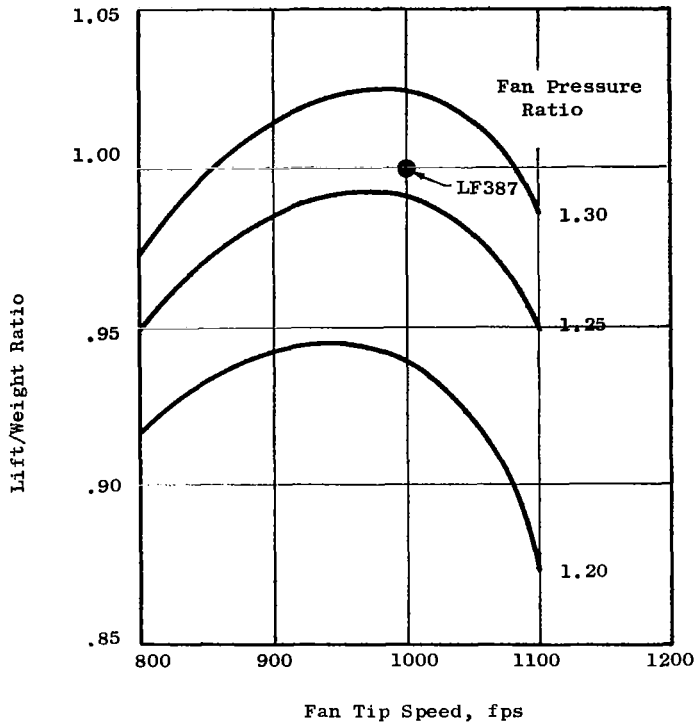


Figure 66. Lift/Weight Ratio vs. Tip Speed and Pressure Ratio, for IGV Fans

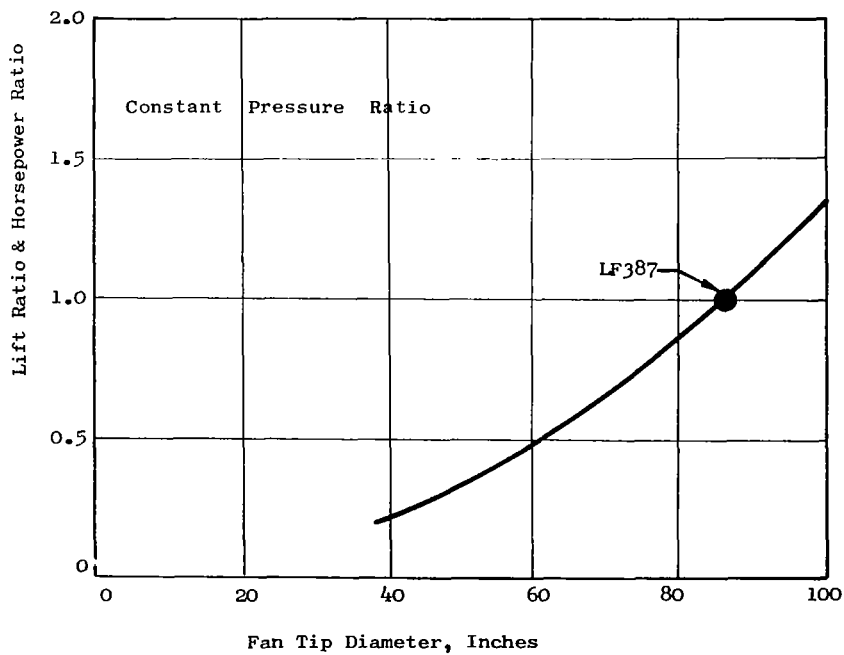


Figure 67. Effect of Input Power on Fan Diameter and Lift, for IGV Fans

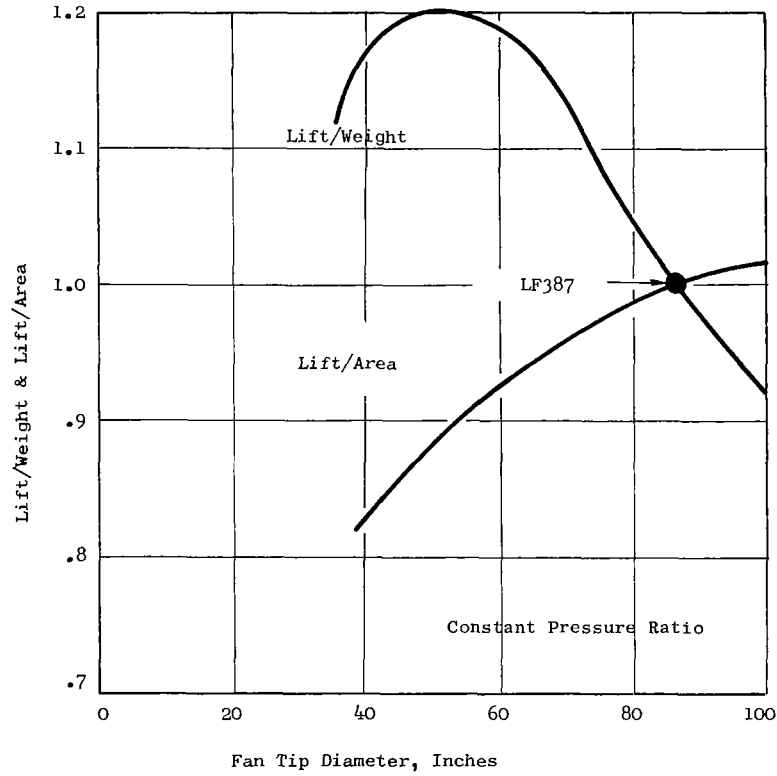


Figure 68 Effect of Fan Diameter on Lift/Weight & Lift/Area Ratios, for IGW Fans

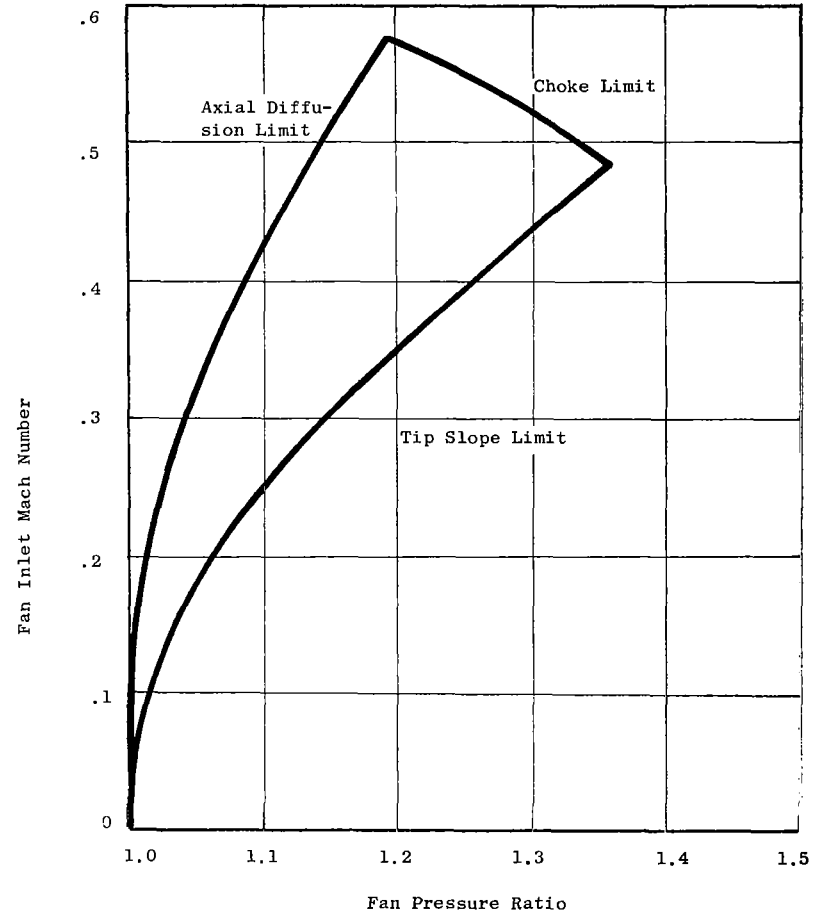


Figure 69 Inlet Mach Number Limits For IGW Lift Fans

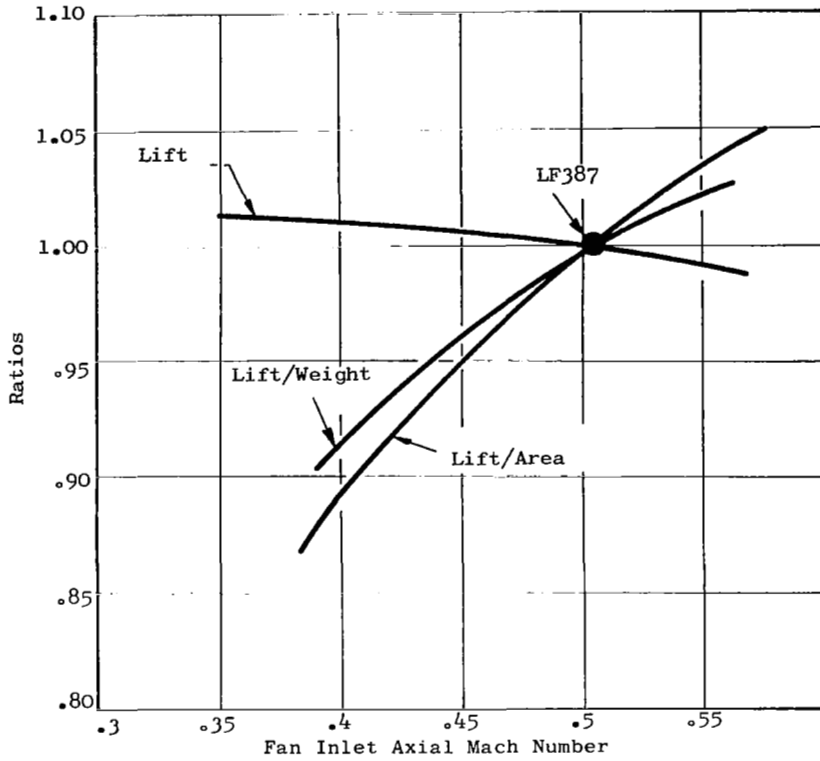


Figure 70. Effects of Fan Inlet Mach Number on Fan Lift, Weight and Area, for IGV Fans

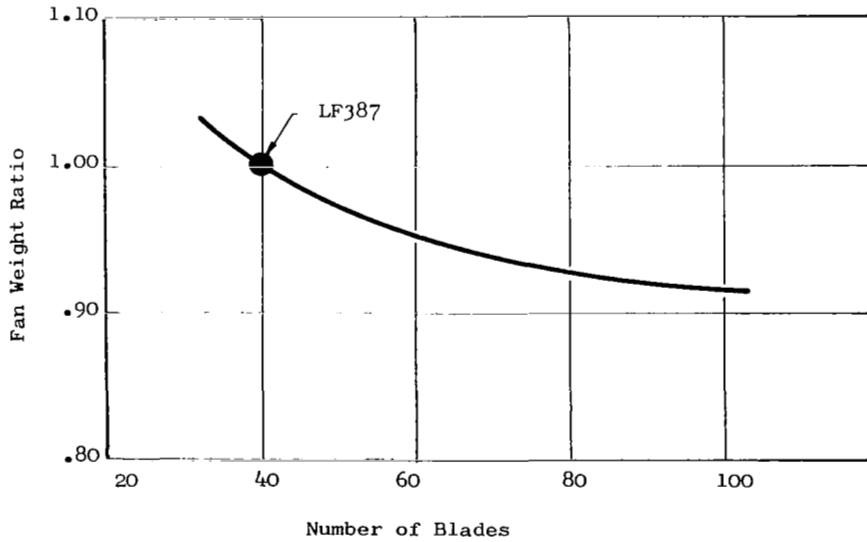


Figure 71. Fan Weight Versus Number of Blades, for IGV Fans

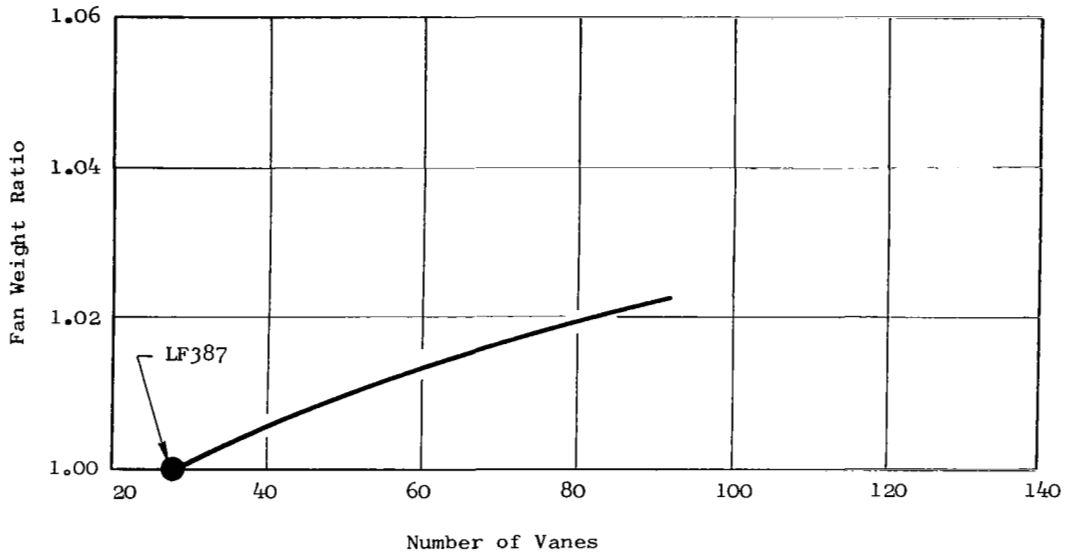


Figure 72. Fan Weight Versus Number of Vanes, for IGV Fans

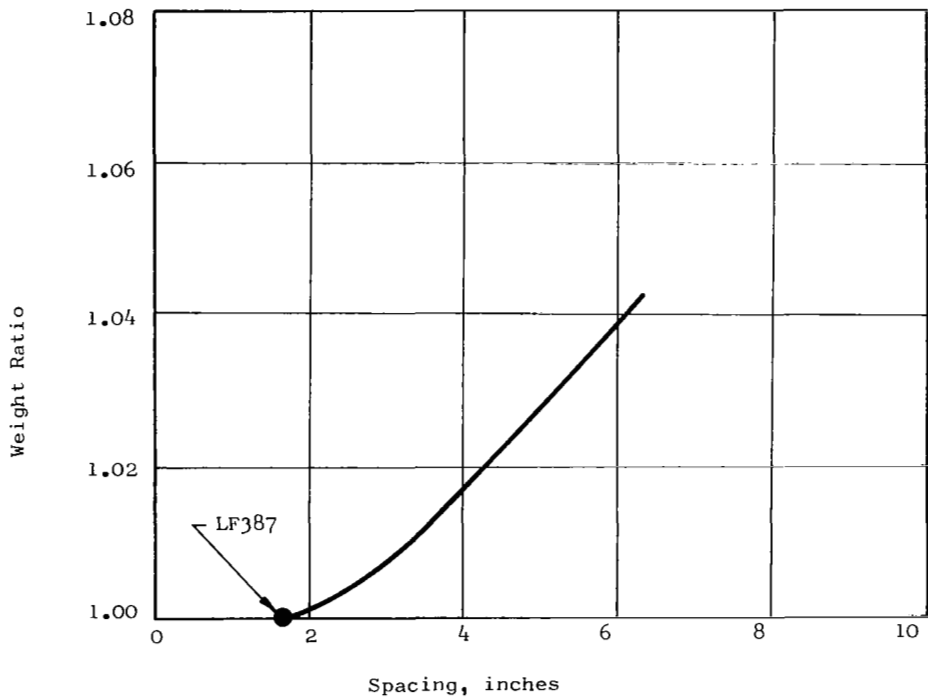


Figure 73. Weight Increase for Rotor-Stator Spacing, for IGV Fans

SELECTIONS OF QUIET FAN DESIGNS

The parametric noise data and parametric performance & installation data can be used to make judgements of reasonable compromises to achieve a quiet fan. For each change in the fan design parameters of a basepoint fan, the incremental noise reduction and the effects on fan performance & installation can be determined using the parametric data. The one criteria defining the quiet fan was that total lift remained the same, thus it was necessary to increase fan size to offset performance losses. This was felt to be a realistic approach to defining the true effect of noise reduction. These incremental noise reductions obtained for changes in individual fan parameters cannot be simply added together. Instead, the resultant fan definition must be reanalyzed to correctly estimate the final noise characteristics of the fan design. The final selected quiet fan designs were run on the fan design & acoustic prediction computer programs to calculate the combined effects of all of the design changes. Finally, the fan changes made to reduce noise are dependent on installation restrictions and judgement. It is believed the following fan designs represent typical cases from the installation standpoint.

Selected OGV Fan Design

Fan Pressure Ratio, Tip Speed & Blade Number. - Figure 10 identifies a potential noise reduction for changing from 1.39 to 1.30 pressure ratio. Further, Reference 12 has reported that a fan pressure ratio of about 1.3 makes an attractive V/STOL Transport. A pressure ratio of 1.3 was therefore selected for the first definition of the OGV quiet fan.

The tip speed was shown to have little effect on noise. However, Figure 43 shows that the maximum lift/weight ratio is obtained at a tip speed of about 1050 fps. Therefore, 1050 fps tip speed was selected for the first definition of the quiet fan.

From Figures 36 & 37, at 1.3 pressure ratio and 1050 fps, the lift is 1.085 of the basepoint fan lift and the diameter is 1.11 of the basepoint fan diameter. These data are for constant input horsepower. To scale these data to constant lift, the ratio of lift/diameter² (disc loading) is held constant:

$$\begin{aligned}L_1 / D_1^2 &= L_2 / D_2^2 \\1.085 / (1.11)^2 &= 1 / D_2^2 \\D_2 &= 1.065\end{aligned}$$

Therefore, a 1.3 pressure ratio fan at 1050 fps must have a fan tip diameter 6.5% larger than the basepoint fan for the same lift. The required fan diameter would be $1.065 \times 75 = 79.9$ inches.

Figure 18 indicates that a blade number increase will result in a noise reduction. Figure 48 shows that 82 blades is the maximum number of blades for an 80 inch fan at 1050 fps tip speed, therefore 82 blades were selected for the first definition of the quiet fan.

When this combination of 1.3 pressure ratio, 1050 tip speed, 80 inch diameter, and 82 blades was run on the computer to define the new noise level, it was found that the same noise reduction could be obtained by only increasing blade number while holding pressure ratio, tip speed, and size constant, as was obtained by changing blade number, pressure ratio, tip speed and fan size together. This result illustrates the statement made previously, that these incremental noise reductions obtained by changes in individual fan parameters cannot be added together, but instead, the resultant total combination of parameters must be reanalyzed to correctly estimate the noise characteristics of a fan design.

The selected quiet fan was therefore redefined to keep the design values of 1.39 pressure ratio and 1100 fps tip speed unchanged, while increasing the blade number to 80 as indicated by Figure 48.

Vane/Blade Ratio. - The vane row having additional vanes in the outer third of the fan annulus was selected for the quiet fan (see Figure 51). There are 56 full-span vanes and 112 part-span vanes in the selected design. There are a total of 168 vanes at the tip, which gives a vane/blade ratio at the tip of 2.1. The fan weight increase, from Figure 55, was estimated to be 8.6%. The incremental noise decrease, from Figure 20, is about 5 PNdB.

Vane Lean. - The circumferential leaning of the stator vanes provides a phasing of the rotor wake interaction and therefore appear attractive as a noise reduction feature. It is difficult to incorporate very high lean angles into a vane row. The increase in vane length increases weight and requires additional stiffening rings. The hub loading is also affected by the acute hub-vane angles. The quiet fan has 30° of lean. The incorporation of lean based on the results of Reference 8 was calculated to be approximately 3 PNdB. The additional fan weight increase was calculated to be about 1%, from Figure 55.

Front Frame Lean. - It is necessary to use a structural front frame in order to incorporate lean into the stator vane row of the OGV fan. These front frame struts have low drag coefficients and perform no aerodynamic function, but, nevertheless, are a source of noise because of the close strut-rotor spacing. The selected quiet design of Figure 74 is shown with front frame lean to offset any noise penalty incurred by changing to a front frame design. The weight increase for an H frame is about 2% of fan weight.

Rotor-Stator Spacing. - A one-chord spacing was selected for the quiet fan. The noise reduction is given in Figure 22. It can be seen, from Figure 58, that this will result in a fan thickness increase of 3 inches, an increase in fan thickness ratio of 0.04, bringing the ratio to 0.24. Figure 59 indicates a corresponding weight increase of 3%.

Larger noise reductions are possible with further increase in rotor-stator spacing. The allowable spacing is closely related to particular installation requirements. In general, for quiet designs, spacing should be as much as the particular wing or pod thickness will allow.

Acoustic Material. - Effective use of acoustic materials in fan-in-wing installations is limited because of the thinness of the installation. However, the study has identified three areas in which acoustic materials can be employed to advantage: The flowpath wall at the fan tip between the rotor and stator; the stator stiffening ring; and the exit louvers.

A half-inch thick lining of acoustic material has been added to the flow-path wall between the rotor and stator. The liner has been incorporated into the fan structure.

A stator stiffening ring is located at the outer third of the fan annulus and supports the ends of the short vanes. This ring, already required as a structural part, has been modified into an acoustic panel by lengthening the chord and adding acoustic treatment to both sides. This assembly, since it is a ring, can be located close to the rotor without compromising the rotor-stator spacing.

The exit louvers have been treated by adding one half inch of acoustic material to each side. The louver assembly consists of twelve vanes which have a 10" chord, a thickness ratio of 10%, and a solidity of 1.5.

The addition of acoustic material treatment in these three areas will decrease the fan noise by an estimated 8 PNdB, a significant reduction. The estimated fan weight increase for the acoustic treatment is 2%. The stator ring acoustic splitter will cause some performance loss which will require that the fan tip diameter be increased by about 1 inch to maintain constant lift. This size increase for constant lift will increase fan weight by another 2%. The total weight increase for acoustic material treatment is therefore 4% for the OGV quiet fan.

The quiet OGV fan is summarized in Table IX. The fan is shown in Figure 74. The basepoint LF475 OGV fan has a 500 feet sideline noise of 119 PNdB. The quiet version of this fan has a 500 feet sideline noise of only 99 PNdB, a reduction of 20 PNdB. The fan lift is unchanged. The fan diameter is increased by 1 inch, the fan weight is increased by 17%, and the fan thickness is increased by 3 inches.

Table IX. OGV Quiet Fan Summary

Noise Reduction

Basepoint Fan 500' Sideline PNdB	119
Quiet OGV Fan 500' Sideline PNdB without Acoustic Treatment	107
Quiet OGV Fan 500' Sideline PNdB With Acoustic Treatment	99
Total PNdB Reduction	20

Design Changes

	LF475	Quiet OGV Fan	Changes		
			Weight	Thick- ness	Diameter
Blade Number	66	80	-1.5%	-	-
Vane/Blade Ratio	0.55	2.1	+8.5%	-	-
Vane Lean, degrees	0	30	+1%	-	-
Front Frame Lean	None	H Frame	+2%	-	-
Spacing, chords	0.23	1.0	+3%	+3"	-
Acoustic Material	None	Tip Wall, Splitter, & Louvers	+4%	-	+1"
Net Change			+17%	+3"	+1"

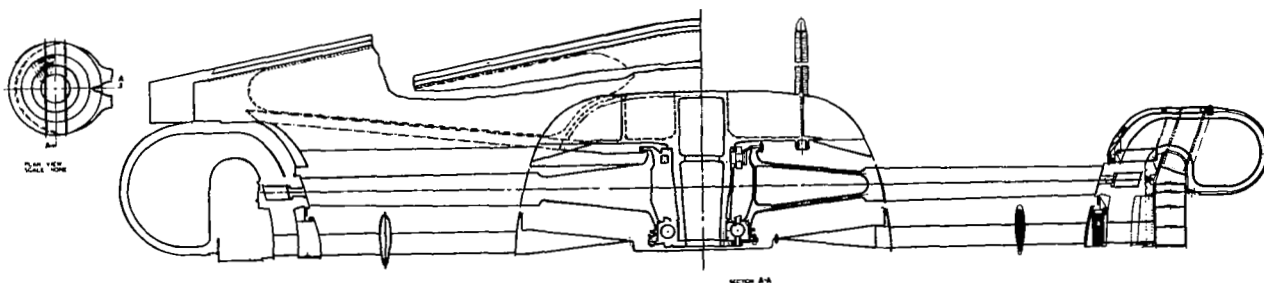


Figure 74. Quiet OGV Fan

Selected IGV Fan Design

Fan Pressure Ratio & Tip Speed. - A decrease in fan pressure ratio from the basepoint fan value of 1.26 to 1.18 will decrease the noise by only about 2 PNdB from Figure 24. But this pressure ratio change will require a size increase of about 9 inches to maintain constant lift, from Figures 61 and 62. This represents an 11% increase in size. Therefore, no change was made to the basepoint fan pressure ratio of 1.26.

The fan tip speed of 1000 ft/sec will give the maximum lift/weight ratio, from Figure 66. Since noise is a weak function of tip speed from Figure 28, no change was made to the basepoint fan tip speed of 1000 ft/sec.

Blade Number. - Figure 48 shows that more blades can be added to the fan. But increased blade number has less effect on noise for the IGV fan than for the OGV fan. This decrease in effectiveness is explained by Figures 15 & 16. The IGV fan has a low fundamental frequency. Increasing the blade number decreases the absolute noise level but increases the annoyance. Larger noise reductions can be obtained for IGV fans by decreasing the vane/blade interaction through increased vane/blade ratio and increased spacing. Any weight savings due to increased blade number would be quickly surpassed by weight increases required to obtain a vane/blade ratio of 2.1, as was the case with the quiet OGV fan. It was decided to keep the present low number of blades (40) for the LF387 rotor and direct the study toward noise reduction by other techniques.

Vane/Blade Ratio. - The basepoint IGV fan has a vane/blade ratio of 0.70. The LF387 basepoint fan has 28 vanes which also serve as structural members. For the IGV quiet fan, the vane number was increased to 84 for a vane/blade ratio of 2.1, and the front frame design was changed by adding major and minor struts as shown in Figure 56 to carry the mechanical loads. The weight increase for the higher vane number is about 2%, from Figure 72.

Vane Lean. - Vane lean can be added to the IGV now by changing the design to incorporate a mechanical rear frame. But this would increase fan weight (due to longer vanes & due to the frame change) and increase fan thickness (due to the minor struts of Figure 56 being in the fan discharge) for a potential noise reduction that at this point can only be assumed. A thickness increase due to increased spacing offers larger noise reductions for IGV fans than would the same thickness increase due to the minor strut being moved to the fan discharge. One could employ the H-frame of Figure 57 for the rear frame design & eliminate the fan thickness increase due to the minor strut, but this would impose complexity, weight & performance penalties on the exit louvers. It was therefore decided not to use leaned vanes in the quiet IGV fan.

Rotor-Stator Spacing. - This IGV fan can have an increase in spacing of 0.60 vane chords without an increase in fan thickness, by moving the IGV's higher up in the fan inlet.

This requires a redesign of the inlet wall curvatures to maintain the stage loading.

A spacing of two chords was selected for the quiet IGV fan. The incremental noise reduction is given in Figure 34. The fan weight will increase about 3%, from Figure 73. The fan thickness ratio (fan thickness/fan tip diameter) will increase from the basepoint LF387 value of 0.18 to 0.22 for the quiet IGV fan, a thickness increase of 4 inches.

Acoustic Material. - The IGV fan and the OGV fan employ the same acoustic treatments to the flowpath tip wall between the stator and the rotor and to the exit louvers. However, a stator vane ring acoustic splitter has not been added to this IGV fan. The study showed that this splitter can reduce the noise only about 1 PNdB. A 1 PNdB noise reduction does not justify the added weight and blockage imposed by the splitter.

The addition of acoustic treatment to the fan flowpath and exit louvers is expected to reduce to the noise by about 5 PNdB, while adding about 1% to the fan weight.

The selected quiet IGV fan design is summarized in Table X. The fan is shown in Figure 75. The LF387 basepoint IGV fan has a 500 feet sideline noise of 131 PNdB. The quiet version of the fan has a 500 feet sideline of 106 PNdB, a reduction of 25 PNdB. The fan lift and size are unchanged. The fan weight is increased by 6% and the fan thickness is increased by 4 inches. This fan could have been made more quiet by increasing the number of blades, leaning the stators, and using an H rear frame, but the penalties in weight would have been as large as with the OGV fan.

Table X. IGV Quiet Fan Summary

Noise Reduction

Basepoint Fan 500' Sideline PNdB	131
Quiet IGV Fan 500' Sideline PNdB Without Acoustic Treatment	111
Quiet IGV Fan 500' Sideline PNdB With Acoustic Treatment	106
Total PNdB Reduction	25

Design Changes

	LF387	Quiet IGV Fan	Changes		
			Weight	Thickness	Diameter
Vane/Blade Ratio	0.70	2.1	+2%	-	-
Spacing, Vane Chords	0.20	2	+3%	+4"	-
Acoustic Material	None	Tip Wall & Louvers	+1%	-	-
Net Changes			+6%	4"	-

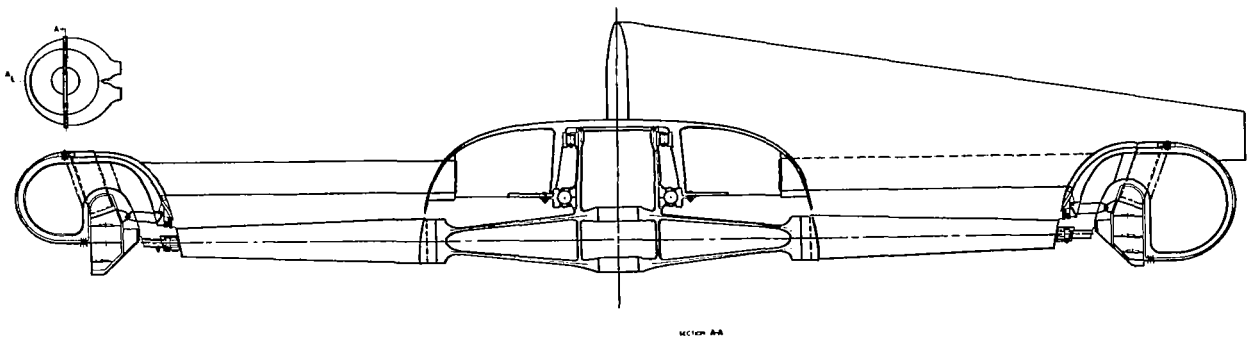


Figure 75. Quiet IGV Fan

CONCLUSIONS

1. The basepoint IGV fan was found to be louder than the basepoint OGV fan even though the OGV fan has over 5% more lift. This is due to the stronger vane - blade interaction of the IGV fan.
2. The quiet IGV fan is louder than the quiet OGV fan. But the quiet IGV fan permits a thinner installation & has a smaller weight penalty for the addition of the quiet features. The noise of the quiet IGV fan could be reduced by making the additional refinements used in the quiet OGV fan (increasing the number of blades, leaning the stators & using an H-frame) but with performance and weight penalties similar to those shown for the quiet OGV fan.
3. Large Spacings (one to two chords) reduced the fundamental tones on both the IGV & OGV fans. A larger reduction was obtained for the IGV fan because of the stronger vane-blade interaction.
4. The use of acoustic materials significantly reduced both pure tone & broad band noise for both IGV & OGV fans.
5. The results of the study indicate that lift fan noise levels of the order of 100 PNdB on the 500 foot sideline can be obtained with small performance & installation penalties.

APPENDIX A¹

THEORETICAL PREDICTION OF AERODYNAMICALLY GENERATED NOISE IN FANS & COMPRESSORS

High frequency sound of the type generated by jet engine fans and compressors is not only disturbing from the standpoint of its sound pressure level, but of its frequency as well. The presently accepted subjective noise scales (see reference 4) indicate that a high frequency noise (2-5 KHz) is potentially far more annoying at a given level than the lower frequency jet noise. The reduction of emitted pure tone noise can be accomplished by two means. First, the generated noise may be suppressed using sound absorbing materials placed in the engine ducting and on other structural members which are exposed to the acoustic waves. Secondly, a more basic approach may be taken that prevents the generation of the noise at the potential source. In order to employ the latter concept, a basic understanding of the mechanisms of pure tone noise generation must be obtained. Then these mechanisms must be related to the basic aero-mechanical design parameters which define the fan or compressor so that judicious design alterations can be made to reduce pure tone noise generation. A method has been developed by which the basic noise generating mechanisms can be directly related to the major aerodynamic and geometric parameters in a fan or compressor. The method is based on internal unsteady aerodynamics, coupled with an acoustic field described in terms of spinning modes. The sound pressure levels generated by the rotor alone, and the potential and wake interaction between adjacent blade rows are calculated. The analysis of the sound propagation in the duct in the presence of axial and circumferential flows is described and incorporated in the prediction method. The analytical results are compared with experimental data and are shown to be in good agreement.

1. Appendix A is based primarily on Reference 3.

Basic Generating Mechanisms

In general, there are two major kinds of blade passing frequency noise generating mechanisms:

1. Those relating to the rotating blade row alone
2. Those that are a result of the interaction of moving blade rows with stationary blade rows

The former mechanism is the result of the rotating steady (in the reference frame attached to the rotor) rotor pressure field. In the absolute reference frame this pressure field appears as a pulsating source with frequency equal to that of the rotor blade passing frequency.

An interaction related noise may result from two major sources:

Viscous wake interaction

Potential field interaction

A viscous wake interaction results when the wake of an upstream blade row impinges on a downstream blade row. The deficient wake velocity results in a change in downwash (or upwash) on the downstream blade which, in turn, causes a fluctuation of the blade's pressure field.

A potential interaction results in a mutual disturbance of the pressure fields of both blade rows. Each blade's pressure field extends out around the blade. When the blade rows are close enough these fields intersect. Thus, each blade experiences a disturbance to its pressure field at the blade passing frequency.

Calculation of Unsteady Circulation

Rotor Alone. - The rotor alone noise is a result of the "steady" rotor circulation.

Thus, the disturbance circulation is computed from basic aerodynamic data and is a direct function of the rotor's loading.

Viscous Wake Interaction. - The unsteady circulation due to a viscous wake interaction may be calculated by the method of Reference 13. Consider the two dimensional tandem cascade of thin airfoils in an incompressible flow, and the wake profile shown in Figures A1 and A2. Then the unsteady upwash on the rotor due to the stator wakes may be expressed as

$$v^r = \frac{1}{2\pi} v_r \sum_{m=1}^{\omega} G_m \exp \left[i \nu_{r,m} \left(t - \frac{x_r}{v_r} \right) \right] \quad (A1)$$

where

$$G_m = 14.622 \frac{v_s}{v_r} \frac{C_d \sin \beta \sigma_s}{\left(\frac{x'}{c_s} + .3 \right) \cos \alpha_s} \sqrt{\frac{x'}{c_s}} \exp \left[- \pi m^2 \left(\frac{.68 \sigma_s}{\sqrt{2} \cos \alpha_s} \right)^2 \frac{C_d x'}{c_s} \right] \quad (A2)$$

$$\frac{x'}{c_s} = \frac{c_r}{c_s} \left(\frac{b}{c_r} \sec \alpha_s + \frac{x_r}{c_r} \frac{v_s}{v_r} \right) - .7 \quad (A3)$$

$$b = b' + c_s \cos \alpha_s + c_r \cos \alpha_r \quad (A4)$$

and
$$\frac{x_r}{c_r} = \frac{1}{2} \quad (A5)$$

Equation (A5) implies that the wake width and velocity decrement are to be evaluated at the quarter chord point on the rotor. Reference 13 shows that the value of x_r/c_r does not significantly affect the results.

Assuming a sinusoidal unsteady motion of a thin airfoil, it can be shown (Reference 14) that the unsteady circulation on the rotor is given by

$$\Gamma_r = 2\pi c_r \sum_{m=1}^{\infty} v_m^r J(m\omega_r) S(m\omega_r) \exp \left[im \left(i\psi_r t - \omega_r \right) \right] \quad (A6)$$

where

$$J(m\omega_r) = J_0(m\omega_r) - i J_1(m\omega_r) \quad (A7)$$

and

$$S(m\omega_r) = \frac{1}{im\omega_r \left[K_0(im\omega_r) + K_1(im\omega_r) \right]} \quad (A8)$$

Potential Interaction. - A similar calculation can be made for the potential interaction of the rotor pressure field on a stator blade by using the method of Reference 15. Consider the geometry shown in Figure A3. In this case the unsteady upwash on the stator is given by

$$v^s = \frac{\Gamma_o^r}{2 n c_s} \sum_{m=1}^{\infty} G_m^s \exp \left(\frac{2 n m}{d_r} e^{-i \alpha_s} x_s \right) e^{i \nu_s^m t} \quad (A9)$$

(A10)

where

$$G_m^s = \frac{n \sigma_s d_s}{d_r} e^{-i \alpha_s} H_m^r \exp \left\{ -n m \sigma_r \left[\frac{b}{c_r} \left(1 + i \tan \alpha_r - \frac{i U}{V_s \cos \alpha_s} \right) - \frac{i U}{V_r} \right] \right\}$$

$$H_m^r = J_0(z_r) + i J_1(z_r) \quad (A11)$$

and

$$z_r = n m \sigma_r e^{-i \left[(n/2) - \alpha_r \right]} \quad (A12)$$

The quantity H_m^r is a function of the vorticity distribution along the rotor chord. Equation (A11) assumed the rotor vorticity distribution to be equivalent to that of an isolated flat-plate airfoil at an angle of attack.

Again, for sinusoidal motion, the unsteady circulation can be shown to have the form

$$\Gamma_s = \Gamma_o^r \sum_{m=1}^{\infty} G_m^s J(\lambda_s^m) S(m \omega_s) \exp \left[i m (\nu_s t - \omega_s) \right] \quad (A13)$$

where

$$\lambda_s = \frac{2\pi c_s}{d_r} e^{i \left[(\pi/2) - \alpha_s \right]} \quad (A14)$$

Additional equations for the viscous wake interaction between a rotor and downstream stator, the potential interaction due to the stator pressure field on the rotor in Figure A3, and the mutual potential interaction of a rotor and downstream stator can be derived by the same processes as those used to deduce Equations (A6) and (A13). In the case of the potential interaction of the steady stator pressure field with a rotor, however, it is more realistic to use an elliptic vorticity distribution along the vane chord in defining Equation (A11). That is,

$$H_m^s = \frac{2 i e^{i\alpha_s}}{m \sigma_s \pi} J_1(z_s) \quad (A15)$$

where

$$z_s = \pi m \sigma_s e^{-i \left[(\pi/2) + \alpha_s \right]}$$

In summary, equations similar to Equations (A6) and (A13) can be written which will define the unsteady circulation due to interactions between rotors and stators in terms of basic aerodynamic and geometric design parameters. While the rotor alone "unsteady" circulation can be obtained from the design aerodynamic loading of the rotor.

Wave Propagation in the Engine Duct

It now remains to relate the unsteady circulation computed in the previous section to the propagation of an acoustic wave in the engine duct. If the annular duct geometry (see References 16, 17 and 18) is as shown in Figure A5, the linear differential equation for small pressure disturbances may be expressed in non-dimensional form, as

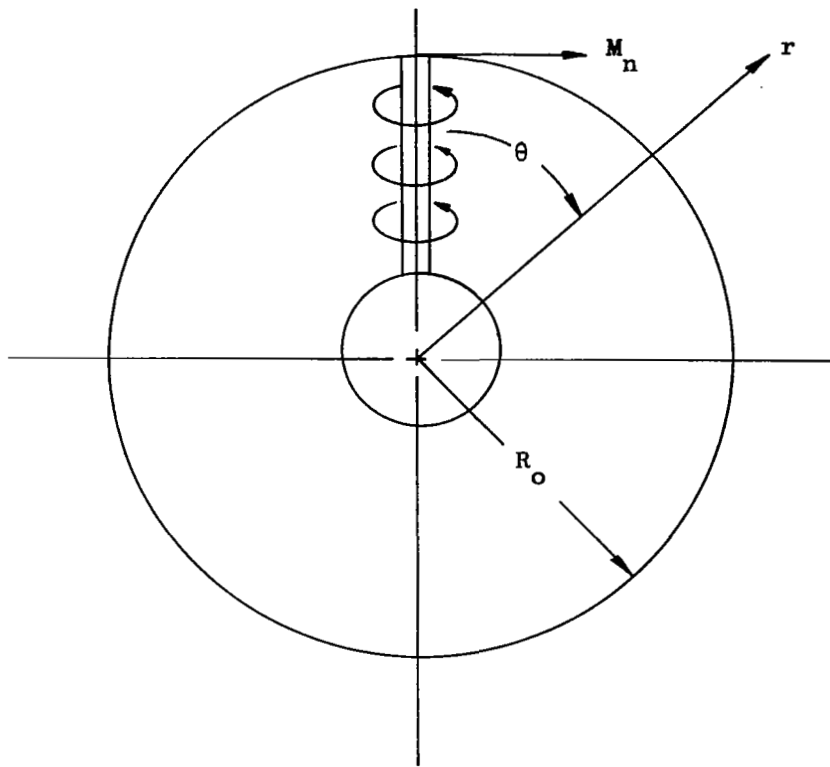


Figure A4. Model of A Rotating Line Vortex

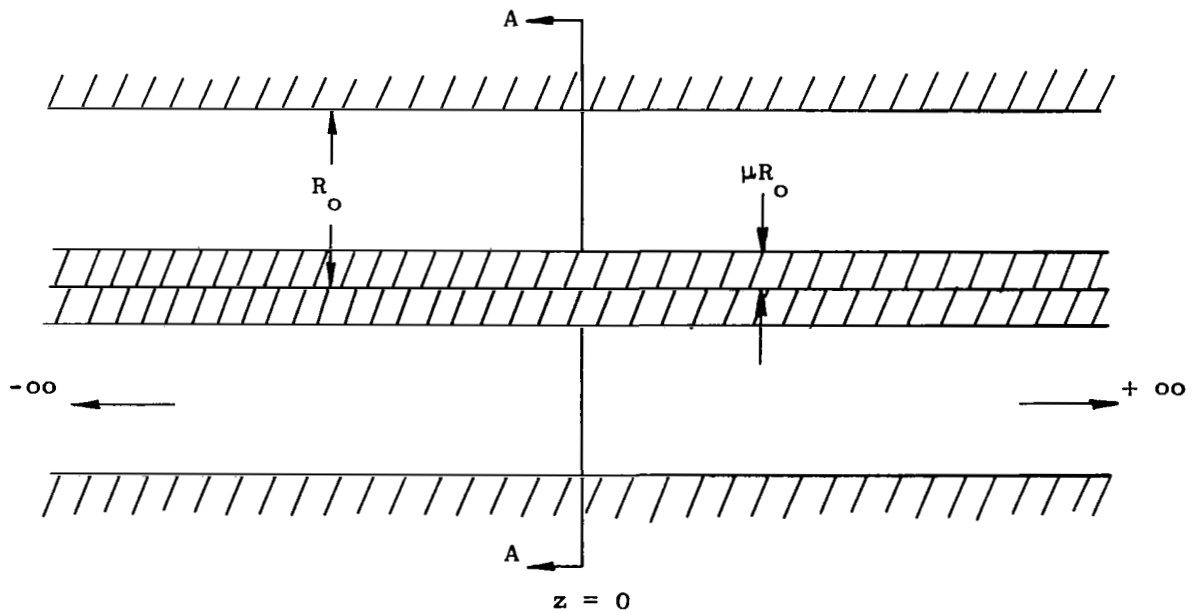


Figure A5. Annular Duct Geometry

$$\nabla^2 \psi = \left[\frac{\partial}{\partial t} + M_z \frac{\partial}{\partial z} + \frac{M_\theta}{r} \frac{\partial}{\partial \theta} \right]^2 \psi \quad (\text{A16})$$

where M_z and M_θ are respectively the axial and tangential Mach numbers, and ψ is defined by

$$\vec{v} = \nabla \psi \quad (\text{A17})$$

If it is assumed that the swirl velocity is representative of a solid body rotation, that is

$$M_\theta = r \bar{M}_\theta \quad (\text{A18})$$

where \bar{M}_θ is a constant, then the solution to Equation (A16) can be expressed as

$$\psi = \sum_{n=-\infty}^{+\infty} \sum_{m=0}^{\infty} e^{i \gamma z} \left[A_1 e^{i \zeta z} + A_2 e^{-i \zeta z} \right] e^{in(\theta - M_n t)} R_n(\lambda_{nm} r) \quad (\text{A19})$$

$$\gamma = \frac{-n M_z (M_n - M_\theta)}{1 - M_z^2} \quad (\text{A20})$$

$$\zeta = \frac{\sqrt{n^2 (M_n - \bar{M}_\theta)^2 - \lambda_{nm}^2 (1 - M_z^2)}}{1 - M_z^2} \quad (\text{A21})$$

and

$$R_n(\lambda_{nm} r) = B_1 J_n(\lambda_{nm} r) + B_2 Y_n(\lambda_{nm} r) \quad (\text{A22})$$

If the walls of the duct are hard, that is, infinitely reactive in the acoustic sense, then a zero velocity condition may be applied at $r = 1.0$ and $r = \mu$. Applying this boundary condition, it is found that

$$\frac{B_2}{B_1} = - \frac{J_n'(\lambda_{nm})}{Y_n'(\lambda_{nm})} \quad (A23)$$

and that the eigenvalue λ_{nm} can be found from the equation

$$Y_n'(\lambda_{nm}\mu) J_n'(\lambda_{nm}) - Y_n'(\lambda_{nm}) J_n'(\lambda_{nm}\mu) = 0 \quad (A24)$$

Referring to Figure A5, it is a requirement of mass continuity that the axial velocity across the plane $z = 0$ be continuous. In terms of Equation (A17)

$$w = c \frac{\partial \phi}{\partial z} \Big|_{z=0} \text{ is continuous} \quad (A25)$$

If the duct of Figure A5 is assumed infinite in both the plus and minus z directions, then

$$\phi_{nm}^+ \Big|_{z=0} = A_1 e^{in(\theta - M_n t)} R_n(\lambda_{nm} r) \quad (A26)$$

and

$$\phi_{nm}^- \Big|_{z=0} = A_2 e^{in(\theta - M_n t)} R_n(\lambda_{nm} r) \quad (A27)$$

From the requirement of Equation (A25) it is seen that

$$A_1 = -A_2 \quad (A28)$$

The assumption of an infinite duct restricts the wave propagation in the duct to one direction and does not allow end reflections. Equation (A19) may be recast for a right-running wave as

$$\phi = \sum_{n=-\infty}^{+\infty} \sum_{m=0}^{\infty} A_{nm} e^{i(\lambda + \gamma)z} e^{in(\theta - M_n t)} R_n(\lambda_{nm} r) \quad (A29)$$

where A_{nm} is a combination of the remaining unknown constants.

Examining Equations (A21) and (A29) it can be seen that the acoustic wave represented by Equation (A29) will decay when ζ is imaginary. That is, when

$$\lambda_{nm} > \frac{n(M_n - \bar{M}_\theta)}{1 - M_z^2} \quad (A30)$$

or in terms of a "cut-off" Mach number

$$M_{nm}^* = \frac{\lambda_{nm}}{n} \sqrt{1 - M_z^2} + \bar{M}_\theta \quad (A31)$$

The Mach number M_{nm}^* is the tip Mach number of the spinning mode (References 16 and 19) at which the (nm) mode begins to propagate down the duct unattenuated. The mode Mach number is related to the rotor tip Mach number by

$$M_n = \frac{\bar{n} M_T B}{n}$$

Figure A6 shows the variation of cut-off Mach number with swirl and axial Mach numbers for the case of $n = 32$, $m = 1$, and $\mu = .29$.

In Equation (A29) one more constant, A_{nm} , remains to be determined by a boundary condition at the plane $z = 0$. Consider the line vortex rotating in the plane $z = 0$, as shown in Figure A5. The tangential velocity at an angle θ will be zero until the line vortex is at the same angle. Expressed mathematically,

$$v = f(r) \delta(\theta - M_n t) \quad (A32)$$

where $f(r)$ is the radial distribution of tangential velocity. The circulation at a given radius may be found by integrating

$$\Gamma(r) = R_0 c \int_0^{2\pi} v r d\theta \quad (A33)$$

where $R_0 c$ is introduced to non-dimensionalize the circulation. Then

$$\Gamma(r) = R_0 c r f(r) \quad (A34)$$

or

$$v = \frac{\partial \phi}{\partial \theta} \Big|_{z=0} = \frac{\Gamma(r)}{R_0 r c} \delta(\theta - M_n t) \quad (A35)$$

Using Equation (A17) the final boundary condition can be expressed as

$$v \Big|_{z=0} = \frac{\Gamma(r)}{R_0 c} \delta(\theta - M_n t) \quad (\text{A36})$$

If there are D such rotating line vortices the boundary condition can be expressed as

$$\frac{\partial \psi}{\partial \theta} \Big|_{z=0} = \frac{\Gamma(r)}{R_0 c} \sum_{k=1}^D \delta\left(\theta - M_n t + \frac{2\pi k}{D}\right) \quad (\text{A37})$$

Applying Equation (A37) to Equation (A29), multiplying the result by

$$e^{-i\hat{n}(\theta - M_n t)} d(\theta - M_n t)$$

and integrating from 0 to 2π , it is found that

$$\Gamma(r) \sum_{k=1}^D e^{\frac{-i\hat{n} 2\pi k}{D}} = R_0 c \sum_{n=-\infty}^{+\infty} \sum_{m=0}^{\infty} 4i\pi n A_{nm} \delta_{\hat{n}\hat{n}} R_n(\lambda_{nm} r) \quad (\text{A38})$$

Examining the left side of Equation (A38), it can be seen that

$$\sum_{k=1}^D \exp \frac{-i\hat{n} 2\pi k}{D} = \begin{cases} D & \text{if } \frac{\hat{n}}{D} = \text{integer} \\ 0 & \text{if } \frac{\hat{n}}{D} \neq \text{integer} \end{cases} \quad (\text{A39})$$

Then, since \hat{n} is a dummy index.

$$\Gamma(r) D = R_o c \sum_{n = -\infty}^{+\infty} \sum_{m = 0}^{\infty} 4 i n \pi A_{nm} R_n (\lambda_{nm} r) \quad (A40)$$

Multiplying both sides of Equation (A40) by $r R_n (\lambda_{n\alpha} r)$ and integrating from 1.0 to μ , it is found that

$$A_{nm} = \frac{D}{4i \pi R_o c n \eta_{nm}} \int_{\mu}^{1.0} \Gamma(r) r R_n (\lambda_{nm} r) dr \quad (A41)$$

where the orthonormal properties of $R_n (\lambda_{nm} r)$ in the space 1.0 to μ have been employed and where η_{nm} is the norm of $R_n (\lambda_{nm} r)$ in the same space given by

$$\eta_{nm} = \frac{1}{2 \lambda_{nm}^2} \left[(\lambda_{nm}^2 - n^2) R_n^2 (\lambda_{nm}) - (\lambda_{nm}^2 \mu^2 - n^2) R_n^2 (\lambda_{nm} \mu) \right] \quad (A42)$$

From the definition of the velocity potential it can be shown that the pressure is expressed as

$$P = - e c^2 \frac{\partial \phi}{\partial t} \quad (A43)$$

neglecting steady duct flow. Using Equations (A29), (A41) and (A43), the rms pressure can be expressed as

(A44)

$$P /_{z=0} = \sum_{n=-\infty}^{+\infty} \sum_{m=0}^{\infty} \frac{e c D M_n}{4\sqrt{2} \pi R_o \eta_{nm}} R_n(\lambda_{nm} r) \int_{\mu}^{1.0} \Gamma(r) r R_n(\lambda_{nm} r) dr$$

The integral in Equation (A44) can be integrated if the radial distribution of unsteady circulation is known. This circulation is the disturbing force which initiates the propagation of the acoustic wave in the annular duct. Thus, it is seen that for rotor alone noise it is the radial distribution of steady rotor circulation which determines the sound generation. Furthermore, for interaction noise, $\Gamma(r)$ is the radial distribution of unsteady circulation of the type defined by Equations (A6) and (A13). In other words, to obtain an analytic expression for $\Gamma(r)$, the circulation can be computed at three radial points: hub, midspan, and tip, and a curve of the form

$$\Gamma(r) = a_0 + a_1 r + a_2 r^2 \quad (A45)$$

fit to the results.

In general, then, the integral in Equation (A44) will have the form

$$I_j = a_j \int_{\mu}^{1.0} r^{j+1} R_n(\lambda_{nm} r) dr \quad (A46)$$

The integral Equation (A46) can be integrated in closed form.

The expression, Equation (A44), is the acoustic pressure resulting from a given generating mechanism (rotor alone or interaction) at the plane of generation. The evaluation of Equation (A44) requires that a sufficient number of terms in the inner summation on m be taken to provide adequate convergence.

The index m physically denotes the successive radial modes which make up the acoustic wave. In general, it has been found that results requiring three-place accuracy can be obtained with ten to twelve terms of the inner series.

The terms of the outer series are determined by the "spinning lobe" theory developed in Reference 16. The number of lobes is determined by

$$n = B - kV \quad (A47)$$

for the fundamental of rotor blade passing frequency. The index k is summed from $-\infty$ to $+\infty$; therefore, in Equation (A44) the index n is replaced by the expression in Equation (A47) and a sufficient number of terms is taken to insure convergence.

In most cases the measure of acoustic power generated will be of major concern. The power may be computed using the relationship

$$W_{nm} = n R_o^2 \int_{\mu}^{1.0} \frac{P_{nm}^2}{e^2 c} r \, dr \quad (A48)$$

for each (nm) mode. Then

$$W_{nm} = \frac{e_{cD}^2 M_n^2}{16 n \eta_{nm}} \left[\sum_{j=0}^2 I_j \right]^2 \quad (A49)$$

where the orthonormal properties of $R_n(\lambda_{nm} r)$ in the space 1.0 to μ have been employed.

The calculated power can then be represented by power level as

$$\text{PWL} = 10 \log \frac{\sum_n \sum_m W_{nm}}{10^{-13} \text{ watts}} \quad (\text{A50})$$

In summary, evaluation of Equation (A50) provides a prediction of the rotor blade passing frequency tone generated by a rotor or rotor/stator interaction in terms of the basic aerodynamic and geometric variables which define the machine.

Comparison With Test Data

The theoretical model presented above has been programmed for the GE 635 computer. The analytical prediction of the blade passing frequency sound power levels was done for a series of vehicles and compared with test data. Some of these comparisons are reported below.

NASA Two-Stage Quiet Fan. - Data were taken on a two-stage fan (TF39 with the outer panel removed) on a 250 ft. arc in the far field, at the General Electric Test Site at Peebles, Ohio. The results are reported in detail in Reference 21. The comparison with the analytical prediction is shown in Figure A7. One can see that the agreement is quite good.

General Electric Model Fan. - Figure A8 shows the comparison between data measured in the far field and the predicted sound power levels, for a model fan tested at the General Electric Test Site at Peebles, Ohio. The agreement is within 2 dB.

NASA Data Taken on a Test Rig at NASA Langley. - The data were taken in the anechoic chamber at Langley (Reference 22), different configurations with and without IGV's, and with different spacing. The comparison between measured and predicted data is shown in Figure A9. Again, the theoretical model checks the data within 1 dB.

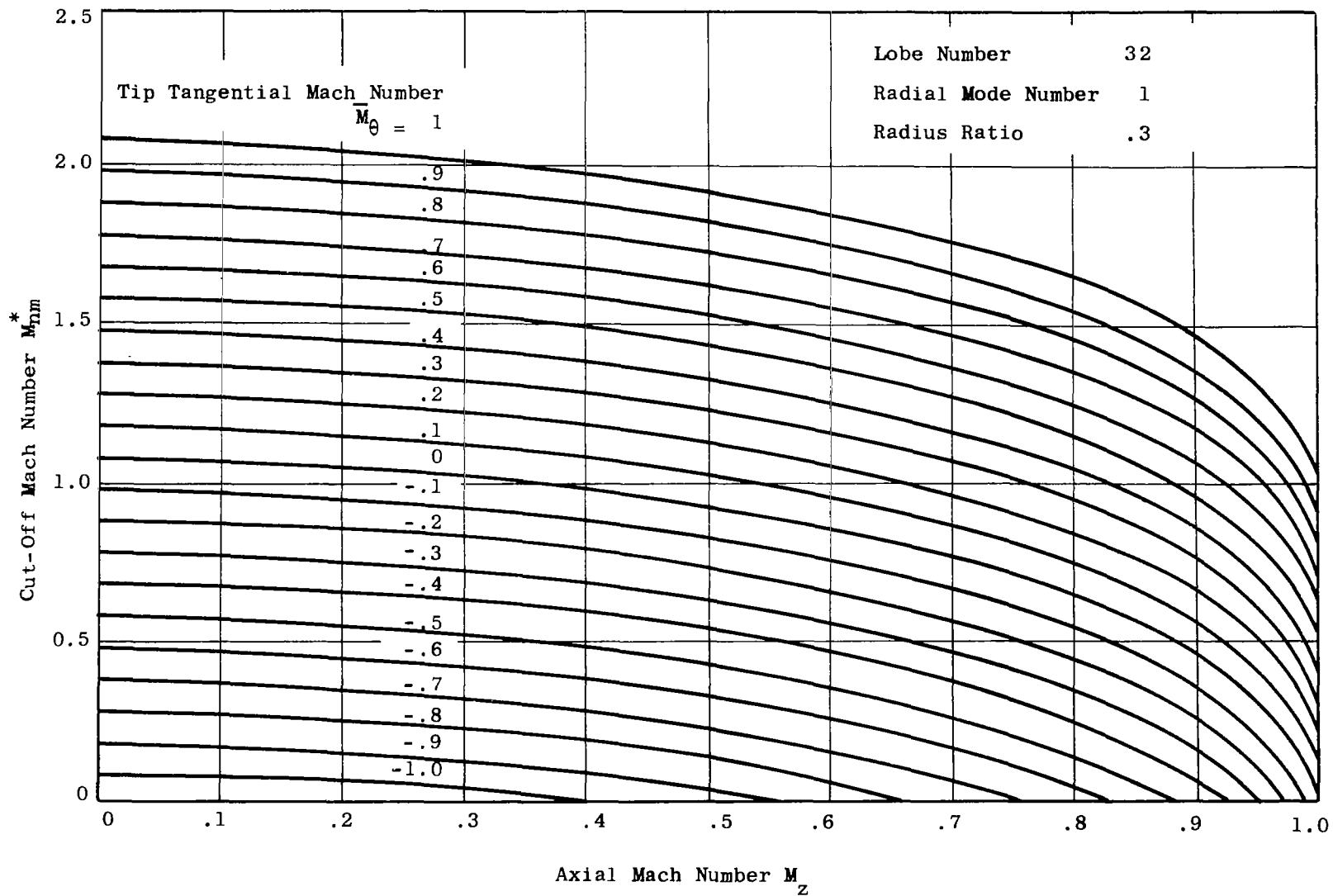


Figure A6. Cut-Off Mach Number Variations With M_z and \bar{M}_{θ}

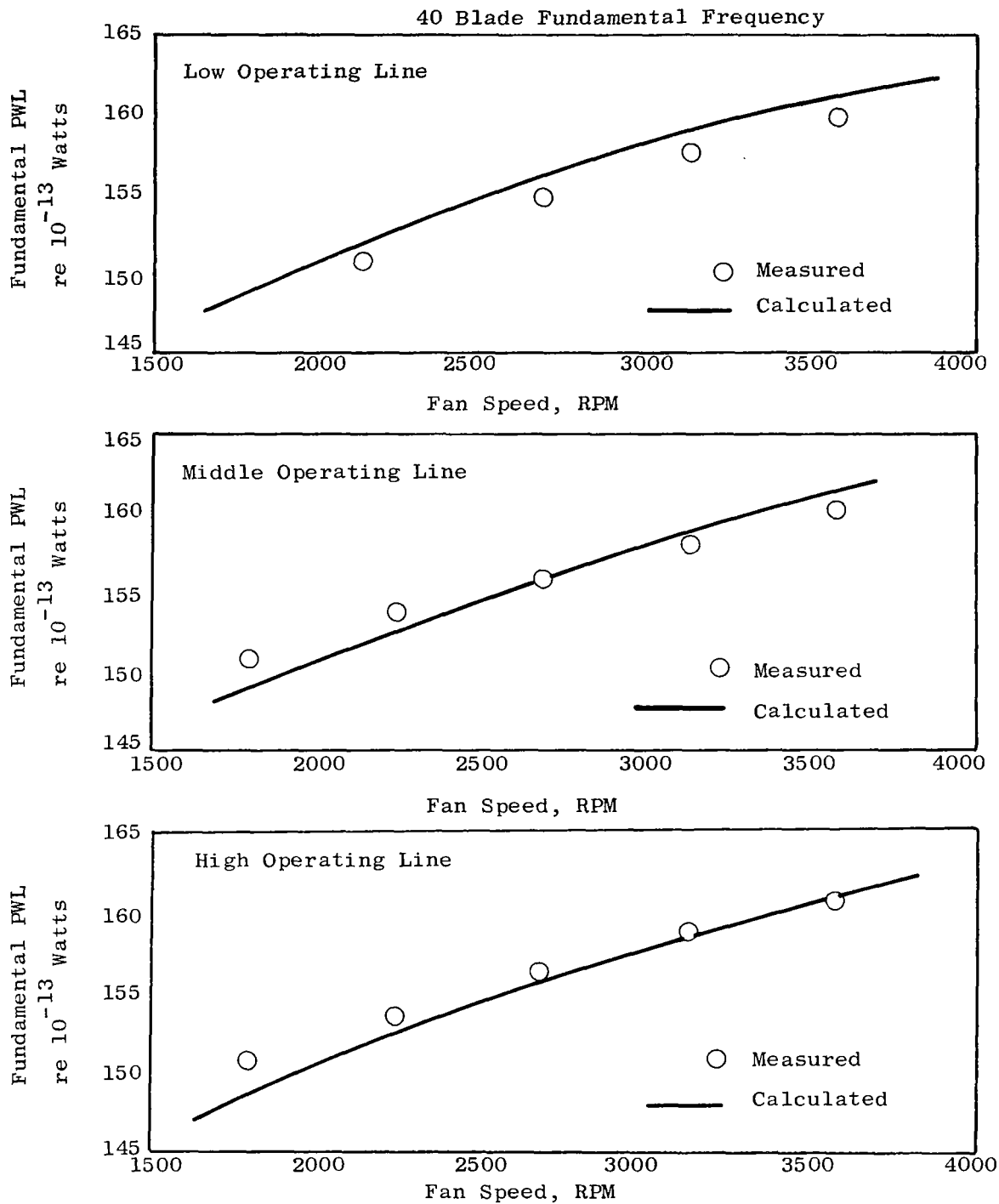


Figure A7. Comparison Between Calculated and Measured Sound Power Levels on the TF39 Inner Panel

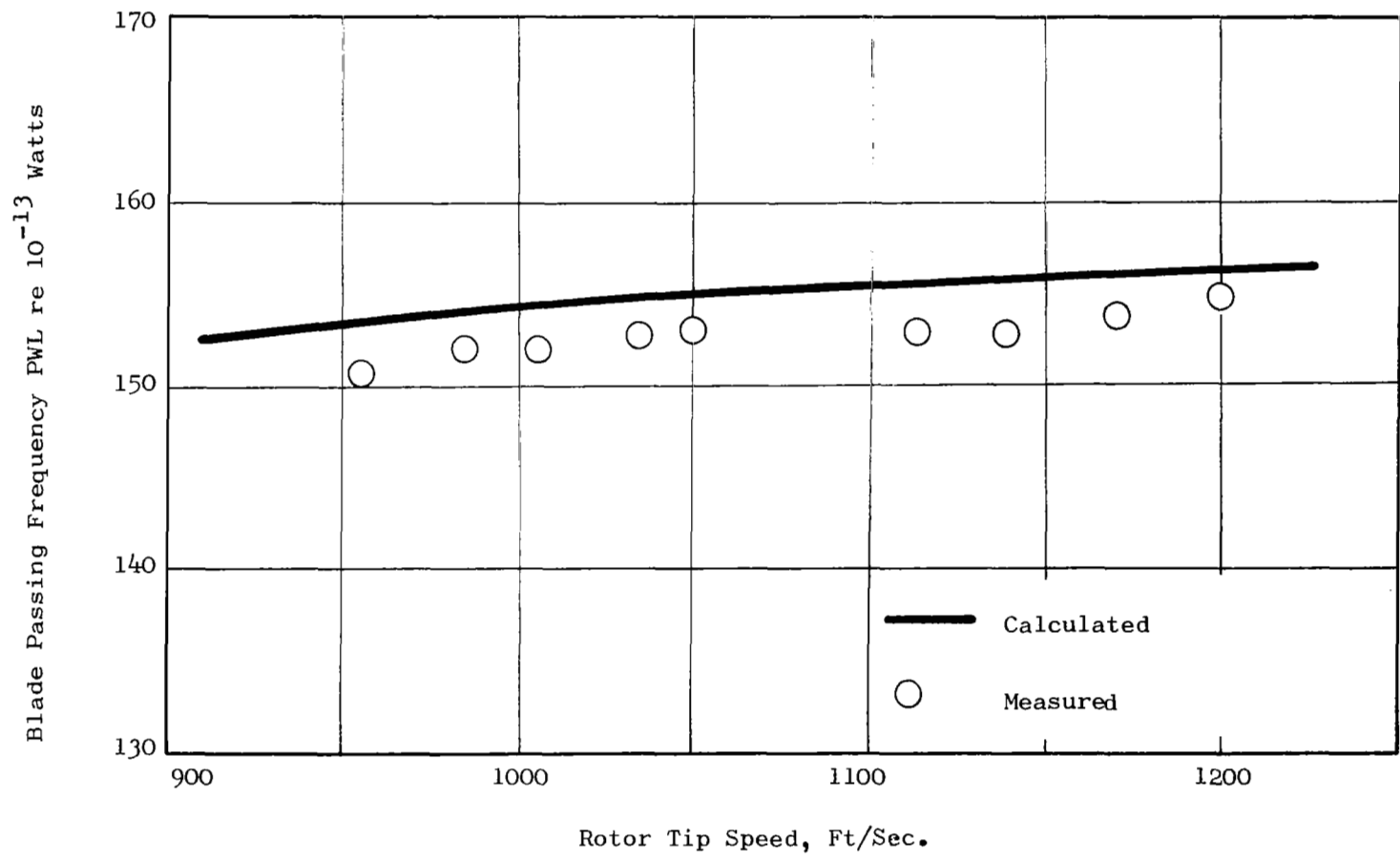


Figure A8. Calculations Compared To Test Data For A Model Turbofan Fundamental PWL

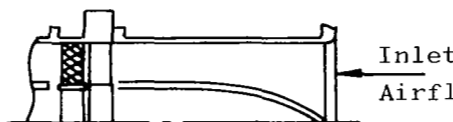
Configuration 1: IGV-Rotor (62 vanes, 53 blades) spacing: 0.535 chord



Measured (NASA Langley) 132 dB

Calculated 132.25 dB

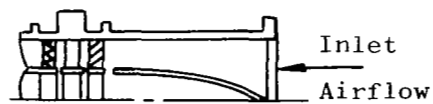
Configuration 2: Rotor-OGV (53 blades, 62 vanes) spacing: 0.535 chord



Measured (NASA Langley) 123 dB

Calculated 123.5 dB

Configuration 3: IGV-Rotor-OGV (62 vanes, 53 blades, 62 vanes) spacing:
(1 R) 0.535 chord, (-0) 0.535 chord



Measured (NASA Langley) 132 dB

Calculated 132.8 dB

Configuration 4: IGV-Rotor-OGV (62 vanes, 53 blades, 62 vanes) spacing:
(1-R) 6.25 chord, (R-0) 0.535 chord



Measured (NASA Langley) 124 dB

Calculated 124 dB

Note: Calculation of PWL from measured SPL was for inlet noise only, and done on the basis of a hemisphere.

Figure A9. Comparison of Measured and Calculated PWL's for NASA 14.75-Inch Diameter Fan With Radius Ratio of 0.727 Operating at Tip Speed of 480 Ft/Sec.

CJ805-23B Turbofan. - Far field data were taken on this aft fan at the General Electric Flight Test Center in California. Figure A10 shows that the predicted levels are within 1.5 dB of the measured data.

LF336 Lift Fan. - A prediction of the perceived noise levels generated by the LF336 lift fan were calculated in November, 1968. The test was conducted at the General Electric Edwards Flight Test Center in January, 1969, and data were taken in the far field. The comparison between predicted and measured data is shown in Figure A11. The predicted and measured data agree very well.

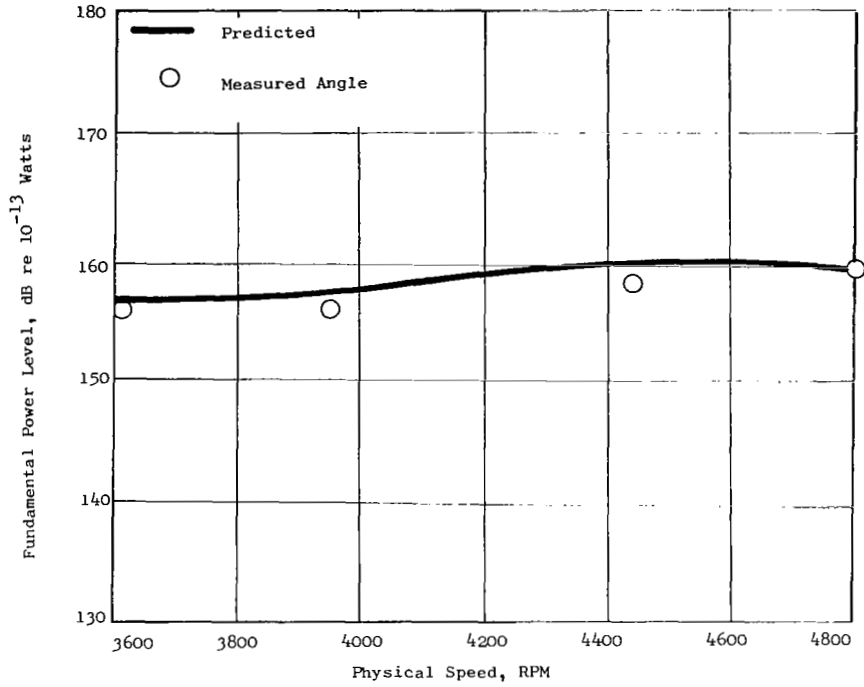


Figure A10. Fundamental PWL - CJ805-23 Calculated and Measured

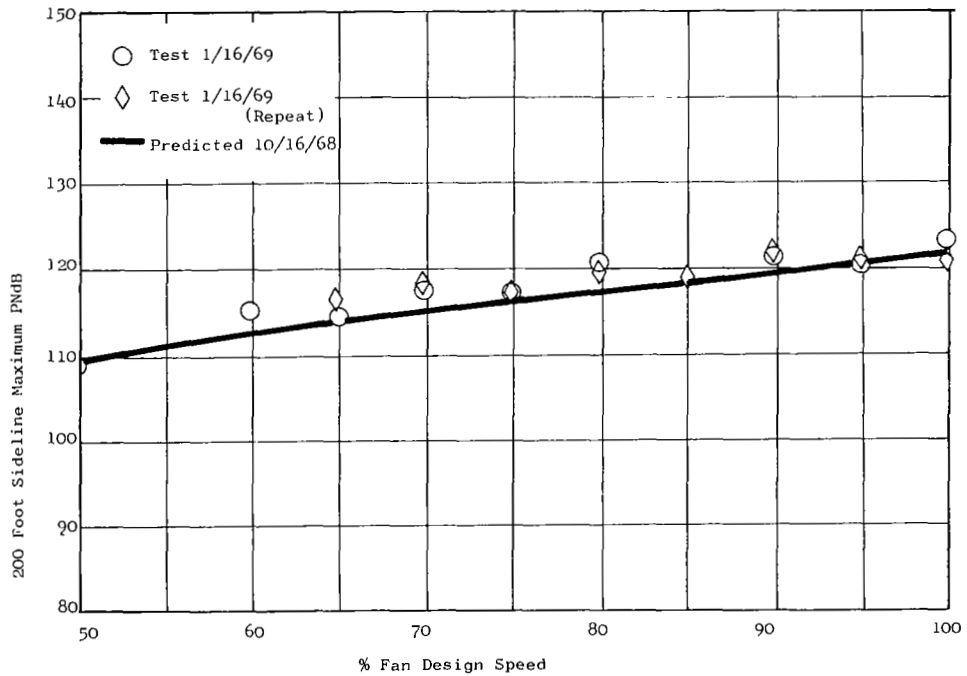


Figure A11. Predicted and Measured Standard Day Max 200' Sideline PNdB For The LF-336A.

APPENDIX B

This appendix contains the aero-acoustic data used to calculate the fan parametric noise curves shown in Figures 9 through 34. The run number on each Appendix B Table refers to the run logs of Tables VI and VII.

Table B1 OGV Fan Aero-Acoustic Data for Run 1

Pressure Ratio	1.20		
Radius Ratio	0.40		
Fan Tip Speed, fps	1114		
Fan Tip Diameter, inches	75.0		
Number of Rotor Blades	66		
Number of Stator Vanes	36		
Vane/Blade Ratio	0.55		
Rotor-Stator Tip Spacing, in blade chords	0.23		
	HUB	PITCH	TIP
Rotor Inlet Radius, inches	15.0	26.3	37.5
Rotor Inlet Absolute Air Angle, α_1 , deg	0	0	0
Rotor Inlet Relative Air Angle, β_1 , deg	31.4	53.0	58.5
Rotor Exit Absolute Air Angle, α_2 , deg	37.4	24.0	21.8
Rotor Exit Relative Air Angle, β_2 , deg	0	47.4	53.0
Rotor Inlet Speed, U_1 , fps	446	780	1114
Rotor Exit Speed, U_2 , fps	464	775	1086
Rotor Blade Chord, C_r , inches	4.75	4.76	4.78
Stator Vane Chord, C_s , inches	5.30	5.30	5.30
Rotor Solidity, σ_r	3.33	2.33	1.34
Stator Solidity, σ_s	2.15	1.51	.864
Rotor Diffusion Factor, D_r	0.38	0.28	0.27
Stator Diffusion Factor, D_s	0.40	0.24	0.38
Rotor Drag Coefficient, C_{dr}	0.0327	0.0217	0.0215
Rotor-Stator Spacing, inches	0.90	1.00	1.10

Table B2 OGV Fan Aero-Acoustic Data for Run 2

Pressure Ratio	1.30		
Radius Ratio	0.41		
Fan Tip Speed, fps	1114		
Fan Tip Diameter, inches	75.0		
Number of Rotor Blades	66		
Number of Stator Vanes	36		
Vane/Blade Ratio	0.55		
Rotor-Stator Tip Spacing, in blade chords	0.23		
	HUB	PITCH	TIP
Rotor Inlet Radius, inches	15.4	26.5	37.5
Rotor Inlet Absolute Air Angle, α_1 , deg	0	0	0
Rotor Inlet Relative Air Angle, β_1 , deg	35.08	53.5	58.5
Rotor Exit Absolute Air Angle, α_2 , deg	35.97	26.93	23.58
Rotor Exit Relative Air Angle, β_2 , deg	0	39.49	44.71
Rotor Inlet Speed, U_1 , fps	457	786	1114
Rotor Exit Speed, U_2 , fps	465	780	1096
Rotor Blade Chord, C_r , inches	4.12	4.45	4.78
Stator Vane Chord, C_s , inches	5.30	5.30	5.30
Rotor Solidity, σ_r	2.89	2.12	1.34
Stator Solidity, σ_s	1.86	1.36	.864
Rotor Diffusion Factor, D_r	0.270	0.285	0.286
Stator Diffusion Factor, D_s	0.420	0.274	0.396
Rotor Drag Coefficient, C_{dr}	0.024	0.029	0.034
Rotor-Stator Spacing, inches	0.90	1.00	1.10

Table B3 OGV Fan Aero-Acoustic Data for Run 4

Pressure Ratio	1.39		
Radius Ratio	0.45		
Fan Tip Speed, fps	1114		
Fan Tip Diameter, inches	75.0		
Number of Rotor Blades	66		
Number of Stator Vanes	36		
Vane/Blade Ratio	0.55		
Rotor-Stator Tip Spacing, in blade chords	0.23		
	HUB	PITCH	TIP
Rotor Inlet Radius, inches	16.88	27.2	37.5
Rotor Inlet Absolute Air Angle, α_1 , deg	0	0	0
Rotor Inlet Relative Air Angle, β_1 , deg	38.3	51.72	60.8
Rotor Exit Absolute Air Angle, α_2 , deg	39.05	34.80	31.75
Rotor Exit Relative Air Angle, β_2 , deg	0	26.63	39.67
Rotor Inlet Speed, U_1 , fps	501	808	1114
Rotor Exit Speed, U_2 , fps	535	796	1057
Rotor Blade Chord, C_r , inches	3.77	4.28	4.78
Stator Vane Chord, C_s , inches	5.30	5.30	5.30
Rotor Solidity, σ_r	2.35	1.65	1.34
Stator Solidity, σ_s	1.67	1.14	0.864
Rotor Diffusion Factor, D_r	0.322	0.399	0.390
Stator Diffusion Factor, D_s	0.243	0.380	0.505
Rotor Drag Coefficient, C_{dr}	0.0315	0.0528	0.0615
Rotor-Stator Spacing, inches	0.90	1.00	1.10

Table B4 OGV Fan Aero-Acoustic Data for Run 4

Pressure Ratio	1.39		
Radius Ratio	0.63		
Fan Tip Speed, fps	800		
Fan Tip Diameter, inches	75		
Number of Rotor Blades	66		
Number of Stator Vanes	36		
Vane/Blade Ratio	0.55		
Rotor-Stator Tip Spacing, in blade chords	0.23		
	HUB	PITCH	TIP
Rotor Inlet Radius, inches	23.63	30.57	37.5
Rotor Inlet Absolute Air Angle, α_1 , deg	0	0	0
Rotor Inlet Relative Air Angle, β_1 , deg	37.7	46.7	49.5
Rotor Exit Absolute Air Angle, α_2 , deg	35.1	37.8	31.8
Rotor Exit Relative Air Angle, β_2 , deg	0	15.2	19.1
Rotor Inlet Speed, U_1 , fps	504	652	800
Rotor Exit Speed, U_2 , fps	546	653	760
Rotor Blade Chord, C_R , inches	4.25	4.52	4.78
Stator Vane Chord, C_S , inches	5.3	5.3	5.3
Rotor Solidity, σ_R	1.89	1.61	1.34
Stator Solidity, σ_S	1.22	1.04	0.864
Rotor Diffusion Factor, D_R	0.24	0.444	0.381
Stator Diffusion Factor, D_S	0.508	0.399	0.473
Rotor Drag Coefficient, C_{dr}	0.023	0.064	0.051
Rotor-Stator Spacing, inches	0.90	1.00	1.10

Table B5 OGV Fan Aero-Acoustic Data for Run 5

Pressure Ratio	1.39		
Radius Ratio	0.51		
Fan Tip Speed, fps	1000		
Fan Tip Diameter, inches	75		
Number of Rotor Blades	66		
Number of Stator Vanes	36		
Vane/Blade Ratio	0.55		
Rotor-Stator Tip Spacing, in blade chords	0.23		
	HUB	PITCH	TIP
Rotor Inlet Radius, inches	19.13	28.31	37.5
Rotor Inlet Absolute Air Angle, α_1 , deg	0	0	0
Rotor Inlet Relative Air Angle, β_1 , deg	37.3	51.5	55.7
Rotor Exit Absolute Air Angle, α_2 , deg	35.2	31.8	26.3
Rotor Exit Relative Air Angle, β_2 , deg	0	28.0	32.9
Rotor Inlet Speed, U_1 , fps	510	755	1000
Rotor Exit Speed, U_2 , fps	547	749	950
Rotor Blade Chord, C_R , inches	4.28	4.53	4.78
Stator Vane Chord, C_S , inches	5.3	5.3	5.3
Rotor Solidity, σ_R	2.35	1.85	1.34
Stator Solidity, σ_S	1.52	1.19	0.864
Rotor Diffusion Factor, D_R	0.205	0.336	0.308
Stator Diffusion Factor, D_S	0.461	0.329	0.425
Rotor Drag Coefficient, C_{dr}	0.020	0.041	0.041
Rotor-Stator Spacing, inches	0.90	1.00	1.10

Table B6 OGV Fan Aero-Acoustic Data for Run 6			
Pressure Ratio	1.39		
Radius Ratio	0.41		
Fan Tip Speed, fps	1200		
Fan Tip Diameter, inches	75		
Number of Rotor Blades	66		
Number of Stator Vanes	36		
Vane/Blade Ratio	0.55		
Rotor-Stator Tip Spacing, in blade chords	0.23		
	HUB	PITCH	TIP
Rotor Inlet Radius, inches	15.38	26.40	37.5
Rotor Inlet Absolute Air Angle, α_1 , deg	0	0	0
Rotor Inlet Relative Air Angle, β_1 , deg	37.86	55.63	60.38
Rotor Exit Absolute Air Angle, α_2 , deg	35.26	28.2	25.2
Rotor Exit Relative Air Angle, β_2 , deg	0	36.82	40.91
Rotor Inlet Speed, U_1 , fps	492	846	1200
Rotor Exit Speed, U_2 , fps	549	845	1140
Rotor Blade Chord, C_R , inches	4.12	4.50	4.78
Stator Vane Chord, C_S , inches	5.3	5.3	5.3
Rotor Solidity, σ_R	2.816	2.08	1.34
Stator Solidity, σ_S	1.82	1.34	0.864
Rotor Diffusion Factor, D_R	0.184	0.272	0.297
Stator Diffusion Factor, D_S	0.431	0.286	0.418
Rotor Drag Coefficient, C_{dr}	0.0193	0.033	0.0419
Rotor-Stator Spacing, inches	0.90	1.00	1.10

Table B7 OGV Fan Aero-Acoustic Data for Run 7			
Pressure Ratio	1.39		
Radius Ratio	0.45		
Fan Tip Speed, fps	1114		
Fan Tip Diameter, inches	36		
Number of Rotor Blades	66		
Number of Stator Vanes	36		
Vane/Blade Ratio	0.55		
Rotor-Stator Tip Spacing, in blade chords	0.23		
	HUB	PITCH	TIP
Rotor Inlet Radius, inches	8.10	13.91	18.00
Rotor Inlet Absolute Air Angle, α_1 , deg	0	0	0
Rotor Inlet Relative Air Angle, β_1 , deg	38.3	51.72	60.8
Rotor Exit Absolute Air Angle, α_2 , deg	39.05	34.80	31.75
Rotor Exit Relative Air Angle, β_2 , deg	0	26.63	39.67
Rotor Inlet Speed, U_1 , fps	501	808	1114
Rotor Exit Speed, U_2 , fps	535	796	1050
Rotor Blade Chord, C_R , inches	1.81	2.05	2.29
Stator Vane Chord, C_S , inches	2.55	2.55	2.55
Rotor Solidity, σ_R	2.35	1.65	1.34
Stator Solidity, σ_S	1.67	1.14	0.864
Rotor Diffusion Factor, D_R	0.322	0.399	0.390
Stator Diffusion Factor, D_S	0.243	0.380	0.505
Rotor Drag Coefficient, C_{dr}	0.0315	0.0528	0.0615
Rotor-Stator Spacing, inches	0.481	0.533	0.587

Table B8 OGV Fan Aero-Acoustic Data for Run 8			
Pressure Ratio	1.39		
Radius Ratio	0.45		
Fan Tip Speed, fps	1114		
Fan Tip Diameter, inches	50		
Number of Rotor Blades	66		
Number of Stator Vanes	36		
Vane/Blade Ratio	0.55		
Rotor-Stator Tip Spacing, in blade chords	0.23		
	HUB	PITCH	TIP
Rotor Inlet Radius, inches	11.25	19.3	25.0
Rotor Inlet Absolute Air Angle, α_1 , deg	0	0	0
Rotor Inlet Relative Air Angle, β_1 , deg	38.3	51.72	60.8
Rotor Exit Absolute Air Angle, α_2 , deg	39.05	34.80	31.75
Rotor Exit Relative Air Angle, β_2 , deg	0	26.63	39.67
Rotor Inlet Speed, U_1 , fps	501	808	1114
Rotor Exit Speed, U_2 , fps	535	796	1057
Rotor Blade Chord, C_r , inches	2.52	2.86	3.19
Stator Vane Chord, C_s , inches	3.53	3.53	3.53
Rotor Solidity, σ_r	2.35	1.65	1.34
Stator Solidity, σ_s	1.67	1.14	0.864
Rotor Diffusion Factor, D_r	0.322	0.399	0.390
Stator Diffusion Factor, D_s	0.243	0.380	0.505
Rotor Drag Coefficient, C_{dr}	0.0315	0.0528	0.0615
Rotor-Stator Spacing, inches	0.602	0.668	0.734

Table B9 OGV Fan Aero-Acoustic Data for Run 9			
Pressure Ratio	1.39		
Radius Ratio	0.45		
Fan Tip Speed, fps	1114		
Fan Tip Diameter, inches	100		
Number of Rotor Blades	66		
Number of Stator Vanes	36		
Vane/Blade Ratio	0.55		
Rotor-Stator Tip Spacing, in blade chords	0.23		
	HUB	PITCH	TIP
Rotor Inlet Radius, inches	22.5	38.7	50.0
Rotor Inlet Absolute Air Angle, α_1 , deg	0	0	0
Rotor Inlet Relative Air Angle, β_1 , deg	38.3	51.72	60.8
Rotor Exit Absolute Air Angle, α_2 , deg	39.05	34.80	31.75
Rotor Exit Relative Air Angle, β_2 , deg	0	26.63	39.67
Rotor Inlet Speed, U_1 , fps	501	808	1114
Rotor Exit Speed, U_2 , fps	535	796	1057
Rotor Blade Chord, C_r , inches	5.04	5.72	6.38
Stator Vane Chord, C_s , inches	7.06	7.06	7.06
Rotor Solidity, σ_r	2.35	1.65	1.34
Stator Solidity, σ_s	1.67	1.14	0.864
Rotor Diffusion Factor, D_r	0.322	0.399	0.390
Stator Diffusion Factor, D_s	0.243	0.380	0.505
Rotor Drag Coefficient, C_{dr}	0.0315	0.0528	0.0615
Rotor-Stator Spacing, inches	1.204	1.336	1.468

Table B10 OGV Fan Aero-Acoustic Data for Run 10

Pressure Ratio	1.39		
Radius Ratio	0.45		
Fan Tip Speed, fps	1114		
Fan Tip Diameter, inches	75		
Number of Rotor Blades	20		
Number of Stator Vanes	11		
Vane/Blade Ratio	0.55		
Rotor-Stator Tip Spacing, in blade chords	0.23		
	HUB	PITCH	TIP
Rotor Inlet Radius, inches	16.88	27.2	37.5
Rotor Inlet Absolute Air Angle, α_1 , deg	0	0	0
Rotor Inlet Relative Air Angle, β_1 , deg	38.3	51.72	60.8
Rotor Exit Absolute Air Angle, α_2 , deg	39.05	34.80	31.75
Rotor Exit Relative Air Angle β_2 , deg	0	26.63	39.67
Rotor Inlet Speed, U_1 , fps	501	808	1114
Rotor Exit Speed, U_2 , fps	535	796	1057
Rotor Blade Chord, C_r , inches	12.46	14.09	15.78
Stator Vane Chord, C_s , inches	5.30	5.30	5.30
Rotor Solidity, σ_r	2.35	1.65	1.34
Stator Solidity, σ_s	1.67	1.14	0.864
Rotor Diffusion Factor, D_r	0.322	0.399	0.390
Stator Diffusion Factor, D_s	0.243	0.380	0.505
Rotor Drag Coefficient, C_{dr}	0.0315	0.0528	0.0615
Rotor-Stator Spacing, inches	2.97	3.30	3.63

Table B11 OGV Fan Aero-Acoustic Data for Run 11

Pressure Ratio	1.39		
Radius Ratio	0.45		
Fan Tip Speed, fps	1114		
Fan Tip Diameter, inches	75		
Number of Rotor Blades	80		
Number of Stator Vanes	44		
Vane/Blade Ratio	0.55		
Rotor-Stator Tip Spacing, in blade chords	0.23		
	HUB	PITCH	TIP
Rotor Inlet Radius, inches	16.88	27.2	37.5
Rotor Inlet Absolute Air Angle, α_1 , deg	0	0	0
Rotor Inlet Relative Air Angle, β_1 , deg	38.3	51.72	60.8
Rotor Exit Absolute Air Angle, α_2 , deg	39.05	34.80	31.75
Rotor Exit Relative Air Angle β_2 , deg	0	26.63	39.67
Rotor Inlet Speed, U_1 , fps	501	808	1114
Rotor Exit Speed, U_2 , fps	535	796	1057
Rotor Blade Chord, C_r , inches	3.11	3.52	3.94
Stator Vane Chord, C_s , inches	5.30	5.30	5.30
Rotor Solidity, σ_r	2.35	1.65	1.34
Stator Solidity, σ_s	1.67	1.14	0.864
Rotor Diffusion Factor, D_r	0.322	0.399	0.390
Stator Diffusion Factor, D_s	0.243	0.380	0.505
Rotor Drag Coefficient, C_{dr}	0.0315	0.0528	0.0615
Rotor-Stator Spacing, inches	0.742	0.823	0.906

Table B12 OGV Fan Aero-Acoustic Data for Run 12

Pressure Ratio	1.39		
Radius Ratio	0.45		
Fan Tip Speed, fps	1114		
Fan Tip Diameter, inches	75		
Number of Rotor Blades	66		
Number of Stator Vanes	9.9		
Vane/Blade Ratio	1.5		
Rotor-Stator Tip Spacing, in blade chords	0.23		
	HUB	PITCH	TIP
Rotor Inlet Radius, inches	16.88	27.2	37.5
Rotor Inlet Absolute Air Angle, α_1 , deg	0	0	0
Rotor Inlet Relative Air Angle, β_1 , deg	38.3	51.72	60.8
Rotor Exit Absolute Air Angle, α_2 , deg	39.05	34.80	31.75
Rotor Exit Relative Air Angle, β_2 , deg	0	26.63	39.67
Rotor Inlet Speed, U_1 , fps	501	808	1114
Rotor Exit Speed, U_2 , fps	535	796	1057
Rotor Blade Chord, C_r , inches	3.77	4.28	4.78
Stator Vane Chord, C_s , inches	1.91	1.91	1.91
Rotor Solidity, σ_r	2.35	1.65	1.34
Stator Solidity, σ_s	1.67	1.14	0.864
Rotor Diffusion Factor, D_r	0.322	0.399	0.390
Stator Diffusion Factor, D_s	0.243	0.380	0.505
Rotor Drag Coefficient, C_{dr}	0.0315	0.0528	0.0615
Rotor-Stator Spacing, inches	0.90	1.00	1.10

Table B13 OGV Fan Aero-Acoustic Data for Run 13

Pressure Ratio	1.39		
Radius Ratio	0.45		
Fan Tip Speed, fps	1114		
Fan Tip Diameter, inches	75		
Number of Rotor Blades	66		
Number of Stator Vanes	138.6		
Vane/Blade Ratio	2.1		
Rotor-Stator Tip Spacing, in blade chords	0.23		
	HUB	PITCH	TIP
Rotor Inlet Radius, inches	16.88	27.2	37.5
Rotor Inlet Absolute Air Angle, α_1 , deg	0	0	0
Rotor Inlet Relative Air Angle, β_1 , deg	38.3	51.72	60.8
Rotor Exit Absolute Air Angle, α_2 , deg	39.05	34.80	31.75
Rotor Exit Relative Air Angle, β_2 , deg	0	26.63	39.67
Rotor Inlet Speed, U_1 , fps	501	808	1114
Rotor Exit Speed, U_2 , fps	535	796	1057
Rotor Blade Chord, C_r , inches	3.77	4.28	4.78
Stator Vane Chord, C_s , inches	1.37	1.37	1.37
Rotor Solidity, σ_r	2.35	1.65	1.34
Stator Solidity, σ_s	1.67	1.14	0.864
Rotor Diffusion Factor, D_r	0.322	0.399	0.390
Stator Diffusion Factor, D_s	0.243	0.380	0.505
Rotor Drag Coefficient, C_{dr}	0.0315	0.0528	0.0615
Rotor-Stator Spacing, inches	0.90	1.00	1.10

Table B14 OGV Fan Aero-Acoustic Data for Run 14

Pressure Ratio	1.39		
Radius Ratio	0.45		
Fan Tip Speed, fps	1114		
Fan Tip Diameter, inches	75		
Number of Rotor Blades	66		
Number of Stator Vanes	36		
Vane/Blade Ratio	0.55		
Rotor-Stator Tip Spacing, in blade chords	0.10		
	HUB	PITCH	TIP
Rotor Inlet Radius, inches	16.88	27.2	37.5
Rotor Inlet Absolute Air Angle, α_1 , deg	0	0	0
Rotor Inlet Relative Air Angle, β_1 , deg	38.3	51.72	60.8
Rotor Exit Absolute Air Angle, α_2 , deg	39.05	34.80	31.75
Rotor Exit Relative Air Angle, β_2 , deg	0	26.63	39.67
Rotor Inlet Speed, U_1 , fps	501	808	1114
Rotor Exit Speed, U_2 , fps	535	796	1057
Rotor Blade Chord, C_r , inches	3.77	4.28	4.78
Stator Vane Chord, C_s , inches	5.30	5.30	5.30
Rotor Solidity, σ_r	2.35	1.65	1.34
Stator Solidity, σ_s	1.67	1.14	0.864
Rotor Diffusion Factor, D_r	0.322	0.399	0.390
Stator Diffusion Factor, D_s	0.243	0.380	0.505
Rotor Drag Coefficient, C_{dr}	0.0315	0.0528	0.0615
Rotor-Stator Spacing, inches	0.391	0.435	0.478

Table B15 OGV Fan Aero-Acoustic Data for Run 15

Pressure Ratio	1.39		
Radius Ratio	0.45		
Fan Tip Speed, fps	1114		
Fan Tip Diameter, inches	75		
Number of Rotor Blades	66		
Number of Stator Vanes	36		
Vane/Blade Ratio	0.55		
Rotor-Stator Tip Spacing, in blade chords	1.0		
	HUB	PITCH	TIP
Rotor Inlet Radius, inches	16.88	27.2	37.5
Rotor Inlet Absolute Air Angle, α_1 , deg	0	0	0
Rotor Inlet Relative Air Angle, β_1 , deg	38.3	51.72	60.8
Rotor Exit Absolute Air Angle, α_2 , deg	39.05	34.80	31.75
Rotor Exit Relative Air Angle, β_2 , deg	0	26.63	39.67
Rotor Inlet Speed, U_1 , fps	501	808	1114
Rotor Exit Speed, U_2 , fps	535	796	1057
Rotor Blade Chord, C_r , inches	3.77	4.28	4.78
Stator Vane Chord, C_s , inches	5.30	5.30	5.30
Rotor Solidity, σ_r	2.35	1.65	1.34
Stator Solidity, σ_s	1.67	1.14	0.864
Rotor Diffusion Factor, D_r	0.322	0.399	0.390
Stator Diffusion Factor, D_s	0.243	0.380	0.505
Rotor Drag Coefficient, C_{dr}	0.0315	0.0528	0.0615
Rotor-Stator Spacing, inches	3.91	4.34	4.78

Table B16 OGV Fan Aero-Acoustic Data for Run 16			
Pressure Ratio	1.39		
Radius Ratio	0.45		
Fan Tip Speed, fps	1114		
Fan Tip Diameter, inches	75		
Number of Rotor Blades	66		
Number of Stator Vanes	36		
Vane/Blade Ratio	0.55		
Rotor-Stator Tip Spacing, in blade chords	2.0		
	HUB	PITCH	TIP
Rotor Inlet Radius, inches	16.88	27.2	37.5
Rotor Inlet Absolute Air Angle, α_1 , deg	0	0	0
Rotor Inlet Relative Air Angle, β_1 , deg	38.3	51.72	60.8
Rotor Exit Absolute Air Angle, α_2 , deg	39.05	34.80	31.75
Rotor Exit Relative Air Angle, β_2 , deg	0	26.63	39.67
Rotor Inlet Speed, U_1 , fps	501	808	1114
Rotor Exit Speed, U_2 , fps	535	796	1057
Rotor Blade Chord, C_r , inches	3.77	4.28	4.78
Stator Vane Chord, C_s , inches	5.30	5.30	5.30
Rotor Solidity, σ_r	2.35	1.65	1.34
Stator Solidity, σ_s	1.67	1.14	0.864
Rotor Diffusion Factor, D_r	0.322	0.399	0.390
Stator Diffusion Factor, D_s	0.243	0.380	0.505
Rotor Drag Coefficient, C_{dr}	0.0315	0.0528	0.0615
Rotor-Stator Spacing, inches	7.82	8.69	9.56

Table B17 IGV Fan Aero-Acoustic Data for Run 1			
Pressure Ratio	1.15		
Radius Ratio	0.40		
Fan Tip Speed, fps	1000		
Fan Tip Diameter, inches	86.5		
Number of Rotor Blades	40		
Number of Stator Vanes	28		
Vane/Blade Ratio	0.70		
Rotor-Stator Tip Spacing, in vane chords	0.20		
	HUB	PITCH	TIP
Rotor Inlet Radius, inches	17.30	30.28	43.25
Rotor Inlet Absolute Air Angle, α_1 , deg	-32.15	-17.48	-14.42
Rotor Inlet Relative Air Angle, β_1 , deg	52.43	56.99	63.14
Rotor Exit Absolute Air Angle, α_2 , deg	0	0	0
Rotor Exit Relative Air Angle, β_2 , deg	30.9	51.3	52.1
Rotor Inlet Speed, U_1 , fps	400	763	1000
Rotor Exit Speed, U_2 , fps	437	751	962
Rotor Blade Chord, C_r , inches	5.21	5.71	6.04
Stator Vane Chord, C_s , inches	7.5	7.5	7.5
Rotor Solidity, σ_r	1.92	1.20	0.890
Stator Solidity, σ_s	2.18	1.10	0.75
Rotor Diffusion Factor, D_r	0.267	0.235	0.167
Stator Diffusion Factor, D_s	-0.334	-0.213	-0.151
Stator Drag Coefficient, C_{ds}	0.0310	0.0443	0.0557
Rotor-Stator Spacing, inches	0.75	1.10	1.50

Table B18 IGV Fan Aero-Acoustic Data for Run 2			
Pressure Ratio	1.26		
Radius Ratio	0.45		
Fan Tip Speed, fps	1000		
Fan Tip Diameter, inches	86.5		
Number of Rotor Blades	40		
Number of Stator Vanes	28		
Vane/Blade Ratio	0.70		
Rotor-Stator Tip Spacing, in vane chords	0.20		
	HUB	PITCH	TIP
Rotor Inlet Radius, inches	19.46	31.36	43.25
Rotor Inlet Absolute Air Angle, α_1 , deg	-46.4	-27.2	-25.0
Rotor Inlet Relative Air Angle, β_1 , deg	61.5	59.3	65.6
Rotor Exit Absolute Air Angle, α_2 , deg	0	0	0
Rotor Exit Relative Air Angle, β_2 , deg	46.9	54.3	59.3
Rotor Inlet Speed, U_1 , fps	450	781	1000
Rotor Exit Speed, U_2 , fps	499	769	964
Rotor Blade Chord, C_R , inches	5.87	5.95	6.04
Stator Vane Chord, C_S , inches	7.5	7.5	7.5
Rotor Solidity, σ_R	1.92	1.21	0.89
Stator Solidity, σ_S	2.18	1.11	0.75
Rotor Diffusion Factor, D_R	0.451	0.336	0.313
Stator Diffusion Factor, D_S	-0.738	-0.364	-0.334
Stator Drag Coefficient, C_{ds}	0.0504	0.0666	0.0939
Rotor-Stator Spacing, inches	0.75	1.10	1.50

Table B19 IGV Fan Aero-Acoustic Data for Run 3			
Pressure Ratio	1.30		
Radius Ratio	0.468		
Fan Tip Speed, fps	1000		
Fan Tip Diameter, inches	86.5		
Number of Rotor Blades	40		
Number of Stator Vanes	28		
Vane/Blade Ratio	0.70		
Rotor-Stator Tip Spacing, in vane chords	0.20		
	HUB	PITCH	TIP
Rotor Inlet Radius, inches	20.24	31.75	43.25
Rotor Inlet Absolute Air Angle, α_1 , deg	-45.5	-26.7	-28.0
Rotor Inlet Relative Air Angle, β_1 , deg	60.7	57.4	67.1
Rotor Exit Absolute Air Angle, α_2 , deg	0	0	0
Rotor Exit Relative Air Angle, β_2 , deg	37.5	50.0	56.5
Rotor Inlet Speed, U_1 , fps	467	781	1000
Rotor Exit Speed, U_2 , fps	536	759	943
Rotor Blade Chord, C_R , inches	6.04	6.04	6.04
Stator Vane Chord, C_S , inches	7.5	7.5	7.5
Rotor Solidity, σ_R	1.92	1.23	0.89
Stator Solidity, σ_S	2.18	1.11	0.75
Rotor Diffusion Factor, D_R	0.331	0.353	0.326
Stator Diffusion Factor, D_S	-0.846	-0.531	-0.388
Stator Drag Coefficient, C_{ds}	.0574	0.0857	0.107
Rotor-Stator Spacing, inches	0.75	1.10	1.50

Table B20 IGV Fan Aero-Acoustic Data for Run 4

Pressure Ratio	1.26		
Radius Ratio	0.55		
Fan Tip Speed, fps	800		
Fan Tip Diameter, inches	86.5		
Number of Rotor Blades	40		
Number of Stator Vanes	28		
Vane/Blade Ratio	0.70		
Rotor-Stator Tip Spacing, in vane chords	0.20		
	HUB	PITCH	TIP
Rotor Inlet Radius, inches	23.96	33.61	43.25
Rotor Inlet Absolute Air Angle, α_1 , deg	-41.1	-29.9	-26.8
Rotor Inlet Relative Air Angle, β_1 , deg	57.0	56.7	60.5
Rotor Exit Absolute Air Angle, α_2 , deg	0	0	0
Rotor Exit Relative Air Angle, β_2 , deg	37.1	47.7	49.5
Rotor Inlet Speed, U_1 , fps	444	651	800
Rotor Exit Speed, U_2 , fps	481	639	768
Rotor Blade Chord, C_r , inches	5.87	5.95	6.04
Stator Vane Chord, C_s , inches	7.5	7.5	7.5
Rotor Solidity, σ_r	1.92	1.21	0.890
Stator Solidity, σ_s	2.18	1.11	0.75
Rotor Diffusion Factor, D_r	0.390	0.388	0.361
Stator Diffusion Factor, D_s	-0.870	-0.553	-0.591
Stator Drag Coefficient, C_{ds}	0.0601	0.0927	0.1531
Rotor-Stator Spacing, inches	0.75	1.10	1.50

Table B21 IGV Fan Aero-Acoustic Data for Run 5

Pressure Ratio	1.26		
Radius Ratio	0.410		
Fan Tip Speed, fps	1100		
Fan Tip Diameter, inches	86.5		
Number of Rotor Blades	40		
Number of Stator Vanes	28		
Vane/Blade Ratio	0.70		
Rotor-Stator Tip Spacing in vane chords	0.20		
	HUB	PITCH	TIP
Rotor Inlet Radius, inches	17.73	30.49	43.25
Rotor Inlet Absolute Air Angle, α_1 , deg	-38.9	-25.2	-26.1
Rotor Inlet Relative Air Angle, β_1 , deg	54.7	59.1	69.6
Rotor Exit Absolute Air Angle, α_2 , deg	0	0	0
Rotor Exit Relative Air Angle, β_2 , deg	38.1	54.4	54.3
Rotor Inlet Speed, U_1 , fps	450	827	1100
Rotor Exit Speed, U_2 , fps	499	810	1030
Rotor Blade Chord, C_r , inches	5.4	5.8	6.04
Stator Vane Chord, C_s , inches	7.5	7.5	7.5
Rotor Solidity, σ_r	1.92	1.21	0.89
Stator Solidity, σ_s	2.18	1.14	0.75
Rotor Diffusion Factor, D_r	0.389	0.323	0.257
Stator Diffusion Factor, D_s	0.907	0.491	0.353
Stator Drag Coefficient, C_{ds}	0.0647	0.0728	0.0841
Rotor-Stator Spacing, inches	0.75	1.10	1.50

Table B22 IGV Fan Aero-Acoustic Data for Run 6

Pressure Ratio	1.26		
Radius Ratio	0.45		
Fan Tip Speed, fps	1100		
Fan Tip Diameter, inches	36.0		
Number of Rotor Blades	40		
Number of Stator Vanes	28		
Vane/Blade Ratio	0.70		
Rotor-Stator Tip Spacing in vane chords	0.20		
	HUB	PITCH	TIP
Rotor Inlet Radius, inches	8.10	13.05	18
Rotor Inlet Absolute Air Angle, α_1 , deg	-46.4	-27.2	-25.0
Rotor Inlet Relative Air Angle, β_1 , deg	61.5	59.3	65.6
Rotor Exit Absolute Air Angle, α_2 , deg	0	0	0
Rotor Exit Relative Air Angle, β_2 , deg	46.9	54.3	59.3
Rotor Inlet Speed, U_1 , fps	450	725	1000
Rotor Exit Speed, U_2 , fps	499	732	964
Rotor Blade Chord, C_R , inches	2.48	2.49	2.50
Stator Vane Chord, C_S , inches	3.1	3.1	3.1
Rotor Solidity, σ_R	1.92	1.21	0.89
Stator Solidity, σ_S	2.18	1.11	0.75
Rotor Diffusion Factor, D_R	0.451	0.336	0.343
Stator Diffusion Factor, D_S	-0.738	-0.364	-0.334
Stator Drag Coefficient, C_{ds}	0.0504	0.0666	0.0939
Rotor-Stator Spacing, inches	0.31	0.47	0.62

Table B23 IGV Fan Aero-Acoustic Data for Run 7

Pressure Ratio	1.26		
Radius Ratio	0.45		
Fan Tip Speed, fps	1000		
Fan Tip Diameter, inches	50		
Number of Rotor Blades	40		
Number of Stator Vanes	28		
Vane/Blade Ratio	0.70		
Rotor-Stator Tip Spacing in vane chords	0.20		
	HUB	PITCH	TIP
Rotor Inlet Radius, inches	11.25	18.13	25.0
Rotor Inlet Absolute Air Angle, α_1 , deg	-46.4	-27.2	-25.0
Rotor Inlet Relative Air Angle, β_1 , deg	61.5	59.3	65.6
Rotor Exit Absolute Air Angle, α_2 , deg	0	0	0
Rotor Exit Relative Air Angle, β_2 , deg	46.9	54.3	59.3
Rotor Inlet Speed, U_1 , fps	450	725	1000
Rotor Exit Speed, U_2 , fps	499	732	964
Rotor Blade Chord, C_R , inches	3.46	3.47	3.48
Stator Vane Chord, C_S , inches	4.3	4.3	4.3
Rotor Solidity, σ_R	1.92	1.21	0.89
Stator Solidity, σ_S	2.18	1.11	0.75
Rotor Diffusion Factor, D_R	0.451	0.336	0.313
Stator Diffusion Factor, D_S	-0.738	-0.364	-0.334
Stator Drag Coefficient, C_{ds}	0.0504	0.0666	0.0939
Rotor-Stator Spacing, inches	0.43	0.70	0.90

Pressure Ratio	1.26		
Radius Ratio	0.45		
Fan Tip Speed, fps	1000		
Fan Tip Diameter, inches	100		
Number of Rotor Blades	40		
Number of Stator Vanes	28		
Vane/Blade Ratio	0.70		
Rotor-Stator Tip Spacing in vane chords	0.20		
	HUB	PITCH	TIP
Rotor Inlet Radius, inches	22.5	36.25	50.0
Rotor Inlet Absolute Air Angle, α_1 , deg	-46.4	-27.2	-25.6
Rotor Inlet Relative Air Angle, β_1 , deg	61.5	59.3	65.6
Rotor Exit Absolute Air Angle, α_2 , deg	0	0	0
Rotor Exit Relative Air Angle, β_2 , deg	46.9	54.3	59.3
Rotor Inlet Speed, U_1 , fps	450	725	1000
Rotor Exit Speed, U_2 , fps	499	732	964
Rotor Blade Chord, C_R , inches	6.8	6.9	7.0
Stator Vane Chord, C_S , inches	8.75	8.75	8.75
Rotor Solidity, σ_R	1.92	1.21	0.89
Stator Solidity, σ_S	2.18	1.11	0.75
Rotor Diffusion Factor, D_R	0.451	0.336	0.313
Stator Diffusion Factor, D_S	-0.738	-0.364	-0.334
Stator Drag Coefficient, C_{ds}	0.0504	0.0666	0.0939
Rotor-Stator Spacing, inches	0.875	1.31	1.75

Pressure Ratio	1.26		
Radius Ratio	0.45		
Fan Tip Speed, fps	1000		
Fan Tip Diameter, inches	86.5		
Number of Rotor Blades	20		
Number of Stator Vanes	14.0		
Vane/Blade Ratio	0.7		
Rotor-Stator Tip Spacing in vane chords	2.0		
	HUB	PITCH	TIP
Rotor Inlet Radius, inches	8.10	13.05	18.0
Rotor Inlet Absolute Air Angle, α_1 , deg	-46.4	-27.2	-25.0
Rotor Inlet Relative Air Angle, β_1 , deg	61.5	59.3	65.6
Rotor Exit Absolute Air Angle, α_2 , deg	0	0	0
Rotor Exit Relative Air Angle, β_2 , deg	46.9	54.3	59.3
Rotor Inlet Speed, U_1 , fps	450	725	1000
Rotor Exit Speed, U_2 , fps	499	732	964
Rotor Blade Chord, C_R , inches	11.74	11.91	12.08
Stator Vane Chord, C_S , inches	15.0	15.0	15.0
Rotor Solidity, σ_R	1.92	1.21	0.89
Stator Solidity, σ_S	2.18	1.11	0.75
Rotor Diffusion Factor, D_R	0.451	0.336	0.313
Stator Diffusion Factor, D_S	-0.738	-0.364	-0.334
Stator Drag Coefficient, C_{ds}	0.0504	0.0666	0.0939
Rotor-Stator Spacing, inches	1.50	2.25	3.0

Table B26 IGV Fan Aero-Acoustic Data for Run 10

Pressure Ratio	1.26		
Radius Ratio	0.45		
Fan Tip Speed, fps	1000		
Fan Tip Diameter, inches	86.5		
Number of Rotor Blades	80		
Number of Stator Vanes	56		
Vane/Blade Ratio	0.7		
Rotor-Stator Tip Spacing, in vane chords	0.20		
	HUB	PITCH	TIP
Rotor Inlet Radius, inches	8.10	13.05	18.0
Rotor Inlet Absolute Air Angle, α_1 , deg	-46.4	-27.2	-25.0
Rotor Inlet Relative Air Angle, β_1 , deg	61.5	59.3	65.6
Rotor Exit Absolute Air Angle, α_2 , deg	0	0	0
Rotor Exit Relative Air Angle, β_2 , deg	46.9	54.3	59.3
Rotor Inlet Speed, U_1 , fps	450	725	1000
Rotor Exit Speed, U_2 , fps	499	732	964
Rotor Blade Chord, C_R , inches	3.0	3.05	3.1
Stator Vane Chord, C_S , inches	3.75	3.75	3.75
Rotor Solidity, σ_R	1.92	1.21	0.89
Stator Solidity, σ_S	2.18	1.11	0.75
Rotor Diffusion Factor, D_R	0.451	0.336	0.313
Stator Diffusion Factor, D_S	-0.738	-0.364	-0.334
Stator Drag Coefficient, C_{dS}	0.0504	0.0666	0.0939
Rotor-Stator Spacing, inches	0.375	0.563	0.75

Table B27 IGV Fan Aero-Acoustic Data for Run 11

Pressure Ratio	1.26		
Radius Ratio	0.45		
Fan Tip Speed, fps	1000		
Fan Tip Diameter, inches	86.5		
Number of Rotor Blades	40		
Number of Stator Vanes	60		
Vane/Blade Ratio	1.5		
Rotor-Stator Tip Spacing, in vane chords	0.20		
	HUB	PITCH	TIP
Rotor Inlet Radius, inches	19.46	31.36	43.25
Rotor Inlet Absolute Air Angle, α_1 , deg	-46.4	-27.2	-25.0
Rotor Inlet Relative Air Angle, β_1 , deg	61.5	59.3	65.6
Rotor Exit Absolute Air Angle, α_2 , deg	0	0	0
Rotor Exit Relative Air Angle, β_2 , deg	46.9	54.3	59.3
Rotor Inlet Speed, U_1 , fps	450	725	1000
Rotor Exit Speed, U_2 , fps	499	732	964
Rotor Blade Chord, C_R , inches	5.87	5.95	6.04
Stator Vane Chord, C_S , inches	3.5	3.5	3.5
Rotor Solidity, σ_R	1.92	1.21	0.89
Stator Solidity, σ_S	2.18	1.11	0.75
Rotor Diffusion Factor, D_R	0.451	0.336	0.313
Stator Diffusion Factor, D_S	-0.738	-0.364	-0.334
Stator Drag Coefficient, C_{dS}	0.0504	0.0666	0.0939
Rotor-Stator Spacing	0.35	0.53	0.70

Table B28 IGV Fan Aero-Acoustic Data for Run 12

Pressure Ratio	1.26		
Radius Ratio	0.45		
Fan Tip Speed, fps	1000		
Fan Tip Diameter, inches	86.5		
Number of Rotor Blades	40		
Number of Stator Vanes	84		
Vane/Blade Ratio	2.1		
Rotor-Stator Tip Spacing, in vane chords	0.20		
	HUB	PITCH	TIP
Rotor Inlet Radius, inches	19.46	31.36	43.25
Rotor Inlet Absolute Air Angle, α_1 , deg	-46.4	-27.2	-25.0
Rotor Inlet Relative Air Angle, β_1 , deg	61.5	59.3	65.0
Rotor Exit Absolute Air Angle, α_2 , deg	0	0	0
Rotor Exit Relative Air Angle, β_2 , deg	46.9	54.3	59.3
Rotor Inlet Speed, U_1 , fps	450	725	1000
Rotor Exit Speed, U_2 , fps	499	732	964
Rotor Blade Chord, C_r , inches	5.87	5.95	6.04
Stator Vane Chord, C_s , inches	2.5	2.5	2.5
Rotor Solidity, σ_r	1.92	1.21	0.89
Stator Solidity, σ_s	2.18	1.11	0.75
Rotor Diffusion Factor, D_r	0.451	0.336	0.313
Stator Diffusion Factor, D_s	-0.738	-0.364	-0.334
Stator Drag Coefficient, C_{ds}	0.0504	0.0666	0.0939
Rotor-Stator Spacing, inches	0.25	0.38	0.50

Table B29 IGV Fan Aero-Acoustic Data for Run 13

Pressure Ratio	1.26		
Radius Ratio	0.45		
Fan Tip Speed, fps	1000		
Fan Tip Diameter, inches	86.5		
Number of Rotor Blades	40		
Number of Stator Vanes	28		
Vane/Blade Ratio	0.7		
Rotor-Stator Tip Spacing, in vane chords	1.0		
	HUB	PITCH	TIP
Rotor Inlet Radius, inches	19.46	31.36	43.25
Rotor Inlet Absolute Air Angle, α_1 , deg	-46.4	-27.2	-25.0
Rotor Inlet Relative Air Angle, β_1 , deg	61.5	59.3	65.6
Rotor Exit Absolute Air Angle, α_2 , deg	0	0	0
Rotor Exit Relative Air Angle, β_2 , deg	46.9	54.3	59.3
Rotor Inlet Speed, U_1 , fps	450	725	1000
Rotor Exit Speed, U_2 , fps	499	732	964
Rotor Blade Chord, C_r , inches	5.87	5.95	6.04
Stator Vane Chord, C_s , inches	7.5	7.5	7.5
Rotor Solidity, σ_r	1.92	1.21	0.89
Stator Solidity, σ_s	2.18	1.11	0.75
Rotor Diffusion Factor, D_r	0.451	0.336	0.313
Stator Diffusion Factor, D_s	-0.738	-0.364	-0.334
Stator Drag Coefficient, C_{ds}	0.0504	0.0666	0.0939
Rotor-Stator Spacing, inches	7.5	7.5	7.5

Table B30 IGV Fan Aero-Acoustic Data for Run 14

Pressure Ratio	1.26		
Radius Ratio	0.45		
Fan Tip Speed, fps	1000		
Fan Tip Diameter, inches	86.5		
Number of Rotor Blades	40		
Number of Stator Vanes	28		
Vane/Blade Ratio	0.7		
Rotor-Stator Tip Spacing, in vane chords	1.5		
	HUB	PITCH	TIP
Rotor Inlet Radius, inches	19.46	31.36	43.25
Rotor Inlet Absolute Air Angle, α_1 , deg	-46.4	-27.2	-25.0
Rotor Inlet Relative Air Angle, β_1 , deg	61.5	59.3	65.6
Rotor Exit Absolute Air Angle, α_2 , deg	0	0	0
Rotor Exit Relative Air Angle, β_2 , deg	46.9	54.3	59.3
Rotor Inlet Speed, U_1 , fps	450	725	1000
Rotor Exit Speed, U_2 , fps	499	732	964
Rotor Blade Chord, C_r , inches	5.07	5.93	6.04
Stator Vane Chord, C_s , inches	7.5	7.5	7.5
Rotor Solidity, σ_r	1.92	1.21	0.89
Stator Solidity, σ_s	2.18	1.11	0.75
Rotor Diffusion Factor, D_r	0.451	0.336	0.313
Stator Diffusion Factor, D_s	-0.738	-0.364	-0.334
Stator Drag Coefficient, C_{ds}	0.0504	0.0666	0.0939
Rotor-Stator Spacing, inches	11.25	11.25	11.25

Table B31 IGV Fan Aero-Acoustic Data for Run 15

Pressure Ratio	1.26		
Radius Ratio	0.45		
Fan Tip Speed, fps	1000		
Fan Tip Diameter, inches	86.5		
Number of Rotor Blades	40		
Number of Stator Vanes	28		
Vane/Blade Ratio	0.7		
Rotor-Stator Tip Spacing, in vane chords	2.0		
	HUB	PITCH	TIP
Rotor Inlet Radius, inches	19.46	31.36	43.25
Rotor Inlet Absolute Air Angle, α_1 , deg	-46.4	-27.2	-25.0
Rotor Inlet Relative Air Angle, β_1 , deg	61.5	59.3	65.6
Rotor Exit Absolute Air Angle, α_2 , deg	0	0	0
Rotor Exit Relative Air Angle, β_2 , deg	46.9	54.3	59.3
Rotor Inlet Speed, U_1 , fps	450	725	1000
Rotor Exit Speed, U_2 , fps	499	732	964
Rotor Blade Chord, C_r , inches	5.87	5.95	6.04
Stator Vane Chord, C_s , inches	7.5	7.5	7.5
Rotor Solidity, σ_r	1.92	1.21	0.89
Stator Solidity, σ_s	2.18	1.11	0.75
Rotor Diffusion Factor, D_r	0.451	0.336	0.313
Stator Diffusion Factor, D_s	-0.738	-0.364	-0.334
Stator Drag Coefficient, C_{ds}	0.0504	0.0666	0.0939
Rotor-Stator Spacing, inches	15.0	15.0	15.0

REFERENCES

1. Przedpelski Z. J.: Lift Fan Technology Studies. NASA CR 761, 1966.
2. Smith, M.J.P.; House, M.E.: Internally Generated Noise From Gas Turbine Engines - Measurement & Prediction. ASME Paper 66-GT/N-43, March, 1966.
3. Benzakein, M.J.; Kazin, S. B.: A Theoretical Prediction of Aerodynamically Generated Noise in Fans and Compressors. Acoustical Society of America, Cleveland, Ohio, November, 1968.
4. Definitions and Procedures for Computing the Perceived Noise Level of Aircraft Noise, SAE, ARP 865, October 16, 1964.
5. Lawson, M.V.: Reduction of Compressor Noise Radiation. Journal of the Acoustical Society of America, Vol. 43, No. 1 pp. 37-50, 1968.
6. Crigler, J.C.; Copeland, W.L.; Morris, G.J.: Turbojet - Engine Noise Studies to Evaluate Effects of Inlet Guide Vane-Rotor Spacing. NASA TN D-4690, 1968.
7. Wells, R. J.; McGraw, J.M.: Model Freon Compressor Acoustical Studies. FAA DS 68-5, February, 1968.
8. Sharland, I.J.: Sources of Noise In Axial Flow Fans. Journal of Sound Vibration Vol. 1. No. 3, pp. 302-322, 1964.
9. Le S. Filleul, N.: An Investigation of Axial Flow Fan Noise. J of SV, Vol. 3, No. 2 pp. 147-165, 1966.
10. Sofrin, G.; McCann, J.: P&W Aircraft Experience in Compressor Noise Reduction. Aircraft Noise Symposium, University of Tennessee, February, 1968.
11. Smith, E.B.; Benzakein, M.J.; Radecki, K.P.: Study and Tests to Reduce Compressor Sounds of Jet Aircraft. FAA Report DS 68-7, February, 1968.
12. Technical & Economic Evaluation of Aircraft for Intercity Short Haul Transportation. FAA-ADS-74, 1, 1966.
13. Kemp, N.H.; Sears, W.R.: The Unsteady Forces Due to Viscous Wakes in Turbomachines. Journal of the Aeronautical Sciences, July, 1955.
14. Sears, W.R.: Some Aspects of Non-Stationary Airfoil Theory and Its Practical Application. J of AS, January, 1941.
15. Kemp, N.H.; Sears, W.R.: Aerodynamic Interference Between Moving Blade Rows. J of AS, September, 1953.

16. Tyler, J.M.; Sofrin, T.G.: Axial Flow Compressor Noise Studies. 1961 SAE Aeronautical Meeting, 345D.
17. Morfey, C.L.; Dawson, H.: Axial Compressor Noise: Some Results From Aero-Engine Research. ASME 11th Annual Gas Turbine Conference, Zurich, March, 1966.
18. Slutsky, S.: Discrete Noise Generation and Propagation by a Fan Engine. AFOSR - UTIAS Symposium on Aerodynamic Noise, Toronto, Canada, May 20, 1968, Paper Number 170.
19. Sperry, W.C.; Benzakein, M.J.: Experimental Results of Vane/Blade Number Effects on Compressor Noise. ASME 13th Annual International Gas Turbine Conference, Washington, D.C., March 17, 1968.
20. Luke, Y.L.: Integrals of Bessel Functions. McGraw-Hill Book Company, 1962.
21. Motsinger, R.E.; et all: Low Tip Speed Fan Noise Demonstration Program. NASA CR 72456, November, 1968.
22. Copeland, W.L.; Crigler, J.L.; Dibble, A.C. Jr.: Contribution of Downstream Stator to the Interaction Noise of a Single Stage Axial Flow Compressor, NASA TN D-3892, April, 1967.